Annual Review
2018

Molecular Photoscience Research Center

Kobe University

Preface

This annual review provides a summary of the research activity of Molecular Photoscience Research Center for the 2018 academic year. We are further promoting advanced research and international collaboration on molecular photoscience and related topics. Any constructive comments and questions, and any suggestion for collaboration research are welcome.

Since 2017 we have been running joint usage/research project on molecular science in the terahertz frequency region, which is open to domestic universities and research institutes. The project is supported by Ministry of Education, Culture, Sports, Science and Technology (MEXT), Japan. In this year 38 joint research projects were accepted, and the research area spans from solid state physics, biophysics, solution chemistry, polymer science, photochemistry, theoretical physics and chemistry, so on. The research center will continue to make efforts to push forward international and domestic collaborative research.

April, 2019

Keisuke Tominaga
Director of Molecular Photoscience Research Center,
Kobe University

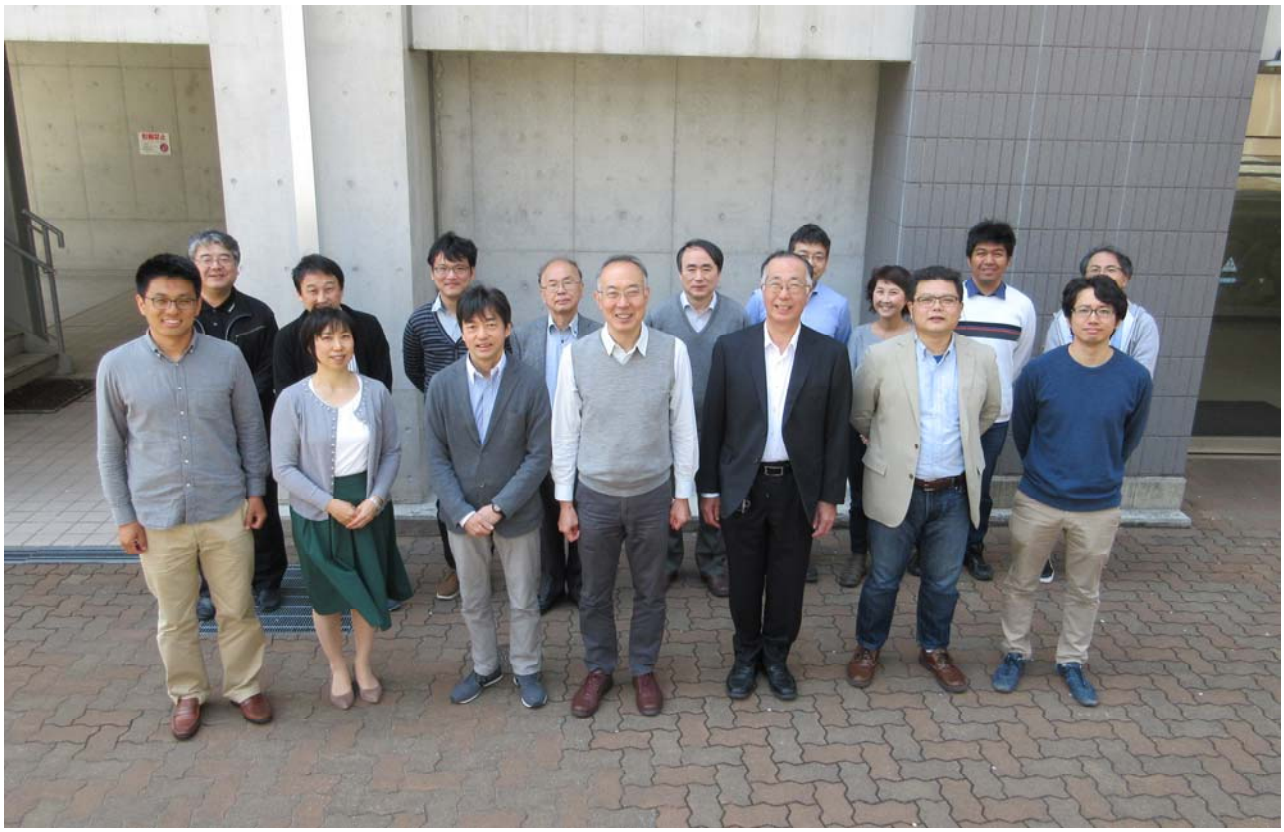

Contents

Members

Keisuke Tominaga	Director
Hitoshi Ohta	Vice-Director
Takako Miyazaki	Assistant
Sachiyo Tombe	Assistant
Kei Kita	Assistant

Laser Molecular Photoscience Laboratory

Yasuhiro Kobori	Professor
Shunji Kasahara	Associate Professor
Takashi Tachikawa	Associate Professor
Hiroki Nagashima	JSPS Postdoctoral Fellow
Morihiko Hamada	Postdoctoral Fellow

Terahertz Molecular Chemistry Laboratory

Keisuke Tominaga	Professor
Kaoru Ohta	Research Associate Professor
Feng Zhang	Postdoctoral Fellow
Masaki Okuda	Researcher
Lou Serafin Lozada	Kobe University Visiting Research Fellow (~ May 2018)
Dustin Loren Almanza	Kobe University Visiting Research Fellow (March 2018 ~)
Harumi Sato	Associate Professor (Supplementary assignment. Main assignment is Graduate School of Human Development and Environment)
Yukihiro Ozaki	Visiting Professor

Terahertz Material Physics Laboratory

Hitoshi Ohta	Professor
Susumu Okubo	Associate Professor
Khalif Benzid	Postdoctoral Fellow (~ September 2018)
Yu Saito	Postdoctoral Fellow (October 2018 ~)
Keigo Hijii	Researcher
Toshiro Kohmoto	Professor (Supplementary assignment. Main assignment is Graduate School of Science)
Eiji Ohmichi	Associate Professor (Supplementary assignment. Main assignment is Graduate School of Science)

I. Laser Molecular Photoscience Laboratory

I-A. SPIN INTERACTIONS STUDIED BY TIME RESOLVED MAGNETIC RESONANCE SPECTROSCOPY

In the natural photosynthesis, the organic solar cells and the photocatalysis, transient radical species or carriers are immediately generated by the light-induced chemical reactions for the photo-energy conversion, providing essential sources of the living energies. However, it has been unclear how those transient molecules are initially interacting each other before the carrier-conductions or charge-dissociation take place. In our group, we are developing experimental methodologies to determine molecular positions, orbital orientations and orbital overlap (electronic coupling) in the initially generated radical-pairs, multiexcitons, and electron-hole pairs in the photoactive proteins, in the solar cells, and in the photocatalysis on the basis of the transient electron paramagnetic resonance (EPR) method. We have clarified several fundamental mechanisms of the energy-conversions in the singlet-fission materials and in the low band gap polymer systems.

Charge-Transfer Character Drives Möbius Antiaromaticity in the Excited Triplet State of Twisted [28]Hexaphyrin

F. Ema, M. Tanabe[1], S. Saito[2], T. Yoneda[2], K. Sugisaki[3], T. Tachikawa, S. Akimoto, S. Yamauchi[1], K. Sato[3], A. Osuka[2], T. Takui[3], Y. Kobori

[1]Tohoku University

[2]Kyoto University

[3]Osaka City University

(*J. Phys. Chem. Lett., 2018*)

Aromaticity is one of the most common concepts that plays an important role in chemistry. Chemical properties and reactivities of π-conjugated macrocyclic molecules depend on their aromatic or antiaromatic character. As a complement of the Hückel rule, Heilbronner predicted that [4n] and [4n+2] π-electronic systems with singly twisted topology show aromaticity and antiaromaticity, respectively. The aromatic molecules show diatropic ring currents, negative nucleus-independent chemical shift (NICS) values at the ring center, and large harmonic oscillator model of aromaticity (HOMA) values. In recent years, Möbius aromatic macrocyclic molecules have been extensively synthesized. Their aromatic or antiaromatic characters have been confirmed experimentally in singlet S0 states, but their excited electronic properties, particularly in T1 states, have been scarcely studied so far. Expanded porphyrins have attracted great attention. Importantly, some expanded porphyrins have been shown to take on twisted conformations exhibiting Möbius aromaticity or antiaromaticity. Meso-aryl-substituted hexaphyrin(1.1.1.1.1.1)s can be a [26] or [28] π-electronic state. Planar [26]hexaphyrin and [28]hexaphyrin display aromatic and antiaromatic characters, respectively, in the S0 states. These aromatic and antiaromatic natures are reversed in the T1 state. The excited-state aromaticity/antiaromaticity of twisted hexaphyrins has received much attention in relation to Baird's

rule. Detailed electronic structures associated with the aromaticity/antiaromaticity, however, have not been investigated in twisted Möbius aromatic molecules in the T1 state. In this study, we examined the T1 states of meso-hexakis(pentafluorophenyl) [26]hexaphyrin(1.1.1.1.1.1) ([26]Hex) and meso-hexakis(pentafluorophenyl) [28]hexaphyrin (1.1.1.1.1.1) ([28]Hex) using an X-band time-resolved electron paramagnetic resonance (TREPR) method in combination with magnetophotoselection (MPS) measurements. We showed that the unpaired electronic orbitals in the T1 state are not uniformly delocalized over the macrocycle of the twisted Möbius [28]hexaphyrin at cryogenic temperature.

Figure 1 shows the delay-time-dependent TREPR spectra of **[28]Hex** obtained by irradiating the depolarized light, the light (***L***) parallel to $\boldsymbol{B_0}$ (***L*** // $\boldsymbol{B_0}$), and the light perpendicular to $\boldsymbol{B_0}$ (***L*** $\perp$ $\boldsymbol{B_0}$). The symmetrical broad EPR spectrum lines were found to be highly dependent upon both the ***L*** direction and the delay time. The magnetophotoselection effects denote that the broad TREPR spectra originate from peak splittings by the anisotropic spin-spin dipolar coupling in the T_1 state as the zero-field splitting (ZFS) interaction whose tensor orientation is defined with respect to the optical transition dipole moment in the molecule. The identifications of the ZFS tensor can thus be performed by the analysis of the TREPR spectra, enabling us to characterize the electronic structures of the T_1 states. The ZFS parameters of D and E are defined in the spin-spin dipolar interaction as, $D = 3(g\beta)^2\langle(r_{12}^2 - z_{12}^2)/r_{12}^5\rangle/4$ and $E = 3(g\beta)^2\langle(y_{12}^2 - x_{12}^2)/r_{12}^5\rangle/4$, where x_{12}, y_{12} and z_{12} are axis components in the separation vector $\boldsymbol{r}_{12}$ between the two spins (1 and 2) in the principal axes system (X, Y, Z) of the triplet state. We performed model calculations of the TREPR spectra based on the line-shape theory for the triplet state.

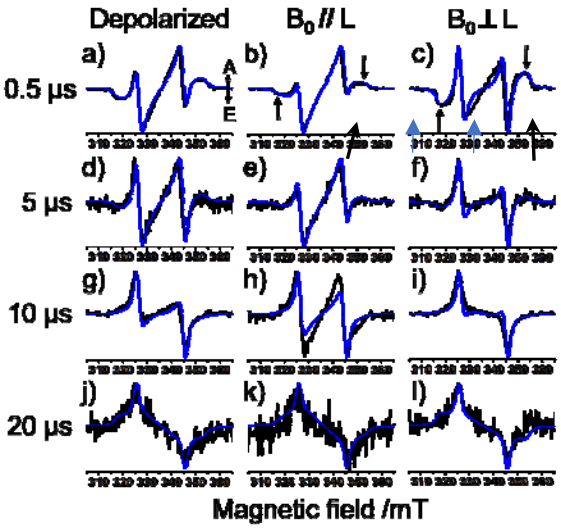

Figure 1. Experimental (black) and simulated (blue) TREPR spectra of **[28]Hex** observed at several delay times after the 650 nm laser irradiations at 77 K in toluene. Depolarized light was employed in the left. $\boldsymbol{B_0}$ // ***L***, and $\boldsymbol{B_0}$ $\perp$***L*** denote that the polarization directions of the laser light (***L***) were parallel and perpendicular to the external magnetic field ($\boldsymbol{B_0}$), respectively.

Further insights into the electronic structure of the T_1 state were obtained by spectrum changes in Figure 1 for t > 5 μs. From Figure 1d, 1g, and 1j, the line-shapes were modulated from the E/A/E/A/E/A pattern to A/A/A/E/E/E by the delay time. In a previous study, time-dependent EPR spectra were interpreted in terms of sublevel-dependent depopulations by a triplet-triplet energy-transfer. In the present case, the A/A/A/E/E/E pattern is explained by a quick T_Z depletion. We quantitatively fitted the delay time

dependence of the transverse magnetizations with taking into account the time-dependent sublevel populations determined by depletion rates from the *X, Y* and *Z* sublevels, respectively. The deactivation kinetics of $k_T = (k_{-X} + k_{-Y} + k_{-Z})/3 = 16$ ms^{-1} is consistent with reported lifetime (90 μs) of ^{3}**[28]Hex*** at 170 K obtained by the transient absorption spectroscopy [1].

In conclusion, we have revealed the electronic structure of the T_1 state of **[28]Hex** by using the TREPR method as the first example of twisted Möbius aromatic molecules. The contribution of the intramolecular CT character together with the LE character at one side in the Möbius strip ring of the macrocycle has been demonstrated. The lack of the spin-spin exchange stabilization between the separated unpaired electrons causes the destabilized triplet state, resulting in antiaromaticity. Besides the energetics and the ring current effects that are used to evaluate the aromaticity/antiaromaticity, the quick SOC-induced triplet deactivation faster than $k_T = 10^4$ s^{-1} can be an alternate important barometer to represent the "antiaromaticity" because of the connection between the orthogonal CT character and the triplet instability.

[1] Kim, K. S.; Yoon, Z. S.; Ricks, A. B.; Shin, J.-Y.; Mori, S.; Sankar, J.; Saito, S.; Jung, Y. M.; Wasielewski, M. R.; Osuka, A. *J. Phys. Chem. A* **2009,** *113*, 4498-4506.

Multiexciton Dynamics Depending on Intramolecular Orientations in Pentacene Dimers: Recombination and Dissociation of Correlated Triplet Pairs

H. Sakai[1], R. Inaya[1], H. Nagashima, S. Nakamura[1], Y. Kobori, N. V. Tkachenko[2], T. Hasobe[1]

[1]Keio University

[2]Tampere University of Technology

(*J. Phys. Chem. Lett., 2018*)

Singlet fission (SF), which involves the ultrafast splitting process of a singlet exciton into two triplet excitons with spin conservation, is an attractive and promising way to overcome the value of Shockley–Queisser limit on the efficiency of single-junction photovoltaics. Efficient SF requires the energy level matching between the energy of the lowest-lying singlet excited state E(S1) and energy of two triplet excited states 2E(T1) [that is, E(S1) ≥ 2E(T1)]. SF populates correlated triplet pairs [(TT)] from a singlet excited state, which subsequently dissociates to generate individual triplet states [(2 × T)]. As the reverse process from [(TT)], triplet-triplet annihilation (TTA) inhibits to generate (2 × T) because of the competitive reaction with the dissociation process of (TT). Therefore, new methodologies to control photophysical processes from (TT) are definitely required for utilization of generated triplet excitons through high-yield SF.

Pentacene is one of representative molecules to meet the above requirement as compared to other molecules. High triplet quantum yields through quantitative SF utilizing covalently linked molecular dyads were recently observed in addition to the occurrence of SF in crystalline and aggregate states of organic molecules. Moreover, the dissociation process from exchanged-coupled triplet pairs (i.e., quintet spin state [5(TT)]) to individual triplet states (2 × T1) was observed by time-resolved electron spin resonance (TR-ESR).

However, there is no example regarding the evaluation of intramolecular orientation- dependent multiexciton dynamics in covalently linked molecular dimers. In particular, no experimental studies have been performed to specify how the transfer-integrals between the chromophores paly roles in the efficient generations of 2 × T1 with inhibiting the energy-wasting TTA processes.

In this study, we arranged and synthesized a series of pentacene dimers bridged by a phenylene linker at ortho and meta-positions [denoted as o-(Pc)2 and m-(Pc)2] to examine the multiexciton dynamics between recombination and dissociation from correlated triplet pairs (TT) generated by SF in pentacene dimers. (Figure 1) The DFT calculations and electrochemical measurements qualitatively suggested the strong intramoleclar chromophore coupling of o-(Pc)2 relative to m-(Pc)2. Femtosecond and picosecond transient absorption measurements combined with time-resolved electron spin resonance (TR-ESR) measurements quantitatively revealed the SF-mediated multiexciton dynamics in these dimers.

Femtosecond and picosecond transient absorption measurements quantitatively revealed the SF-mediated multiexciton dynamics including quintet states in these dimers. The multiexciton dynamics are largely dependent on the orientation between two pentacene units in covalently linked dimers with different intramolecular chromophore couplings. Moreover, multiexciton quintet spin states [^{5}(TT)] of triplet pairs were observed in both dimers by the TR-ESR, by which only *m*-$(Pc)_2$ demonstrated the dissociation process to the individual triplets [(2 × T)] from the quintet states [^{5}(TT)]. The k_{SF} value have been revealed to be two orders of magnitude larger in *o*-$(Pc)_2$ than those in *m*-$(Pc)_2$ and are interpreted by the orientation–dependent $LUMO_m$–$HOMO_m$ coupling rather than the $LUMO_m$–$LUMO_m$ and $HOMO_m$–$HOMO_m$ couplings. This is the first observation and manifestation of the intramolecular orientation–dependent control of the dissociation and recombination processes from the multiexciton states. Such rational controls of the transfer integrals in molecular assemblies provide a new perspective for the higher efficiencies of $\Phi_{(2 \times T)}$ to yield the dissociated excitons to contribute to constructions of optoelectronic, spintronic, and energy conversion devices.

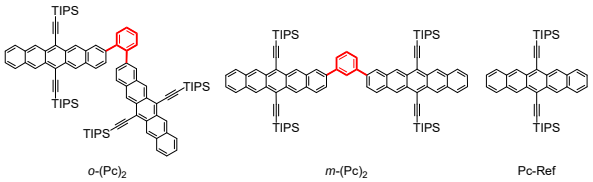

Figure 1. Chemical structures of pentacene dimers and a reference compound in this study.

Time-Resolved EPR Study on Singlet-Fission Induced Quintet Generation and Subsequent Triplet Dissociation in TIPS-Phenyl-Tetracene Aggregates

H. Nagashima, S. Kawaoka[1], Y. Matsui[1], T. Tachikawa, H. Ikeda[1], Y. Kobori

[1]Osaka Prefecture University

(*J. Photopolym. Sci. Technol., 2018*)

Much attention has been attracted on the development of organic photovoltaic devices as the next generation thin-film solar cells that can be low-cost, flexible and light. In this respect, the

singlet fission (SF) process is highly expected to overcome the theoretical limit of the solar cell efficiency (Shockley–Queisser limit) because of a potential of generating two charge-separations from the one high-energy photon. The SF reactions have been observed in limited organic molecules, i.e. tetracene (Tc), pentacene (Pn), hexacene, their derivatives, *etc.* 6,13-Bis(triisopropylsilylethynyl)-pentacene (TIPS-Pn) and 6,11-bis(triisopropylsilylethynyl)tetracene (TIPS-Tc) are representative molecules because of high stability under air, solubility to organic solvents, and high SF efficiencies (up to 200%), in comparison with the parent Pn or Tc. Since applications of the SF to the organic solar cells are still challenging, it is desired to clarify the triplet separation dynamics and its energetics to obtain guidelines for designing highly efficient SF systems.

The SF requires that the energy of the excited singlet state is larger than the twice of the T_1 energy. Pn and their derivatives satisfy this requirement of $E(S_1) > 2E(T_1)$. In contrast, Tc and their derivatives would be classified to another case: the S_1 energy is slightly smaller than the twice of T_1 energy within the thermal energy of k_BT. In this case, a geminate triplet–triplet pair may recombine to the S_1S_0 pair (triplet fusion, TF). This reverse process may follow the SF when the difference between $E(S_1)$ and $2E(T_1)$ is comparable to k_BT. When $E(S_1) << 2E(T_1)$, separately produced two triplet species may encounter a leading to the S_1 formation. This free pair reaction is known as the triplet–triplet annihilation (TTA). Detailed mechanisms of the SF, TF, and TTA are still under discussion on the organic semiconductors.

The electron paramagnetic resonance (EPR) spectroscopy has been a powerful tool to detect unpaired spins and investigate their electronic structures, geometries and dynamics. Recently, the SF-born quintet state, corresponding to ^{5}(TT), was observed by the time-resolved EPR (TREPR) method in thin films and macrocrystals of TIPS-Tc [19]. Intramolecular SF-born quintet states have also been reported on covalently linked dimers of TIPS-Pn. Because the SF is spin-allowed process, the SF-born quintet states are initially populated at a sublevel of $m_s = 0$. Allowed EPR transitions from $|0\rangle$ to $|\pm1\rangle$ are thus detected in the EPR measurements. The primary SF kinetics have been investigated on the covalently linked dimer molecules. It is highly desired, however, that the primary SF dynamics is clarified for the *intermolecular* systems in the solid state, since such kinetics are informative for the practical applications to the organic solar cells. Although the intermolecular SF dynamics have been extensively investigated in the solid crystals and thin-films, the SF and triplet dissociation kinetics have not well been clarified in amorphous solids. In this study, we showed that the quintet (TT)s are generated via SF in solute aggregates, accompanying exothermic microsecond triplet dissociation dynamics from the quintet state by using the TREPR measurements in frozen solutions for newly synthesized 2-phenyl-6,11- bis(triisopropylsilylethynyl)tetracene.

When a 0.1 mM TIPS-Ph-Tc solution was frozen in MTHF, which is a good solvent to solve the substrate, no TREPR signal was observed. On the other hand, clear Q and T signals were obtained for the TIPS-Ph-Tc sample dissolved in *n*-hexane even with a lower concentration of 50 μM. These findings suggest that solute aggregates are produced

by freezing the solutions at 77 K when the poor solvents are employed, contributing to the intermolecular SF.

To analyze the delay time dependence of the EPR signals, the time profiles of the peak intensities in Q in T were reproduced by solving a coupled rate equation determined by the kinetics of ^{5}(TT) and T_1 + T_1. The coupled equation is represented by the dissociation rate constant, k_{QT} for ^{5}(TT) –> T_1 + T_1, the geminate back–reaction rate constant, k_{QT} for T_1 + T_1 –> ^{5}(TT), and the spin-lattice relaxation rate constants of k_{1Q} and k_{1T} for ^{5}(TT) and T_1 + T_1, respectively. The resultant rate constants were obtained to be k_{QT} = 0.53 μs^{-1}, k_{TQ} = 0.30 μs^{-1}, k_{1Q} = 0.63 μs^{-1} and k_{1T} = 0.29 μs^{-1}. From the dissociation and back reaction rates constants, the free energy change (ΔG_{diss}) for the triplet dissociation was estimated to be ΔG_{diss} = –3.6 meV by $\Delta G_{diss} = -k_B T \ln(k_{QT}/k_{TQ})$. This energy is well consistent with ΔG_{diss} = –4.2 meV obtained from the temperature dependence of the ratio of the quintet to triplet formation in the thin films of TIPS-Tc, representing that the dissociation energy would be an upper bound of the intermolecular spin–spin exchange coupling (J) of (TT). The magnitude of $2J$ (= ΔG_{diss}) for (TT) is also coincident with the strongly coupled regime to form the quintet spin state, since the ZFS interaction in the present system is much weaker than the J coupling. The present microsecond dissociation dynamics in the frozen aggregate is however highly different from the quick equilibrium between ^{5}(TT) and T_1 + T_1 in the previously reported thin film of TIPS-Tc. This would be due to a disordered morphology formed by freezing the diluted solution in the present system, since the diffusion coefficients of the triplet excitons are known to be extremely smaller in amorphous environments than those in crystalline phases. To check whether the geminate recombination (or TF) occurs from ^{5}(TT) to the S_1S_0 pair we also measured the fluorescence decay in the present frozen solution system using a streak scope with a picosecond light pulser. Although a double exponential decay profile was detected in the nanosecond time scale, we were unable to detect the TF-induced emission in the submicrosecond region. This result and $\Delta G_{diss} < 0$ obtained above suggest that the free energy (G) of the S_1S_0 pair, ^{5}(TT) and T_1 + T_1 obeys the relationship, $G(S_1) > G[^5(TT)] > G(T_1 + T_1)$, indicating that the SF-requirement of $E(S_1) > 2E(T_1)$ is fulfilled in the present low-temperature aggregate.

In conclusion, by using the TREPR method (the 532-nm laser excitation, 77 K), we have characterized the SF-induced T_1 + T_1 dissociation dynamics and the exchange coupling of the strongly correlated triplet pair in the frozen aggregates of TIPS-Ph-Tc. It has been finally revealed that the microsecond triplet dissociation occurs due to the amorphous morphology in the solute aggregate which is simply produced by freezing the diluted solution, suggesting that ^{5}(TT) is generated as a trapped state. However, the T + T dissociation can follow the trap generation probably due to the repulsion, whose energy were determined by the negative J coupling in (TT) even in the amorphous solid state. The present fundamental energetic and kinetic properties are highly informative for designing efficient energy-conversion systems for the OPV devices.

Singlet-Fission-Born Quintet State: Sublevel Selections and Trapping by Multiexciton Thermodynamics

H. Nagashima, S. Kawaoka[1], S. Akimoto, T. Tachikawa, Y. Matsui[1], H. Ikeda[1], Y. Kobori

[1]Osaka Prefecture University

(*J. Phys. Chem. Lett., 2018*)

Singlet fission (SF) is a reaction that one singlet exciton separates to two triplet excitons. Theoretical limit of the photovoltaic efficiency (Shockly – Queisser limit) can be exceeded by the SF because of a potential of generating two charge-separations from the one high-energy photon. In addition, the SF is applicable for photodetectors, photocatalysis. The SF reactions have been observed in limited organic molecules and TIPS-Tc are representative molecule because they are soluble and stable, in comparison with Pn or Tc and their efficiencies are high (up to 200%). Because application of the SF to the inorganic photovoltaics or the others is still challenging, clarification of the mechanisms and guidelines for design of new SF materials are required.

The singlet exciton localized in one molecule interacts with the neighboring ground state molecule (S_0), generating the correlated intermolecular triplet pair ^{1}(TT) with the singlet character. The ^{1}(TT) state can be converted to quintet state ^{5}(TT). These triplet pair separate into independent triplets. The SF requires that the energy of the excited singlet state is larger than the twice of the T_1 energy. Pn and their derivatives satisfy this requirement of $E(S_1) > 2E(T_1)$. In contrast, tetracene and their derivatives would be classified to the other case: the S_1 energy is slightly smaller than the twice of T_1 energy. In this case, a geminate triplet-triplet pair may recombine to the S_1S_0 pair (triplet fusion, TF). This reverse process may follow the SF when the energy difference between $E(S_1)$ and $2E(T_1)$ is comparable to k_BT. When $E(S_1) << 2E(T_1)$, separately produced two triplet species may encounter leading to the S_1 formation. This free pair reaction is known as the triplet-triplet annihilation (TTA). Detailed mechanisms of SF, TF, and TTA are still under discussion in the organic semiconductors.

For the efficient SF process to yield the correlated TT pair, an orbital overlap between the molecules is required. From this reason, the intermolecular SFs have been observed in highly concentrated solutions, solid crystals and thin-films. For the concentrated solutions in the liquid phase, the SF is reported to take place via the excimer. In nanoparticles, absorption spectra exhibit slight red-shift attributable to a strong chromophore interaction within the particle. In the solid state, large chromophore couplings were reported because Pn molecules are highly ordered to form the π-stacking structures. Recent study however showed an efficient SF in an amorphous environment. It is also important for the OPV applications that the two triplets are efficiently separated in high quantum yield from the correlated TT pair without going back to the S_1S_0 pair. Since the S_1S_0 pair is the singlet, efficient production of the quintet states (^{5}TT pair) is highly desired for preventing the unwanted TF. However, details of the SF-born spin-conversion mechanism are not understood. The electron paramagnetic resonance (EPR) spectroscopy is a powerful tool to directly detect unpaired spins and to investigate their electronic structures, geometries and dynamics. Recently, time- resolved EPR (TREPR) spectra were reported for the SF-born quintet states from

the correlated TT pair. The spin polarization in the EPR spectrum was interpreted by initially population of the quintet states at a sublevel of m_S = 0, i.e. $|^5TT_0>$. This $|^5TT_0>$ generation was observed in TIPS-Tc and in covalently linked dimers of TIPS-Pn, although the origin of the quintet generation is still unclear. Since SF is spin-allowed process, the quintet state generation is required to be accompanied by the singlet-quintet (SQ) mixing from the initially produced singlet character. If the spin-orbit coupling is negligible, the $|^1TT>$ -> $|^5TT_0>$ (S-Q_0) mixing is possible when the energy difference between Q_0 and S is smaller than the zero-field splitting (ZFS) interactions (D) of the individual triplets (i.e. $|E_Q - E_S| < |D|$). It was hypothesized that an intermediate TT pair with a significantly weak J would play a role for the spin polarization. Since TF causes the S_1S_0 pair not from the ^{5}TT pair but from the ^{1}TT pair as the geminate recombination, clarification of the ^{5}TT formation mechanism is a key to regulate SF and TF for the OPV applications to contribute to the complete triplet dissociations reaching 200 %. The SF and triplet dynamics are typically in order of fs – ps, which are too fast to track the initial SF, the spin conversion, and the dissociation by the multiexciton dynamics by using TREPR. In this study, we prepared disordered aggregates of the SF materials from 5,12-bis(triisopropylsilyl) ethynyl-pentacene (TIPS-Pn) and from newly synthesized 2-phenyl-6,11-bis(triisopropyl- silylethynyl) tetracene (TIPS-Ph-Tc) by freezing diluted solution in dichloromethane (CH_2Cl_2). These disordered aggregates will inhibit the rapid exciton process, allowing us to characterize the multiexciton dynamics in more details using TREPR. (Figure 1A)

To characterize the sublevel populations and the geometries of the correlated ^{5}TT from the TREPR spectrum (Figure 1A), we have performed spectrum simulations of the TREPR spectra. Using nine basis spin functions from the quintet, triplet, and singlet TT pairs, the spin Hamiltonian was diagonalized to obtain the nine state-energies in the presence of the Zeeman interaction, the spin-spin dipolar coupling and the exchange interaction. Among the nine eigenvalues, the energetically highest five states are shown as Q_2, Q_1, Q_0, Q_{-1}, and Q_{-2} in Figure 1B under a strong negative J. The internal orientation (Figure 1D) of the ZFS principal axis system (X_2, Y_2, Z_2) in $\boldsymbol{D}_2$ was set by the Euler angles (α, β, γ) with respect to the axis system (X_1, Y_1, Z_1) in $\boldsymbol{D}_1$. The absorptive feature of the spin polarization is completely explained by the preferential populations at m_S = –2, –1 and 0, while highly limited populations are conclusive in the upper sublevels of m_S = 1 and 2. As shown by the red computed spectra in Figure 1A and 1B, the delay time dependences of the EPR spectra were also explained by the preferential relative populations at m_S = –2, –1, and 0 for |Q> and by the populations at m_S = –1 and 0 (Figure 1C right) for the dissociated |T>, denoting that the absorptive spin polarization is conserved during the T + T dissociations from the quintet states.

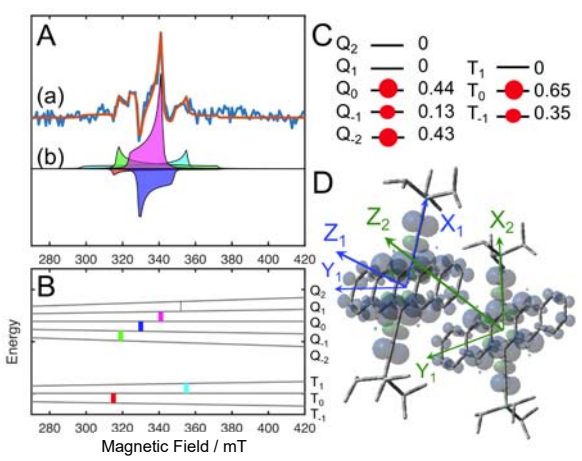

Figure 1. (A, B) Decompositions of the EPR transitions in the TIPS-Pn aggregate at the 0.2 μs delay time. (a) The blue and red lines in panel A show the experimental and simulated TREPR spectra, respectively. Spectra (b) in panel A show the decomposed components integrated by all possible $\boldsymbol{B}_0$-directions. Panel B shows the sublevel energy profiles when the $\boldsymbol{B}_0$ is parallel to the X_1 axis in the TT pair and in the separated T. Quintet states (Q_n) of the strongly coupled TT pairs and the isolated triplet (T_m) are shown. The bars in B show the allowed EPR transitions at the frequency of ω_{MW} = 9.410 GHz for the components in (b) of the panel A. The dashed bar shows the allowed transition but missing in the EPR spectra because of the absence of Q_2 and Q_1 populations. (C) Sublevel populations in |Q> and |T> to account for the TREPR spectra. (D) Representative geometry of the excited quintet states of the TT pair estimated from the orientation setting of α = 30° and β = 20° in the principal axes of the $\boldsymbol{D}_2$ tensor with respect to (X_1, Y_1, Z_1) in TIPS-Pn.

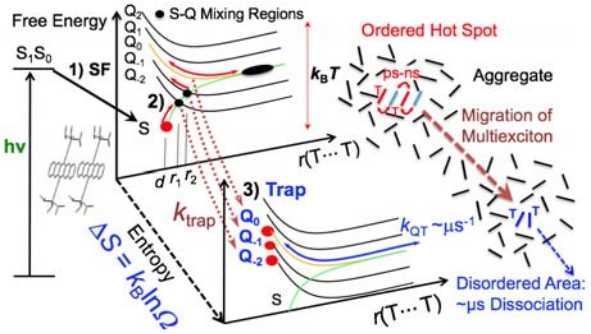

Figure 2. Schematic view of free energy landscape of the TT pairs with respect to the T-T separation (r) and to the reaction coordinate (entropy: ΔS). 1) The SF takes place at the limited ordered area of "hot spot" in the disordered aggregate at a contact separation of $r = d$. 2) When ΔS is constant, the exchange couplings contributing to the SQ gaps are treated to obey $J = J_0 \exp\{-\lambda(r-d)\}$ in which the magnitude of the J_0 is comparable to the thermal energy of k_BT. ΔS is however increased for $r > d$, allowing the exergonic SQ mixings during the ps-ns multiexciton dynamics to generate the CIDEP by the SQ level crossings. 3) After the exciton migration, the coupled TT pairs are spontaneously trapped as indicated by the dotted arrows at the dominant disordered region as the entropy-driven process (lower potentials), resulting in the absorptive Q and Q' signals.

To account for the sublevel populations, we propose a chemically induced dynamic electron polarization (CIDEP) mechanism in SF systems. Figure 2 shows the potential energy landscape drawn with respect to the T-T separation (r) and to a reaction coordinate denoted by an entropy change (ΔS) in the multiexcitons in the solid state.

The SF-born singlet TT pair is initially populated at the minor ordered regions as the "hot spot" using a large electronic coupling, as indicated by the black arrow with 1) SF in Figure 2. The

spin-conversion from $^1|TT\rangle$ (= $|S\rangle$) to $|Q_n\rangle$ should be initially forbidden because these levels are separated from each other by a strong J coupling (J_0) at a contact separation of $r = d$ in Figure 2. Nevertheless, the triplet-exciton diffusion may be initially effective within the geminate multiexciton because of the ordered molecular stacking conformations to induce SF, as shown by the red solid arrows in Figure 2. This primary multiexciton dynamics (as schematically drawn at the upper right in Figure 2) leads to the weakly coupled TT pair, $^1|T...T\rangle$ for $r >> d$. In this case, the singlet state is mixed with the $|Q_0\rangle$ state (SQ_0 mixing). In addition, SQ_{-2} and SQ_{-1} mixings can take place at the level crossing regions of $r = r_1$ or r_2 in Figure 2 by using ZFS, resulting in the populations of $|Q_{-2}\rangle$ and $|Q_{-1}\rangle$, when translational diffusion constant (D_r) of the triplet is small enough. This ZFS-induced level-crossing mechanism was clarified in the CIDEP by radical-triplet pairs for $D_r < 10^{-5}$ cm^2s^{-1} [1]. This D_r range is also in line with the reported triplet diffusion in amorphous TIPS-Pn films [2].

In conclusion, the ps-ns multiexciton diffusion around the ordered "hot-spot" where SF preferentially takes place plays a crucial role on the quintet multiexciton. The SQ mixing regions in Figure 2 are accessible from the initial singlet TT pair due to the entropy enhancement of $\Delta S = k_B \ln \Omega > k_B$. Additionally, ΔS causes the multiexciton trapping at the disordered region, ultimately leading to the μs T+T dissociations. This ΔS may play an important role for the exergonic SFs to result in T + T even in the endothermic SF materials of tetracene derivatives if SF occurs from the weakly coupled singlet states. These new findings are highly informative for rational designs of efficient SF and TTA induced up-conversion systems with preventing the unwanted deactivations by controlling both the molecular π-stacking and the disordered trapping area.

[1] Kobori, Y.; Takeda, K.; Tsuji, K.; Kawai, A.; Obi, K. *J. Phys. Chem. A* **1998,** *102*, 5160-5170.

[2] Grieco, C.; Doucette, G. S.; Pensack, R. D.; Payne, M. M.; Rimshaw, A.; Scholes, G. D.; Anthony, J. E.; Asbury, J. B. *J. Am. Chem. Soc.* **2016,** *138*, 16069-16080.

Identifying triplet pathways in dilute pentacene films

D. Lubert-Perquel[1], E. Salvadori[2], M. Dyson[1], P. N. Stavrinou[3], R. Montis[1], H. Nagashima, Y. Kobori, S. Heutz[1], C. W. M. Kay[4]

[1]Imperial College London

[2]University College London

[3]Oxford University

[4]University of Saarland

(*Nat. Commun. 2018*)

Interest in the photophysics of singlet fission (SF) has dramatically increased in recent years due to the possibility of overcoming thermodynamic limitations in the efficiencies of organic electronic, organic spintronic and hybrid organic/inorganic structures. SF is the photophysical process by which a single photon absorbed by a pair of interacting chromophores generates two triplet excitons. These initially are strongly coupled triplets and may dissociate into free triplets or recombine via triplet-triplet annihilation. In

its basic description, SF requires an incoming photon energy more than double that of the generated triplets. Being a spin-allowed process, it can be fast enough to outcompete prompt fluorescence. Harnessing this mechanism holds the promise to exceed the Shockley-Queisser limit and quantum efficiencies >100% have been reported. Only a few molecules are known to undergo SF, of which polyacenes are the most extensively investigated. Recent studies identify the bound nature of coupled triplets and show evidence of the quintet nature of coupled triplets in isotropic frozen solutions and amorphous films. However, much remains unknown as to the precise nature of the multiexciton (paramagnetic) states and how the coupling between chromophores depends upon their geometry.

To allow detection and characterisation of the high-spin intermediates formed upon SF, we investigated ordered films of pentacene in a *p*-terphenyl matrix at different concentrations. Pentacene was selected as the benchmark molecule for SF, whilst *p*-terphenyl provides a well-defined host. The crystal structure of the pentacene in *p*-terphenyl has been documented – pentacene substitutes into one of two inequivalent sites, due to the herringbone structure of the host lattice. As assessed by optical spectroscopy, dilution has been shown to have little effect on the efficiency of singlet fission; however in combination with oriented samples and EPR spectroscopy, it would allow the kinetics of the distinct spin species to be derived. Furthermore, as *p*-terphenyl is not a conjugated system, charge transfer between host and dopant should be suppressed.

XRD characterisation did not enable firm conclusions to be drawn about the orientation of pentacene in the host matrix. However, this could be achieved by exploiting the anisotropy of the zero-field splitting (zfs) interaction using time-resolved EPR spectroscopy (tr-EPR). Figure 1a shows the full rotation pattern for the 0.5% film over a rotation of 180°, where the angle specifies the orientation between the applied magnetic field and the normal to the substrate. Simulation of the rotation pattern (orange trace) closely resembles that obtained for a pentacene doped *p*-terphenyl crystal. Increased in-plane disorder when the *y, z*-orientation is parallel to the field resulted in a weaker signal at those orientations. At 20 ± 5° between the normal and the magnetic field, a single pair of peaks with a splitting of 55 mT (i.e. 1550 MHz, corresponding to the D+3E transition, where D and E are zfs parameters) can be identified as the pure x-orientation. This indicates that the molecules have a contact angle of ~70° on the substrate, slightly further off the normal than the host contact angle (76°) with an experimental error of ±5°. When rotated by 90°, the *y, z*-orientations (splitting ~46 mT and ~100 mT, corresponding to the D-3E and 2D transitions respectively) are predictably resolved with no *x*-contribution. It was therefore concluded that all pentacene molecules are aligned along the x axis but that there is no preferential orientation in the *y, z* plane.

Figure 2a depicts a 2D mapping of the tr-EPR spectrum of the 10% pentacene: p-terphenyl blended film with the applied magnetic field parallel to the x-axis, with a schematic in Figure 6b detailing the time evolution of triplet dynamics. Four pairs of peaks are visible, with the two inner peak separations about 1/3 of the outer peak separations. This suggests two pairs of strongly exchange coupled triplets, where the exchange coupling $J > D$ the zfs parameter, forming quintet states with $S = 2$. The quintet lifetime of the innermost peaks (^{5}(TT)|| at 334 and 349 mT),

which is most apparent in the emissive line, is ~300 ns, and its decay coincides with a rise in the corresponding triplet (T) signal (at 315 and 369 mT). This implies a short-lived high-spin state that efficiently separates into free triplets, which in turn are very long-lived (> 3 µs). On the other hand, the second pair of quintets (at 331 and 351 mT), has a lifetime of ~1 µs and appears to coexist with the weak, outermost triplet signal (at 312 and 372 mT). This could result from a thermally activated equilibrium between the quintet and triplet states. Due to the inefficient dissociation, these would result in trap-states within the functional layer of an optoelectronic device.

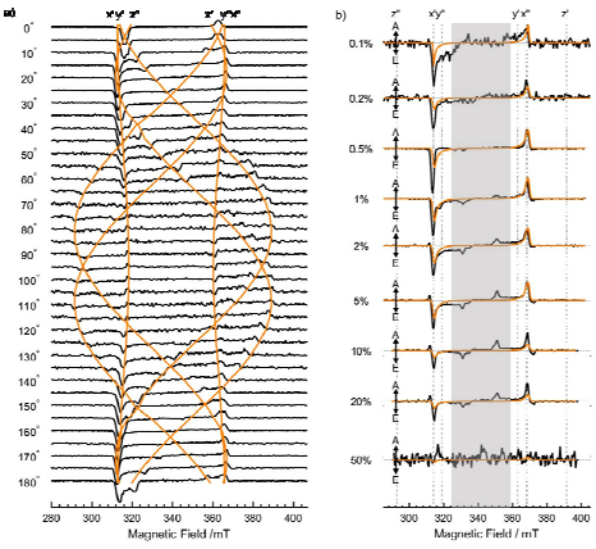

Figure 1. tr-EPR spectroscopy of ordered pentacene films as a function of orientation and concentration. a, tr-EPR spectra of the 1µm 0.5% pentacene doped p-terphenyl film at different orientations within the magnetic field. Angles are defined as between the normal to the substrate and the magnetic field direction. The orange trace is a simulation of the rotation pattern calculated for two inequivalent sites in the crystal lattice. b, tr-EPR spectra acquired in the *x*-orientation as a function of pentacene concentration with the simulated triplet contribution shown in orange. The inner peaks found in the shaded area, which do not belong to isolated triplets, are assigned to long-lived strongly-coupled triplet states.

Only recently quintet formation has been observed by EPR spectroscopy at cryogenic temperatures from pentacene dimers in solution and TIPS-tetracene cast as amorphous films. A major ambiguity in the understanding of singlet fission stems from the poor experimental correlation between molecular geometry and spin coupling. We exploited our growth method to bridge the gap between covalent dimers in solution and monomers in films but crucially at room temperature and with highly controlled molecular orientation. Remarkably, the use of ordered structure and a progressive increase in pentacene concentration allowed the unique observation and characterisation of two strongly coupled quintet states. Indeed, EPR spectroscopy is the sole technique able to unambiguously identify and distinguish between triplets and quintets. Two features provide the signature of a quintet states: the peak splitting in the EPR spectrum three times smaller than that of the corresponding triplets and the nutation frequency $\sqrt{3}$ times larger than that of free triplets. Moreover, dilution inhibits excitation/spin diffusion, significantly enhancing the excitation lifetime. An optimal dilution would provide a compromise between singlet fission efficiency and competing pathways. We have provided direct evidence for two distinct spin coupled states that can be assigned to pairs of pentacenes by their relative orientations. This unambiguously proves that the structure of the pentacene dimers directly affects the properties and dynamics of the corresponding triplet and quintet

high-spin states and that specific geometries are likely to promote the efficiency of SF and to extend the lifetime of the triplet excitons. We have demonstrated that the parallel configuration of dimers undergoes efficient dissociation and is therefore most favorable to generate charges in photovoltaic devices. In contrast, the herringbone configuration results in a trap-state that would hinder triplet harvesting in a device, although the strong coupling on μs timescale could provide opportunities for the exploitation of spin interactions in memory applications. In light of the results presented here, selecting and controlling specific geometries of correlated-triplet pairs can be used to design more efficient triplet harvesting layers; specifically altering the structure into a brick stack arrangement would lead to a reduction in trap-states and improve optoelectronic device efficiency.

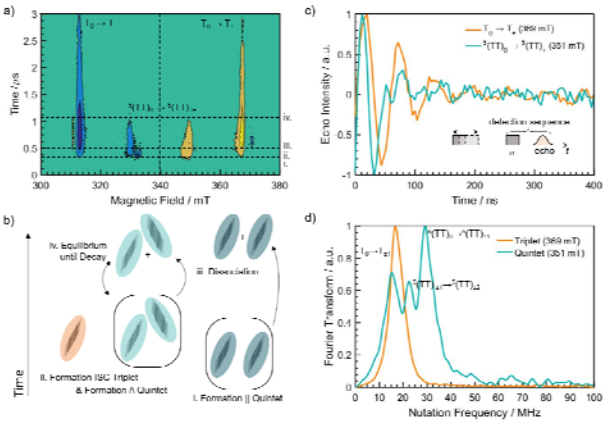

Figure 2. Identifying quintet states at room temperature via EPR spectroscopy and nutation experiments of the (TT) and isolated T states. a, Tr-EPR of the 10% pentacene in p-terphenyl 1 μm film. The innermost peaks from the centre-field belong to strongly-coupled triplets from parallel dimers with the next pair of peaks originating from strongly-coupled triplets with a herringbone geometry. The penultimate and strongest pair of peaks belong to dissociate parallel triplets and isolated ISC crossing triplets, (T). Finally, the outermost peaks are the dissociated triplets from the herringbone quintet. Timescales for the formation and dissociation of spin species are labelled i-iv. b, Schematic of the triplet and quintet kinetics c, Nutation experiment for the high-field quintet and triplet transitions, with the pulse sequence shown in the inset. d, Fourier Transform of data in c showing a ratio of 1.74 between the triplet and quintet nutation frequencies (16.85 and 29.3 MHz respectively), in accord with the nominal value of $\sqrt{3} = 1.73$.

Quantitative Sequential Photoenergy Conversion Process from Singlet Fission to Intermolecular Two-Electron Transfers Utilizing Tetracene Dimer

S. Nakamura[1], H. Sakai[1], H. Nagashima, Y. Kobori, N. V. Tkachenko[2], T. Hasobe[1]

[1]Keio University

[2]Tampere University of Technology

(*ACS Energy Lett. 2019*)

Singlet fission (SF) generates two triplet excitons from one photon absorption. This photophysical process theoretically enables to perform the sequential photo-energy conversion process from SF to electron transfer (ET), yielding the radical ion pairs at ~200% quantum yield. Although the related and conceptual systems were recently published,

the quantitative photoinduced process from SF to two-electron transfers has yet to be reported, so far. The typical examples for intramolecular SF (ISF) are covalently linked pentacene (Pc) dimers with high-yield triplet quantum yields (Φ_T). However, the high-yield intermolecular ET through ISF is generally difficult to achieve for a few reasons. Firstly, the faster recombination of triplet excited states relative to the conventional intersystem crossing (ISC) pathways preclude the intermolecular ET process considering the diffusion-limited reaction. This means that the longer lifetime of the triplet excited state through ISF is required for the high-yield intermolecular reaction. The other reason also includes the relatively low excitation energies of triplet excited states considering energy matching condition between a singlet and two triplet excited states [$E(S_1) \geq 2E(T_1)$]. For example, the triplet excitation energy of Pc is ~0.8 eV. The oxidation potential of the triplet excited state of Pc: [$E(Pc^{\bullet+}/^3Pc^*)$] is ~+0.1 V vs. SCE considering the oxidation potential of Pc ground state: $E(Pc^{\bullet+}/Pc)$ = ~0.9 V vs. SCE. It's quite difficult to find appropriate electron acceptor molecules for ISF-mediated intermolecular ET. Therefore, the strong oxidation property of the triplet excited state with the long lifetime is definitely essential for the achievement of high-yield intermolecular ET through ISF. In contrast, tetracene (Tet) is a good candidate for ISF-mediated intermolecular ET considering the $E(T_1)$: ~1.3 eV and long-lived triplet excited state (0.63 ms). It should be noted that there is no example of covalently linked Tet dimers with the quantitative ISF yield and long-lived triplet state in homogeneous solution regardless of a large number of reports on SF. To attain the high-yield and long-lived triplet excited states, we employed a 2,2'-biphenyl unit as a linker of Tet dimer because of the appropriate control of the electronic coupling between two chromophores. We previously reported the high-yield and long-lived triplet excited states by ISF using 2,2'-biphenyl-bridged Pc dimer. On the other hand, tetrachloro-1,4-benzoquinone, i.e., chloranil (Ch) is a good electron acceptor according to the reported reduction potential (~0 V vs SCE). Herein, we demonstrated the quantitative sequential process from ISF to intermolecular two-electron transfers using 2,2'-biphenyl-bridged Tet dimer (Tet-BP-Tet). The obtained high-yield and long-lived triplet excited states of Tet-BP-Tet by ISF (Φ_T = 175 ± 5% and τ_T = 0.29 ms) resulted in the quantitative intermolecular two-electron transfer process with Ch in benzonitrile (PhCN) (Φ_{ET} = 173 ± 5%).

To carefully examine the transient spectra of Tet-BP-Tet in the longer time scale, nanosecond transient absorption (nsTA) spectra were measured. With increasing the time, the spectral shapes became similar to the pristine T-T absorption spectrum confirmed by energy transfer process. The trace of Tet-BP-Tet at 530 nm was fully fitted by a biexponential function. The initial and faster component is attributable to the mixtures of singlet and correlated triplet-triplet (TT) states because of the competitive reaction between ISF and TTA. The other much slower one corresponds to the individual triplet states (T + T) according to the previous report. Thus, we clearly identified the T-T absorption of Tet-BP-Tet. The individual triplet quantum yield (Φ_T) of Tet-BP-Tet was quantitatively calculated to be 175 ± 5% following the calculation process [1.] Additionally, the rate constant of the dissociation of TT (k_D) (i.e., the

transition from TT to T + T) was determined to be 6.4×10^6 s^{-1}. Finally, microsecond transient absorption (μsTA) spectra demonstrated the long lifetime species of ^{3}Tet*-BP-^{3}Tet*. The lifetime of ^{3}Tet*-BP-^{3}Tet* was also determined to be $\tau_T = 0.29$ ms (i.e., $k_T = 3.4 \times 10^3$ s^{-1}) by monoexponential fitting. Moreover, to confirm the direct evidence of ISF in Tet-BP-Tet, the quintet state of ^{5}(TT) was observed using the time-resolved electron spin resonance measurements (TRESR), as shown in Figure 1.

Additionally, absorption spectral changes from Tet to $Tet^{\bullet+}$ and from Ch to $Ch^{\bullet-}$ were successfully observed by spectroelectrochemical methods. Based on the above results, intermolecular ET between ^{3}Tet*-BP-^{3}Tet* (D) to 2Ch (A) were studied in PhCN by μsTA measurements. The excitation wavelength was chosen to be 532 nm to excite selectively the only Tet unit. The T-T absorption of Tet-BP-Tet was immediately seen at 520 nm after laser pulse excitation. The decay of T-T absorption of Tet-BP-Tet coincides with the developments of Ch radical anion ($Ch^{\bullet-}$) at 450 nm and Tet radical cation ($Tet^{\bullet+}$) at 1000 nm, indicating the occurrence of intermolecular ET from ^{3}Tet*-BP-^{3}Tet* to Ch. The decay of the absorbance at 450 nm arises from the back electron-transfer (BET) reaction. The second-order plot for the decay of $Ch^{\bullet-}$ was obtained from the absorbance at 450 nm and molar absorption coefficient of $Ch^{\bullet-}$ determined by the electrochemical reduction of Ch (3,850 M^{-1} cm^{-1} at 450 nm). From the slope of the linear plot, the second-order rate constant of the back electron transfer (BET) from $Ch^{\bullet-}$ to $Tet^{\bullet+}$ was calculated to be 5.0×10^9 M^{-1} s^{-1}. This value is very close to the diffusion-limit in PhCN (5.6×10^9 M^{-1} s^{-1}). The decay rate constant of the T−T absorption at 520 nm increased with increasing the concentrations of Ch (0 - 0.72 mM).The second-order rate constant of intermolecular ET from ^{3}Tet*-BP-^{3}Tet* to Ch was determined to be 4.8×10^8 M^{-1} s^{-1}. This value is slightly smaller than that of diffusion limited value in PhCN (5.6×10^9 M^{-1} s^{-1}). The possible reason may be due to a small driving force of the intermolecular ET from ^{3}Tet* to Ch or two-electron transfer processes in Tet-BP-Tet.

Finally, the intermolecular ET yield (Φ_{ET}) was quantitatively estimated to be 167 ± 7% at 0.25 mM Ch utilizing the ε of $Ch^{\bullet-}$. The maximum Φ_{ET} value attains up to 173 ± 5% with increasing the concentrations of Ch (the maximum concentration of Ch: 0.72 mM). In conclusion, we demonstrated the quantitative sequential photoenergy conversion process from ISF to intermolecular two-electron transfers using Tet-BP-Tet (SF and donor molecule) and chloranil (electron acceptor). The initial ISF process was confirmed by transient absorption and TRESR measurements. The high-yield and long-lived individual triplet pairs of Tet-BP-Tet by intramolecular SF ($\Phi_T = 175 \pm 5\%$ and $\tau_T = 0.29$ ms) resulted in the quantitative intermolecular two-electron transfer process ($\Phi_{ET} = 173 \pm 5\%$) with chloranil in homogeneous solution (benzonitrile). Such a molecular system provides a new perspective for construction of future solar energy conversion systems (e.g., photocatalysis and photovoltaics).

[1] Sakai, H.; Inaya, R.; Nagashima, H.; Nakamura, S.; Kobori, Y.; Tkachenko, N. V.; Hasobe, T., *J. Phys. Chem. Lett.* **2018**, *9*, 3354-3360.

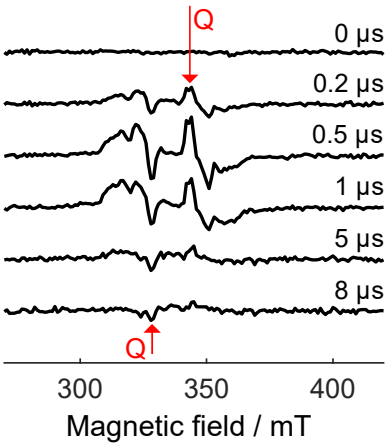

Figure 1. TR-ESR spectra of Tet-BP-Tet in 2-methyl THF at 77 K. The negative ESR intensities with respect to the horizontal baselines denote the microwave emission (E) signals, while the positive intensities the microwave absorptions (A). The E/A polarized peaks labeled by Q exhibit 16 mT separations. This is explained by the zero-field splitting (ZFS) from the excited quintet state of the TT pairs for the field directions perpendicular to Z principal axes of the ZFS tensor, because this splitting is identical with the corresponding splitting reported in quintet state generated in the microcrystals and disordered aggregates of TIPS-Tc.

Singlet-Fission-Born Quintet State: Sublevel Selections and Trapping by Multiexciton Thermodynamics

H. Nagashima, S. Kawaoka[1], S. Akimoto, T. Tachikawa, Y. Matsui[1], H. Ikeda[1], Y. Kobori

[1]Osaka Prefecture University

(*Spin Physics, Spin Chemistry, Spin Technology (SPCT2018), Invited*)

Singlet fission (SF) is expected to exceed the theoretical limit of the efficiency on the organic photovoltaics (OPV). The electron paramagnetic resonance (EPR) spectroscopy is a powerful tool to directly detect unpaired spins and to investigate their electronic structures, geometries and dynamics. Recently, time-resolved EPR (TREPR) spectra were reported on the SF-born quintet states as correlated TT pairs.[1] The spin polarization in the EPR spectrum was interpreted by initial population of the quintet states at a sublevel of $m_S = 0$. This Q_0 generation was observed in covalently linked dimers of TIPS-Pn[2,3], although the origin of this is unclear. When the SF is the spin-conservation process, the quintet generation is required to be accompanied by the singlet–quintet (SQ) mixing from the initially produced singlet character. It was hypothesized that an intermediate TT pair with a significantly weak J would play a role for the Q_0 populations.[1] Little is however known on the primary multiexciton spin dynamics following the intermolecular SF. In this study, we have revealed intermolecular multiexciton dynamics leading to dissociation of two triplet excitons in aggregated 6,13-bis(triisopropylsilylethynyl)pentacene (TIPS-Pn) in diluted frozen solution. We have demonstrated sublevel selective generations of excited quintet states ($|Q_0\rangle$, $|Q_{-1}\rangle$ and $|Q_{-2}\rangle$) by singlet–quintet (SQ) mixings during triplet-exciton diffusions within geminate multiexcitons in the presence of exchange couplings, as was reported in the level-crossing chemically induced dynamics electron polarization (CIDEP) mechanism by the radical-triplet pairs.[4] The present fundamental characteristics of the quintet generations shows strong impact of coexistence of molecularly ordered “hot spot” and disordered regions for exergonic SQ mixings driven by entropy, thereby paving a new

avenue for rational designs of organic devices with controlled multiexciton dynamics by optimizing thin film morphologies.

[1] Weiss, L. R.; Bayliss, S. L.; Kraffert, F.; Thorley, K. J.; Anthony, J. E.; Bittl, R.; Friend, R. H.; Rao, A.; Greenham, N. C.; Behrends, J., *Nat. Phys.* **2017,** *13*, 176-181.

[2] Tayebjee, M. J. Y.; Sanders, S. N.; Kumarasamy, E.; Campos, L. M.; Sfeir, M. Y.; McCamey, D. R., *Nat. Phys.* **2017,** *13*, 182-188.

[3] Sakai, H.; Inaya, R.; Nagashima, H.; Nakamura, S.;Kobori. Y.; Tkachenko, N. V.; Hasobe, T., *J. Phys. Chem. Lett.* **2018** *9*, 3354-3360

[4] Kobori, Y.; Takeda, K.; Tsuji, K.; Kawai, A.; Obi, K., *J. Phys. Chem. A* **1998,** *102*, 5160-5170.

Time-Resolved EPR Study on Photoinduced Charge-Transfer Trap States in Thiophene-Thiazolothiazole Copolymer Films

Yasuhiro Kobori, Yuta Yamamoto, Takumi Ako, Takashi Tachikawa, Itaru Osaka[1]

[1]Hiroshima University

(*233rd ECS Meeting*, *Invited*)

Great attentions have been attracted on the organic photovoltaic (OPV) devices as the next generation thin-film solar cells that can be low-cost, flexible and light [1]. Conjugated polymers have extensively been utilized in various organic electronic devices including the solar cells, field-effect transistors (FET) [2] and light-emitting diodes [3] (LED). The spin coating method from mixed solutions consisting of the conjugated polymers as the electron donors (D) and fullerene derivatives as the acceptors (A) has been employed to produce the solid photoactive layer of the OPV cells [1]. In the organic photoactive layers, it is well known that the polymer molecules are self-organized to generate the bulk heterojunction (BHJ) [4] interfaces. Apart from the OPV applications, pristine films of the conjugated polymers are also utilized for the FET and LED applications [5]. The polymers usually form two dimensional lamellae structures as a result of close interchain packing interaction [4]. Such crystalline phases are known to play a key role for the mobilities of the charges and the excitons in the organic devices. Recent studies suggested that non-fluorescent CT characters exist as a competitive channel of the formation of emissive exciton-type states and determine the light emission efficiencies of the LED films [5].

Despite the significance of the non-fluorescent CT state, no study has experimentally characterized geometry and electronic character of the photoinduced CT state in the pristine polymer films. Consequently, the optoelectric properties of the polymer films have not been fully understood. In our previous study, the geometry and the electronic coupling in the charge-separated states were clarified as the transient radical pairs in regioregular poly(3-hexylthiophene)–fullerene (P3HT–C60) linked dyad molecules [6]. In this study, we have directly observed the photoinduced CT state for a pristine film by thiophene–thiazolothiazole copolymer (PTzBT–BOHD) [7] fabricated by the spin–coating method using time-resolved EPR (TREPR) method to characterize the orbital geometries, the electronic property of the polymer CT state. We show that a long-lived interchain CT states ($P^{+\bullet}$ $P^{-\bullet}$) are generated as a trap state at

disordered region as defects at a cryogenic temperature. We have characterized the interspin separation and the exchange coupling of the interchain CT states in the pristine polymer film of PTzBT–BOHD generated by the 532 nm laser excitation at T = 77 K. It has been revealed that the triplet CT state is generated at the disordered regions of the polymer films as the deep trap site via the triplet exciton. These stable charge─traps would be produced at the polymer defect site possessing the large reorganization energy of ≈ 1 eV. These characteristics of the trapped charges may limit the device performances in the OPV, FET and LED applications. Thus, the TREPR method can provide us with the informative optoelectronic and structural properties of the polymer films for evaluations, designs, and developments of the highly efficient OPV, FET and LED systems.

[1] G. Yu, J. Gao, J. C. Hummelen, F. Wudl and A. J. Heeger, *Science* 270 (1995) 1789.

[2] C. B. Nielsen and I. McCulloch, *Prog. Polym. Sci*. 38 (2013) 2053.

[3] I. F. Perepichka, D. F. Perepichka, H. Meng and F. Wudl, *Adv. Mater.* 17 (2005) 2281.

[4] Y. Kim, S. Cook, S. M. Tuladhar, S. A. Choulis, J. Nelson, J. R. Durrant, D. D. C. Bradley, M. Giles, I. Mcculloch, C. S. Ha and M. Ree, *Nat. Mater.* 5 (2006) 197.

[5] Z. J. Hu, A. P. Willard, R. J. Ono, C. W. Bielawski, P. J. Rossky and D. A. Vanden Bout, *Nat. Commun.* 6 (2015) 8246.

[6] T. Miura, R. Tao, S. Shibata, T. Umeyama, T. Tachikawa, H. Imahori and Y. Kobori, *J. Am. Chem. Soc.* 138 (2016) 5879.

[7] I. Osaka, M. Saito, T. Koganezawa and K. Takimiya, *Adv. Mater.* 26 (2014) 331.

I-B. SINGLE-MOLECULE STUDIES ON PHOTO-ENERGY CONVERSION PROCESSES

To design a more efficient solar energy conversion system (light energy to electrical or chemical energy), it is important to reveal and understand the mechanisms of various chemical reactions at heterogeneous interfaces. We have investigated the photochemical and photophysical processes occurring on a variety of light energy conversion systems such as photocatalysis and solar cells using advanced single-molecule, single-particle spectroscopy techniques and gain new insights related to spatial and temporal heterogeneities in reactions and structures, which are always masked by ensemble averaging.

Direct Observation of Charge Collection at Nanometer-Scale Iodide-Rich Perovskites during Halide Exchange Reaction on $CH_3NH_3PbBr_3$

Izuru Karimata, Kaoru Ohta, Yasuhiro Kobori, and Takashi Tachikawa

(*ACS Appl. Mater. Interfaces, 2018*)

Partial halide substitution in organolead halide perovskites $MAPbX_3$ (MA = $CH_3NH_3^+$, X = Cl^-, Br^-, or I^-) leads to semiconductor heterostructures with precisely tuned band-gap energies, which facilitates efficient charge extraction or separation for high-performance solar cells and optoelectronic devices. In this study, partially iodide-substituted $MAPbBr_3$ perovskites were prepared through a halide-exchange reaction in the liquid phase, and in situ space and time-resolved photoluminescence

profiles were acquired by means of confocal microscopy. A rise in the PL of $MAPbBr_{3-x}I_x$ (red trace) is clearly evident in Figure 1, which is suggestive of charge transfer from the bulk to the surface $MAPbBr_{3-x}I_x$ domains. Each PL profile was nicely fitted to a triexponential function to determine decay and rise times. The $MAPbBr_3$ phase exhibits three decay components (τ_1 = 0.1 ns, τ_2 = 2.6 ns, and τ_3 = 60 ns), while the profile for $MAPbBr_{3-x}I_x$ was well reproduced by a single rise component (τ_{rise} = 0.45 ns) and two decay components (τ_1 = 3.7 ns and τ_2 = 10 ns). Importantly, the rise time did not coincide with the decay time of the $MAPbBr_3$ phase. The rates of charge transfer from the bulk $MAPbBr_3$ to the surface $MAPbBr_{3-x}I_x$ domains, which are widely distributed over a single crystal, were found to greatly depend on the excitation-power density. In particular, an abnormally slow charge-transfer process, lasting a few nanoseconds, was observed at higher excitation density. To explain the dependence of this rate on the excitation density, and its correlation with the charge-trapping rate in the bulk $MAPbBr_3$, we propose a plausible mechanism in which trap filling associated with surface-trapped holes induces band bending within the space charge region. This band bending modulates carrier dynamics near the surface, thereby leading to efficient charge extraction from the bulk.

To validate the mechanism, the carrier dynamics was numerically simulated using a diffusion model that includes the effect of the localized electric field. To validate our simulation, the excitation-density dependence of the PL intensity was further simulated. Our findings provide significantly deeper insight into the carrier dynamics within heterostructured perovskites with nanoscale heterogeneities, and a robust route for manipulating the photogenerated charges in various types of perovskite devices.

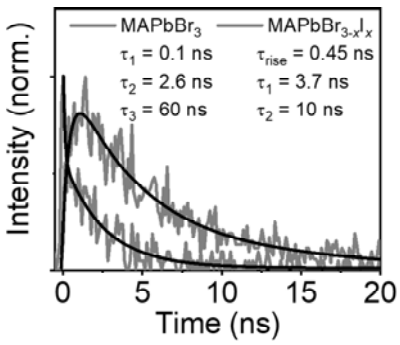

Figure 1. A typical PL intensity trajectory showing the bursts. Inset indicates burst emission spots (marked by red circles) on a single $MAPbBr_3$ crystal during the halide exchange reaction.

Mechanistic Insights into Photochemical Reactions on $CH_3NH_3PbBr_3$ Perovskite Nanoparticles from Single-Particle Photoluminescence Spectroscopy

Yuki Kimura, Izuru Karimata, Yasuhiro Kobori, and Takashi Tachikawa

(*ChemNanoMat, 2019*)

Metal halide perovskites have attracted considerable attention in applications such as photovoltaic cells and light-emitting diodes. The performance and durability of perovskite devices are significantly dependent on the nature of structural defects, but the underlying mechanisms of structure-related photochemical reactions are not yet fully elucidated. This study demonstrates that

the photoluminescence (PL) from individual perovskite nanoparticles (NPs) can be utilized to resolve the different trapping pathways of the photogenerated charges, and hence, obtain a correlation between the pathways. Figure 2 shows the typical PL intensity trajectory of a single $MAPbBr_3$ nanoparticle. The PL intensity is strong immediately after light irradiation, but weakens significantly within a few seconds (referred to as PL deactivation). In addition to the decrease in the PL intensity, the PL decay lifetimes were considerably shortened without any noticeable spectral peak shift. After continuous excitation for a few of tens of seconds, the NPs start emitting again and regain their initial intensity (referred to as PL activation). This gradual increase indicates the light-induced passivation of the nonradiative intrinsic defects, known as photoactivation. From the detailed analysis, it was found that PL deactivation and activation were mainly attributed to nonradiative Auger recombination by the trapped charges and the passivation of surface traps by oxygen, respectively. Single-particle spectroelectrochemical techniques were further employed to explore the possible origin of the effective charge trap states. When negative bias was applied using cyclic voltammetry, the PL intensity sharply decreased at around -0.9 V vs NHE, followed by the recovery in intensity at a less negative voltage. It is suggested that this state is related to the PL deactivation and possibly originates from Br vacancy. Consequently, this study unravels the complex effects of the structural defects on the charge carrier dynamics in perovskites.

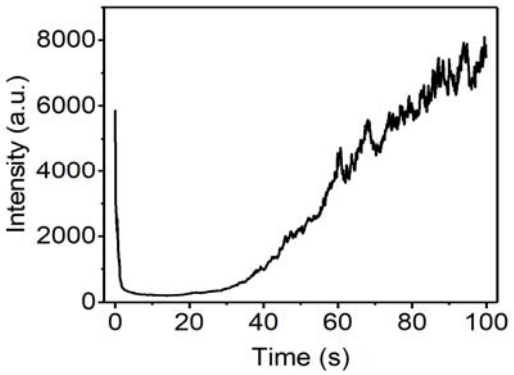

Figure 1. The PL intensity trajectory of a single $MAPbBr_3$ nanoparticle observed during 405-nm laser irradiation in ambient air.

Rapid Formation of Small Mixed-Valence Luminescent Silver Clusters via Cation-Coupled Electron-Transfer in Redox-Active Porous Ionic Crystal Based on Dodecamolybdophosphate

Sayaka Uchida,[1] Tomoki Okunaga,[1] Yuki Harada,[1] Shotaro Magira,[1] Yasuto Noda,[2] Takashi Mizuno,[3] and Takashi Tachikawa

[1]The University of Tokyo

[2]Kyoto University

[3]JEOL RESONANCE Inc.

(*Nanoscale, 2019*)

Redox-active porous ionic crystals based on polyoxometalate (POM) were utilized to form and stabilize small mixed-valence luminescent silver clusters via cation-coupled electron-transfer (CCET) reactions. Reduction-induced ion-exchange between Cs^+ and Ag^+ via CCET took less than 1 min to complete and consisted of two steps: Electron transfer from reduced POM to Ag^+ and subsequent formation of a silver cluster, and diffusion of the silver cluster and exchange with Cs^+. Notably, simple ion-exchange took more than

24 h. The compound containing the silver cluster showed high affinity toward unsaturated hydrocarbon guests. The photoluminescence (PL) spectra of Ag_2-ox and Ag-ox as a reference were measured with excitation at 405 nm. It was found that Ag-ox is not emissive, suggesting that the silver species exists as Ag^+. On the other hand, Ag_2-ox is emissive and gives a broad PL band with a maximum of ca. 550 nm.

Efficient and versatile mechanochromic luminescence of phenanthroimidazolylbenzothiadiazoles: tricolor switching and directional control over the chromism

Sayaka Nagai,[1] Maho Yamashita, Takashi Tachikawa, Takashi Ubukata,[1] Masatoshi Asami,[1] and Suguru Ito[1]

[1]Yokohama National University

(*J. Mater. Chem. C, 2019*)

Mechanochromic luminescence (MCL) refers to the mechanical-stimuli-responsive reversible color change of solid-state emissive dyes. In spite of recent extensive studies on the development of MCL dyes, most of these display bicolor MCL that usually manifests in bathochromic shifts of the emission color in response to mechanical stimuli. Herein, phenanthroimidazolylbenzothiadiazoles are described as a new class of highly emissive solid-state fluorophores that exhibit more versatile MCL properties. Depending on the substituent on the phenyl group of the benzothiadiazole ring, bathochromically or hypsochromically shifted bicolor MCL as well as tricolor MCL are observed for these dyes. Powder X-ray diffraction and differential scanning calorimetry measurements for the bicolor MCL systems indicated that the mechanism of the emission-color change upon grinding is based on typical crystalline-to-amorphous phase transitions. To investigate the tricolor MCL system in detail, single-particle-level fluorescence microscopy has been applied for the first time, which allowed distinguishing three states with different emission properties. The versatility of the present MCL system was attributed to the formation of different crystal structures by introducing various substituents on the aforementioned phenyl group. These results provide useful insights into generating diverse MCL dyes in the future and thus promote the practical applications of MCL systems.

I-C. HIGH-RESOLUTION SPECTOSCOPY OF POLIATOMIC MOLECULES

Doppler-free high-resolution spectroscopic techniques are powerful tools for studying the structure and dynamics of excited polyatomic molecules in detail and unambiguously. Single-mode auto-scan laser systems in UV-Visible-NIR region, the absolute wavenumber measurement system, and several Doppler-free high-resolution spectroscopic measurement systems have been constructed to investigate the excited molecules. High-resolution and high-accuracy measurement of the spectral lines enable to observe rotationally-resolved electronic transition and to find out the excited state dynamics such as internal

conversion (IC), intersystem crossing (ISC), and intramolecular vibrational redistribution (IVR) through the fairly deviation of the spectral line position, intensity anomaly and the change of the spectral linewidth. Recently, we observed the high-resolution spectrum and Zeeman effects of the π-π* transition of several aromatic molecules such as benzene, naphthalene, anthracene, etc. and these molecular constants were determined in high-accuracy.

High-resolution laser spectroscopy of $S_1 \leftarrow S_0$ transition of fluorene and carbazole

Shunji Kasahara, Shinji Kuroda, and Shoya Ueda

(*34th Symposium on Chemical Kinetics and Dynamics, 2018*)

High-resolution laser spectroscopy is a powerful tool for studying the structure and dynamics of excited polyatomic molecules in detail and unambiguously. High-resolution and high-accuracy of the spectral lines enable to observe rotationally-resolved electronic transition and to find out the excited state dynamics through the fairly deviation of the spectral line position, intensity anomaly and the change of the spectral linewidth. In this study, we have observed the rotationally-resolved high-resolution fluorescence excitation spectra of the $S_1 \leftarrow S_0$ transition of fluorene and carbazole molecules (Figure 1). The magnetic effect was also measured up to 1.2 T was obtained by expanding of Fluorene vapor with Ar gas through a pulsed nozzle into the vacuum to consider the excited state dynamics.

A molecular beam was obtained by expanding of fluorene or carbazole vapor with Ar gas through a pulsed nozzle into the vacuum chamber and collimated by using a skimmer (ϕ 2 mm) and slit (0.5 mm). Sub-Doppler fluorescence excitation spectra were measured by crossing a single-mode UV laser beam (Coherent CR699-29 with SpectraPhysics WavetrainSC) perpendicular to a collimated molecular beam. Absolute wavenumber was calibrated with accuracy 0.0002 cm^{-1} by measuring the Doppler-free saturation spectrum of iodine and a fringe pattern of the stabilized etalon.

Rotationally-resolved high-resolution fluorescence excitation spectra were observed for the $S_1 \leftarrow S_0$ transition of fluorene and carbazole. For both molecules, the typical linewidth is about 25 MHz. For fluorene, 7 bands were observed from the 0^0_0 band (Figure 2) to $0^0_0 + 1228$ cm^{-1} band in the region of 33770-35005 cm^{-1}, and their molecular constants were determined with high accuracy. The obtained molecular constants of the 0^0_0 band are good agreement with the reported ones. [1] For the other six vibronic bands were also assigned and determined their molecular constants, but some bands show the difficulty of the rotational assignment. Especially, the typical energy shift was found for the $0_0^0 + 204$ cm^{-1} band, due to the local perturbation with another vibronic level in S_1 state. For carbazole, 3 bands were observed from the 0^0_0 band to $0^0_0 + 1122$ cm^{-1} band in the region of 30800-31935 cm^{-1}, and their molecular constants were also determined. The obtained molecular constants of the 0^0_0 band are good agreement with the reported ones. [1] The Zeeman broadening were observed for the 0^0_0 bands of carbazole up to 1.2 T, however, it was not found for the fluorene.

[1] J. T. Yi, L. Alvarez-Valtierra and D. W. Pratt, *J. Chem. Phys.* **124**, 244302 (2006).

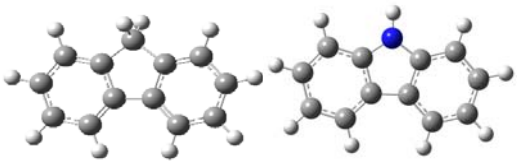

Figure 1. Fluorene (left) and carbazole (right)

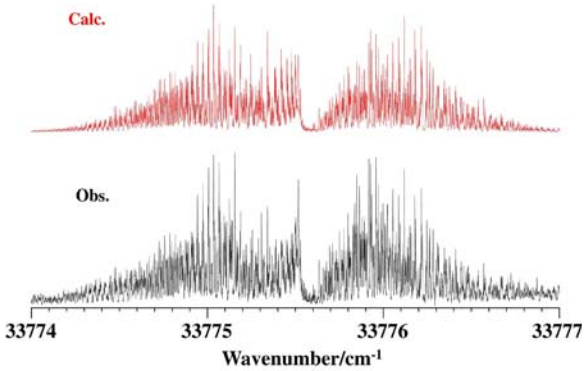

Figure 2. Observed high-resolution spectrum of 0-0 band (lower) and the calculated spectrum (upper).

I-D. HIGH-RESOLUTION SPECTROSCOPY OF NO_2 AND NO_3 RADICAL

Doppler-free high-resolution spectroscopy was applied to investigate the electronic states of radicals. The radicals are very sensitive to the magnetic field because the spin quantum number is a half integer, it is expected to observe large Zeeman splitting even in the small magnetic field. The Zeeman splitting is very useful to assign the observed rotational lines even in the strong perturbing region. Nitrogen dioxide NO_2 and nitrate radical NO_3 have been known as an important intermediate in chemical reaction in the atmosphere. These radicals are the prototype molecules to understand vibronic interaction, and therefore these radicals become one of the model molecule for understanding the Renner-Teller effect for NO_2, and the Jahn-Teller (JT) and pseudo Jahn-Teller (PJT) effects for NO_3. The optically allowed transition has been observed as strong absorption and LIF excitation spectra by several groups. For NO_2 radical, hyperfine splittings are observed in high-resolution spectrum, and the amount of the hyperfine constants suggest the electronic excited state is mixed with the ground state through the vibronic interaction. Recently, we reported the hyperfine-resolved high-resolution spectrum NO_2 A-X system for the 14500-16800 cm^{-1} region.

High-resolution laser spectroscopy of nitrogen dioxide in the region of 14500-16800 cm^{-1}

Shunji Kasahara, Takumi Yoshizawa, Michihiro Hirata, and Kohei Tada

(*25th International Conference on High Resolution Molecular Spectroscopy*)

The nitrogen dioxide (NO_2) is one of the important stable free radicals to investigate the intra-molecular interactions of polyatomic molecules. The visible absorption spectrum shows complexity which comes from the fine structure due to the spin $S = 1/2$ of the unpaired electron and the hyperfine structure due to the nuclear spin $I = 1$ of the ^{14}N atom. Several previous studies examined the hyperfine structures of $N = 1$ levels of the excited electronic states, and reported that the hyperfine interaction constants correlated with the state mixing of the X and A states [1-5]. In this study, we observed hyperfine-resolved high-resolution fluorescence excitation spectra of the $A\ ^2B_2 \leftarrow X\ ^2A_1$ electronic transition of $^{14}NO_2$

radical in 14500-16800 cm^{-1} energy region by crossing a single-mode laser beam perpendicular to a collimated molecular beam [6]. In the observed region, the $^{q}R_0(0)$ lines (k = 0, N = 1 ← 0 transition) were observed for more than 80 vibronic bands, and their hyperfine interaction constants; the Fermi contact interaction constants and the dipole-dipole interaction constants were determined. The determined Fermi contact interaction constants in the 14500-16100 cm^{-1} region were found to be intermediate in magnitude between those in lower and higher energy region reported by other groups. On the other hand, a sharp decreasing of the Fermi contact interaction constant was found in 16 200 – 16 600 cm^{-1} region, and it may be caused by the interaction with the dark $C\,^2A_2$ state.

[1] R. E. Smalley, L. Wharton, and D. H. Levy, *J. Chem. Phys.* **63**, 4977 (1975).

[2] C. A. Biesheuvel, D. H.A. ter Steege. J. Bulthuis, M. H. M. Janssen, J. G. Snijders, and S. Stolte, *Chem. Phys. Lett.* 269, 515 (1997).

[3] C. A. Biesheuvel, J. Bulthuis, M. H. M. Janssen, S. Stolte, and J. G. Snijders, *J. Chem. Phys.* 109, 9701 (1998).

[4] G. Persch, H. J. Vedder, and W. Demtröder, *J. Mol. Spectrosc.*123, 356 (1987).

[5] J. Xin, S. A. Reid, F. Santoro, and C. Petrongolo, *J. Chem. Phys*. 115, 8868 (2001).

[6] K. Tada, M. Hirata, and S. Kasahara, *J. Chem. Phys.* 147, 164304 (2017).

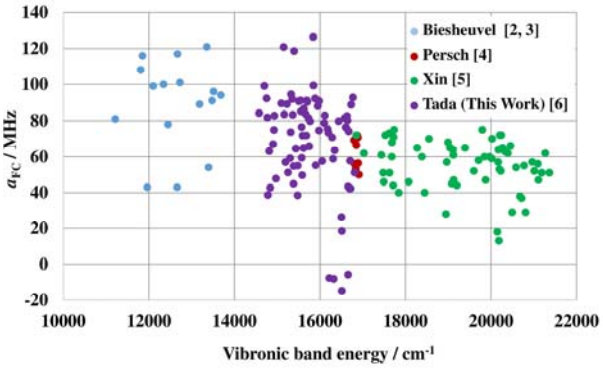

Figure 1. Fermi contact interaction constants vs. the vibronic energy.

II. Terahertz Molecular Chemistry Laboratory

II-A. LIQUID DYNAMICS STUDIED BY NONLINEAR INFRARED SPECTROSCOPY

Molecular dynamics in liquids are strongly affected by the nature of intermolecular interactions. It is greatly important to obtain the molecular description on relation between the dynamics and interactions in liquids in order to elucidate the solvent dynamical effect on chemical reactions. Fluctuations of the vibrational transition energies, which are characterized by time correlation functions of the frequency fluctuations, are very sensitive to the dynamics of surrounding environments. Vibrational energy relaxation is also affected by short-range solvent-oscillator interaction. Furthermore, orientational relaxation reflects microscopic viscosity around the oscillator. In recent years, a great deal of effort has been devoted to investigate solute-solvent interactions with infrared (IR) nonlinear spectroscopy. The vibrational frequency fluctuations can be investigated by three-pulse photon echo and two-dimensional IR spectroscopy. By polarization-sensitive pump-probe spectroscopy in the IR region we can study vibrational energy relaxation and orientational relaxation.

Hydrogen-bond dynamics of 9-fluorenone derivatives in water probed by 2D-IR spectroscopy

Masaki Okuda, Kaoru Ohta and Keisuke Tominaga

(*International Symposium of Nonlinear Optical Spectroscopy*)

In aqueous solution, hydrogen bond (HB) between solute and solvent molecules strongly perturbs dynamic and static properties of the solute molecules, which affects the reactivity of chemical reaction in solution. Vibrational frequency is well-known to be sensitive to the environmental change around solute molecules in solution. Two-dimensional infrared (2DIR) spectroscopy is a powerful tool to quantify the vibrational frequency fluctuation of solute molecules, which results from the temporal fluctuation in solute-solvent interaction on an ultrafast time scale (sub-ps ~ ps time scale).

In this study, by using 2DIR spectroscopy, we have investigated the vibrational frequency fluctuations of two different 9-fluorenone derivatives (FL-2COO^- and FL-4COO^-) in D_2O. From the center line slope analyses for their 2D-IR spectra, we found that the frequency-frequency time correlation function (FFTCF) of the CO stretching mode of FL-4COO^- has a decay time constant of 2.65 ps, which is much longer than those of ionic vibrational probe molecules (~1 ps) observed in many studies so far. The decay time of FFTCFs of the related compounds shows a strong correlation with the size of the hydrocarbon part, which is hydrophobic in nature; acetaldehyde, the smallest size molecule has a time constant of 1.45 ps. Consequently, our 2D-IR results clearly demonstrate that the size of the hydrocarbon part plays an important role in the vibrational frequency fluctuations in water. To understand the effect of the hydrocarbon part on local environment at a molecular level, we conducted the theoretical analyses with classical molecular dynamics (MD) simulations for the

FL-4COO$^-$/water system. We found that the hydrogen bond dynamics between solute and water and the reorientational relaxation of a single water molecule in the vicinity of solute are similar to those in the bulk, which suggests that the slow decay of the FFTCF is not solely due to single-molecule dynamics around the solute. By calculating the radial dependence of the Coulomb electrostatic potential on the vibrational probe from water molecules, we found that the solute interacts electrostatically with water molecules in a sphere of a radius 8 Å from the solute, which can be explained in terms of the low dielectric environment caused by the large aromatic ring. From this result, we conclude that collective water dynamics, which is intrinsically slower than the single-molecule dynamics, makes a strong impact on the vibrational frequency fluctuations of FL-4COO$^-$ in water.

On the other hand, the IR spectrum of FL-2COO$^-$ in D_2O exhibits the asymmetric lineshape, which likely results from two different types of solute-water HB complexes. We found that the relative amplitude of the cross peak (S_{AB}) to the diagonal peak signals (S_{AA}) becomes larger with population time T, which reflects the making and breaking of a HB between FL-2COO$^-$ and a water molecule. Based on these 2DIR results, we conclude that the position of the COO$^-$ group plays an important role for the solute-water HB dynamics.

II-B. DYNAMICS OF ELECTRONICALLY EXCITED STATE IN CONDENSED PHASES

Understanding of dynamics in the electronically excited state is a key issue to elucidate mechanisms in various photochemical reactions in condensed phases. It is also important for designing and developing new materials which have characteristic functions. We employ various kinds of ultrafast technique to monitor photochemical and photophysical invents in sub-pico- to picoseconds time scales. By femtosecond fluorescence up-conversion technique, dynamics in the electronically excited state can be observed with a time resolution up to 100 fs. Vibrational dynamics in the electronically excited can be investigate by UV/VIS-pump IR probe technique. Moreover, low-frequency responses by photoexcitation are investigated by UV/VIS-pump THz probe experiment. Such responses include change of low-frequency vibrational modes induced by photoexcitation and photo-induced changes of charge carrier dynamics.

Ultrafast charge carrier dynamics in diketopyrrolopyrrole-linked tetrabenzoporphyrin films studied by time-resolved terahertz spectroscopy

Kaoru Ohta, Yuichi Hiramatsu, Kohtaro Takahashi[1], Mitsuharu Suzuki[1], Hiroko Yamada[1] and Keisuke Tominaga

[1]Division of Materials Science, Graduate School of Science and Technology, NAIST

(*43rd International Conference on Infrared, Millimeter and Terahertz Waves*)

Organic semiconductors are important materials for plastic solar cells. They have a couple of great advantages over inorganic-based ones because cost-effective and flexible devices can be produced by using solution processing. Tetrabenzoporphrin (BP) is a well-known p-type organic semiconductor that possesses excellent photophysical properties such as a strong absorption in the visible region and high hole mobility. In this work, we studied the charge carrier dynamics of diketopyrrolopyrrole-linked tetrabenzoporphyrin thin films where the diketopyrrolopyrrole unit has two *n*-butyl groups, abbreviated as C4-DPP-BP. We use time-resolved terahertz (THz) spectroscopy to track charge carrier dynamics with excitations at 400 nm and 800 nm. In contrast to BP, C4-DPP-BP exhibits broad and intense absorption, ranging from the visible and near infrared region. Recent study showed that the power conversion efficiency of the C4-DPP-BP-based BHJ solar cell is high (5.2%) compared with BP-based ones. Therefore, it is very interesting to see whether the charge carrier dynamics in C4-DPP-BP:$PC_{61}BM$ BHJ film is different from BP or not. Time-resolved THz measurements of C4-DPP-BP:$PC_{61}BM$ blend films at 800-nm excitation showed that the amplitude of the picosecond decaying components depends on the excitation fluence (Fig. 1).

As the excitation fluence decreases, the amplitude of the fast decaying components decreases. When the excitation fluence was 140 (540) μJ/cm^2, we found that the transient THz signal decays with time constants of 1.4 (0.5) ps and 36 (15) ps. We considered that the fast decaying components in C4-DPP-BP:$PC_{61}BM$ blend films originate from the annihilation of charge pairs at higher excitation fluence. At lower fluence, the charge transfer from C4-DPP-BP to $PC_{61}BM$ at the interfacial region occurs efficiently before quenching of the charge carriers occurs. This could be the reason why the amplitude of the fast decaying component is smaller in C4-DPP-BP:$PC_{61}BM$ blend films compared with C4-DPP-BP thin films. At a higher excitation fluence, charge pair annihilation may also contribute to the fast decaying components of the transient THz signals even in C4-DPP-BP films. It is noted that similar fluence dependence was observed in BHJ conjugated polymer:fullerene blend films, which result from charge pair annihilation occurring at the high carrier densities.

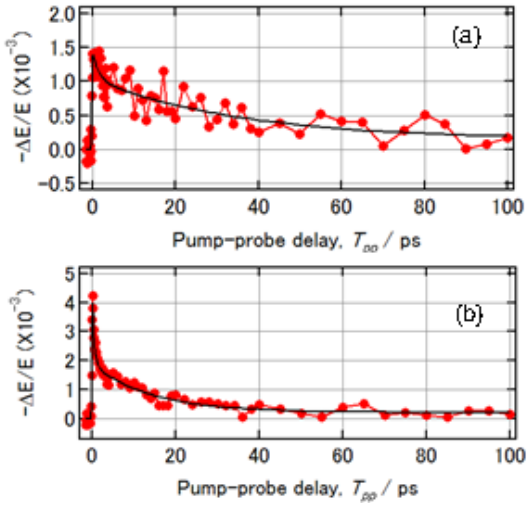

Figure 1. (a) Photoinduced change of the THz electric field amplitude in C4-DPP-BP:$PC_{61}BM$ blend films measured at the peak of the THz transmission. The excitation fluences were (a) 140 μJ/cm^2 and (b) 540 μJ/cm^2, respectively. The excitation wavelength was 800 nm.

II-C. MOLECULAR DYNAMICS IN THE TERAHERTZ FREQUENCY REGION IN CONDENSED PHASES

Vibrational spectroscopy has been widely used to investigate structures, interactions and dynamics of molecules and molecular complexes. The low-frequency region below several terahertz (THz; 1 THz = 33.3 cm^{-1}) corresponds to intermolecular modes of complexes and intramolecular modes with a weaker potential force and/or larger reduced mass. Intermolecular interactions such as hydrogen bonding, van der Waals forces and charge-transfer interactions play important roles in various chemical and biological processes. Moreover, the low-frequency spectra also reflect molecular dynamics on a time scale from picoseconds to femtoseconds. There has been dramatic progress in the generation and detection techniques of freely propagating THz radiation in the past two decades. The examples of the generation technique include photoconductive switching, optical rectification, and the surface photocurrent of semiconductors. Because the pulse duration of the THz radiation is in a sub-picosecond time region, it is possible to measure the electric field of the radiation by coherent detection methods, which consequently allows us to conduct THz time-domain spectroscopy (TDS). By THz-TDS we can obtain the refractive index and extinction coefficient of a medium by measuring the phase and amplitude of the radiation. THz-TDS is an attractive method for studying dynamics in condensed phases with time scales of sub-picoseconds and picoseconds. We have applied THz-TDS to investigate various kinds of condensed materials, including neat liquids and mixtures of liquids, biological polymers, and charge carrier dynamics in semiconductors and conducting polymers.

THz dynamics of hydrated phospholipid studied by broadband dielectric spectroscopy

Yu Kadomura, Naoki Yamamoto[1] and Keisuke Tominaga

[1]Jichi Medical University

(*43rd International Conference on Infrared, Millimeter and Terahertz Waves*)

Cell membrane is mainly formed from self-assembled phospholipid bilayer. Phospholipid bilayer plays an important role in biochemical functions such as ion and molecule transportation. In addition, the functions are observed under certain temperature and hydration condition. Therefore, it is important to investigate effects of thermal excitation and hydration on dynamics of phospholipid bilayer in order to understand biological functions.

Broadband dielectric spectroscopy (BDS) has been used for investigation of dynamics of materials because complex dielectric constant reflects microscopic properties such as intermolecular interactions and molecular motions. The complex dielectric spectra correspond to the Fourier transform of the time correlation function of the total dipole moment of the system. Usually, the frequency range of the electric field used in BDS is 10^{-6} Hz - 10^{12} Hz. By this method, we can mainly investigate rotational relaxation modes, vibrational modes, and conductivity of the materials. Water has spectral components from 10^{7} Hz to 10^{14} Hz. Therefore, it is necessary to measure the spectra in

a wide frequency region in order to understand the dynamics of hydration water around phospholipids. In this work, we studied dynamics of the DMPC bilayer in a broad frequency region including the THz region.

The dielectric spectrum of the dehydrated sample (R = 3.4) does not have a relaxational mode and can be analyzed by two underdamped components. The imaginary part of the complex dielectric spectra slightly decreases as the temperature decreases, which suggests that these vibrational modes are anharmonic. Two and three relaxational components were required for R = 7.1 and R = 7.9, respectively, in addition to the vibrational components. The main relaxational mode of R = 7.9 sample in the GHz region (24 ps, β = 0.83) is slow and broad compared to that of liquid water (9.6 ps, $\beta = 1$) at 293 K. This suggests that the relaxational mode is caused by coupling of water with the phospholipid head group. The relaxational mode has an intensity in the THz region, which is overlapped with the low-frequency underdamped vibrational modes in the high-temperature region. This relaxational mode blue-shifts as the temperature rises. In addition, a fast relaxational mode was observed in the sub-THz region as we reported before.

We compared the results of this study with those of proteins in previous studies. Lysozyme is a globular protein and purple membrane is a protein-phospholipid complex. Here, we focused on the main Cole-Cole relaxational component in the GHz region. The relaxational mode of the hydration water around protein is slow and broad compared to that of phospholipid. The difference of the parameters can be caused by the hydration level, the surface structure of the molecules, the strength of interaction between hydration water and hydrophilic group of the molecules, and so on. Interestingly, the main relaxational mode spreads from the GHz region to the THz region and overlaps with vibrational modes at room temperature among all the studies. This fact may indicate that the thermal activation of the vibrational modes by the relaxational mode is important for the functional expressions of these biomolecules.

Structure analysis of disorder in a molecular crystal with terahertz spectroscopy and solid-state density functional theory

Feng Zhang, Hong-Wei Wang[1], Keisuke Tominaga, Michitoshi Hayashi[1] and Tetsuo Sasaki[2]

[1]National Taiwan University, [2]Shizuoka University

(*43rd International Conference on Infrared, Millimeter and Terahertz Waves*)

For determining atomic positions of a molecular crystal, X-ray crystallography has been the mainstay for 100 years. Despite all the advances, two problems remain challenging. One is that hydrogen atoms are invisible owing to their weak interactions with X-ray. The other is that the determination of the distribution of disordered atoms is far from routine. THz spectroscopy is a promising complement to X-ray. In this work, we aim to elucidate the possibility of applying THz spectroscopy to the structure analysis of disorder.

Form I of diflunisal represents one of the simplest molecular crystals with occupational

disorder. In this system, the pair of hydrogen and fluorine that occupy the two 2,6-ortho sites (highlighted by the circles in the right scheme) of the fluorine-containing ring are disordered; each site has an occupation factor of 0.5. As a result, each molecule can access to two configurations. Since each unit cell contains two molecules, there are in total four unit cell configurations, being denoted as A, B, C, and D.

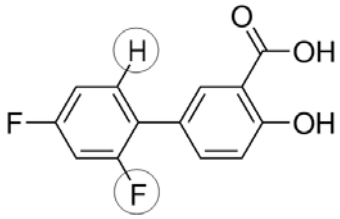

Considering the symmetries of distribution patterns of the four types of unit cell configurations A, B, C, and D, we categorize three classes of packing models. The first class represents the repetitive arrangement of one of the four types of unit cells; the second class denotes the repetitive arrangement of a unit cell constructed through a combination of A, B, C, and D; and the third class stands for the random arrangement of A, B, C, and D. Through an explicit examination of the symmetric properties of vibrational modes arising from the three classes, we concluded that the first class is the only possible distribution pattern of physical significance. On this basis, we proposed an alternating-distribution model of the repetitive-packing segments of unit cells A, B, C, and D.

Using this structural model, we satisfactorily reproduced the THz spectra in a broad frequency region of 15-200 cm^{-1}. One can readily find in Fig. 1 the one-to-one correspondence between experiment and theory for all the observed THz peaks.

According to the line shapes of THz peaks, the whole frequency region divides into three parts, being designated as Regions I, II, and III. Peaks in Regions I and III can all be perfectly fitted with Lorentzian line shapes; while peaks in Region II cannot. We then analyzed the relative strengths of the disordered hydrogen and fluorine atoms with respect to the root-mean-square displacements of all atoms in each modes. The relative strengths of the disordered atoms are all below the average in Region I and III, indicating the marginal importance of the disorder to the THz vibrations in the two regions. Using a one-dimension packing model, AAAAABBBBBCCCCCDDDDD, for a discussion, for a certain mode in Regions I and III, all the unit cells, A, B, C, and D, vibrate collectively in the whole length and at a single frequency, as if the disorder does not exist at all. This situation corresponds to a phonon mode with rather long lifetime. As a result, we observe sharp Lorentzian line shapes in Regions I and III.

In Region II, disordered atoms play non-ignorable roles in the determination of the nature of THz vibrations. We can unambiguously assign peaks *d*, *f* to the short-range repetitive arrangements of unit cells *A* and *D*, respectively, and assign peak *e* to both the short-range repetitive arrangements of unit cells *B* and *C*. Thus Region II displays the fingerprint peaks of the short-range arrangement of the disordered atoms. Let us again use the one-dimension packing model, AAAAABBBBBCCCCCDDDDD, for a discussion. For a certain THz mode in Region II, owing to the remarkable effects of disorder atoms, has distinct frequencies as in different segments, e.g. in AAAAA and BBBBB. In other words, the THz vibrations in Region II are restricted in each

short-range segment. This situation corresponds to the phonon modes confined within small dimensions. Consequently, the phonon modes have very short lifetime and show broad line shapes in THz spectroscopy.

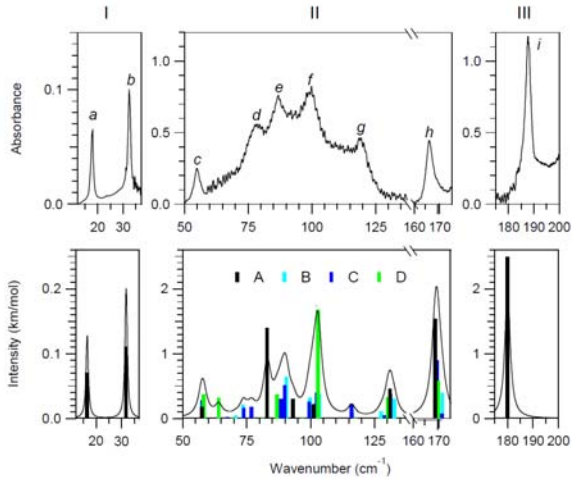

Figure 1. Comparison between experiment and simulation for Form I of diflunisal. The upper panel shows the experimental THz spectra. The lower panel shows the simulated THz modes. Lorentzian line shapes with FWHM of 1.1, 3.5, and 2.5 cm^{-1} are convolved into the modes in Regions I, II, and III, respectively. The intensities of all the line shapes are magnified equally for clarity.

Temperature dependence of THz conductivities of polyaniline emeraldine salt/bentonite pellets

Alvin Karlo G. Tapia[1], Lou Serafin M. Lozada[1], and Keisuke Tominaga

[1]University of the Philippines Los Baños College

(*43rd International Conference on Infrared, Millimeter and Terahertz Waves*)

Polymer-clay systems present many advantages over its parent materials. In conducting polymers or conjugated polymers, conduction takes place through pi-conjugated structures. However, they have poorer thermal processability. Clays when combined with polymers improve the thermal properties of the resulting material. Probing the charge dynamical properties of the conducting polymer-clay systems is essential for designing technological applications. THz spectroscopy has been used to probe charge dynamics in bulk and nanomaterials owing to the relaxation times of charges that lie within the timescale in the THz region.

In this work, polyaniline emeraldine base (PAni-EB) and bentonite clays (Ben) were used for the THz conductivity measurements. PAni-EB was doped with 1 M of HCl yielding PAni emeraldine salt (PAni-ES). PAni-ES/Ben was mixed by mechanical grinding before making pellets. Temperature-dependent THz conductivities from 80 to 290 K were measured using photoconductive-antenna-based THz time-domain spectrometer with cryogenic system.

Figure 1 shows the temperature-dependent THz conductivities of PAni-ES/Ben pellets. The pellets have increasing THz conductivities with increasing amount of PAni-ES and increasing temperatures. The THz conductivities were fitted using combined Drude- Smith and Drude-Lorentz conduction models (DSL). Results show dominant

backscattering of charges for all sample compositions. THz conductivities increase with increasing PAni-ES composition and with increasing temperature. Charges are more mobile for samples with more bentonite. Larger charge densities are observed for samples with more PAni-ES. The Mott-Davis hopping model described well the temperature-dependent conduction of pure PAni-ES. The conduction in the samples was described by backscattering of charges described by the DS term and charges affected by localized oscillators by the DS term.

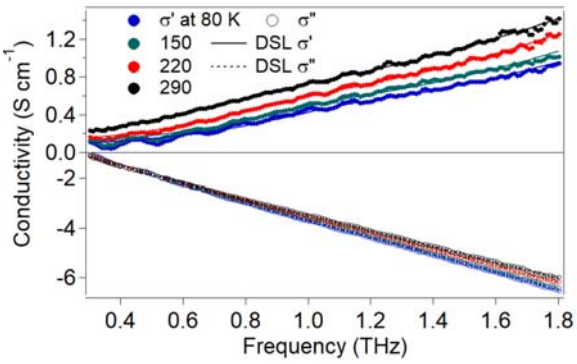

Figure 1. Temperature-dependent complex conductivities of PAni-ES/bentonite pellets fit by Drude-Smith-Lorentz (DSL) model (filled circles-real conductivities and unfilled circles-imaginary conductivities).

II-D. INTERMOLECULAR INTERACTIONS OF POLYMER STUDIED BY TERAHERTZ SPECTROSCOPY

Low-frequency vibrational bands observed in the Raman and terahertz (THz) spectra originate from the higher-order structure, crystalline structure, and intermolecular interactions. Therefore, THz spectroscopy and low-frequency Raman spectroscopy are unique techniques for analyzing higher-order conformations and intermolecular interactions in semicrystalline polymers. However, the band assignment of THz spectra of polymers has not been studied well. Therefore, it is necessary to develop band assignment methods in order to establish THz spectroscopy as a powerful and unique method for exploring the structure and physical properties of polymers.

Polymer structure in water studied by THz-Raman spectroscopy

Harumi Sato, Tomoki Nagahama, Tatsuro Nasu, Yukihiro Ozaki[1]

[1]Kwansei Gakuin University

(*3rd Aquaphotomics International Symposium*)

A collagen model polypeptide $(Pro\text{-}Pro\text{-}Gly)_{10}$, $\{(PPG)_{10}\}$ is a polymer that forms a collagen-like triple-helical structure in aqueous solution. Interestingly, this triple helix folding is thermally reversible. However, short collagen peptides like a $(Pro\text{-}Pro\text{-}Gly)_5$, $\{(PPG)_5\}$ cannot form a triple helical structure due to their low molecular weight or length. Gough et al reported that the $(PPG)_{10}$ adopts a structure in which side chains are mostly exposed to solvent, and the amide group in the backbone forms hydrogen bonds with each molecules, and it was stabilized its helical structure with bound waters [1]. Shikata et al. reported that the hydration number of PPG5 was about 9 per amino acid residue, while that of the PPG10 in the triple helix state in solution was about two per amino acid residue. In the present

study, the structure change and hydration behavior of a collagen model polypeptide $(PPG)_{10}$ and $(PPG)_5$ were investigated in deuterated water over a wide temperature range.

The super absorbent polymer of acrylate type are widely used for commercialized polymer materials such as baby nappies and adults pads, water-holding materials for plants, and so on. As well known the super absorbent polymer can absorb and retain extremely large amounts of a liquid relative to their own mass. The cross-linked poly(acrylic acid) can form a three-dimensional network structure, and water molecules are held tightly in the network by hydrogen-bonding. The hydration with polymer and the comparison between held tightly water molecules and free water will be discussed.

Spectroscopy in THz region reveals intermolecular interaction such as hydrogen bonding between polymer chains. Especially, in the case of the polymer solution, low frequency Raman spectroscopy is powerful tool for investigating these intermolecular hydrogen bonding. We have investigated intermolecular hydrogen bonding between collagen model peptide and water, super absorbent polymer and water by low frequency Raman spectroscopy. In the present study, the results of the structure change and hydration behavior of a collagen model polypeptide $(PPG)_{10}$ and $(PPG)_5$ in deuterated water over a wide temperature range, and the hydration with polymer and the comparison between held tightly water molecules and free water will be discussed.

[1] Gough CA, Anderson RW, Bhatnagar RS, *J Biomol Struct Dyn*. 15(6):1029-37 (1998).

[2] T. Shikata, A. Minakawa and K. Okuyama, *J. Phys. Chem. B*, 113, 43, 14504-14512 (2009)

Molecular dependence of collagen model peptide stuidied by low frequency Raman spectroscopy

Tomoki Nagahama, Mitsuru Yasuda[1], Yukihiro Ozaki[1], Harumi Sato

[1]Kwansei Gakuin University

(*3rd Aquaphotomics International Symposium*)

Low frequency Raman spectra reflects the intermolecular vibration and the interactions between molecular chains. Especially, low frequency Raman spectroscopy is a powerful tool for monitoring higher-order structures of polymer in water. Therefore, we tried to investigate the structural changes of collagen model peptide by low frequency Raman spectroscopy.

Two kinds of collagen model peptides ($(Pro\text{-}Pro\text{-}Gly)_{10}$ (PPG10) and $(Pro\text{-}Pro\text{-}Gly)_5$ (PPG5)) are used as samples (Figure 1). PPG10 and PPG5 are dissolved in D_2O. HR-800-LWR (HORIBA) and SureBlock XLF (Ondax) are used for this study. Each renge of measurements are from 70 cm^{-1} to 3200 cm^{-1} and from 20 cm^{-1} to 1590 cm^{-1}. T95-HS (LINKAM) is used as a temperature controller.

PPG10 forms a triple-helical structure like collagen in aqueous solution, and denatures when it is heated. This structural change from a triple-helix to a random coil in aqueous solution occurs reversibility in PPG10 [1]. However, PPG5 does not show such a conformational change [2]. Figure 2 shows temperature dependent low frequency Raman spectra and their second derivative of PPG10/D_2O and PPG5/D_2O from 27.8ºC to 63.2ºC. They were given by denoising by singular value decomposition, curve fitting,

normalization, and subtraction (each data –70ºC). There are three peaks appeared at around 259 cm^{-1}, 178 cm^{-1}, and 106 cm^{-1} in the 80-300 cm^{-1} region. Figure 3 shows the change of the peak position at around 178 cm^{-1} and 106 cm^{-1}. During cooling process, the peak at around 178 cm^{-1} of PPG10 showed a shift to lower frequency region. While that of PPG5 did not change with temperature (Figure 3 (a)). Moreover, the peak at around 106 cm^{-1} of PPG10 shifted to the higher frequency region, while that of PPG5 did not change with temperature (Figure 3(b)). It is already reported that the peak at 178 cm^{-1} due to the water and 106 cm^{-1} reflected to the intermolecular hydrogen bond in the amide group [3,4]. Therefore, the lower frequency shift of the peak at 178 cm^{-1} due to water indicated that the hydrogen bond between water-to-water is disturbed by collagen model peptide when temperature is higher, but it is not interfered when temperature is lower because triple-helical structure is formed. And the higher frequency shift of 106 cm^{-1} indicated that the intermolecular hydrogen bond in the amide group of the collagen model peptide is stronger because triple-helical structure is formed. These results show that the triple-helical structure of collagen model peptide are formed between 40 to 50ºC. We were able to demonstrate that structural changes from helix to random coil by low frequency Raman spectroscopy.

[1] T. Shikata, N. Yoshida, A. Minakawa, K. Okuyama, *J. Phys. Chem. B* (2009), **113** (43), 14504-14512.

[2] T. Shikata, N. Yoshida, A. Minakawa, K. Okuyama, *J. Phys. Chem. B* (2009), **113** (27), 9055-9058.

[3] Hans R. Zelsmann, *J. Molecular Structure* (1995), **350**, 95-114.

[4] O. F. Nielsen, D. H. Christensen, O. H. Rasmussen, *J. Molecular Structure* (1991), **242**, 273-282.

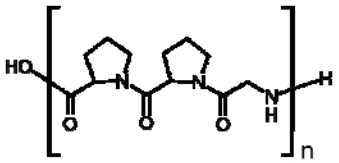

Figure 1. Chemical structure of PPG10 (n = 10) and PPG5 (n = 5).

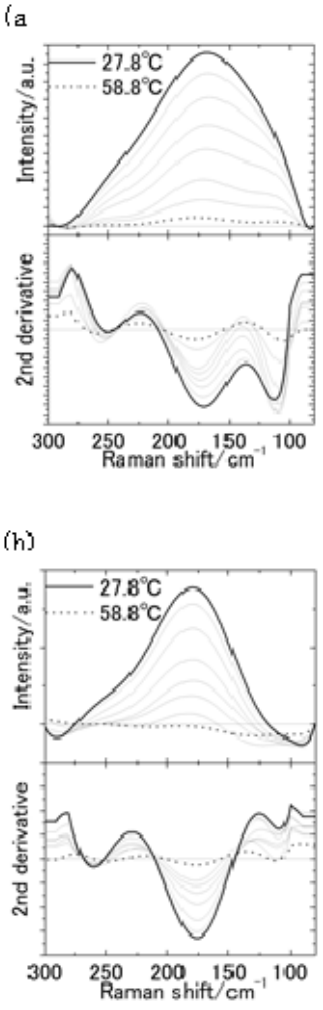

Figure 2. The Raman spectra and their 2nd derivative spectra of (a) PPG10 (b)PPG5.

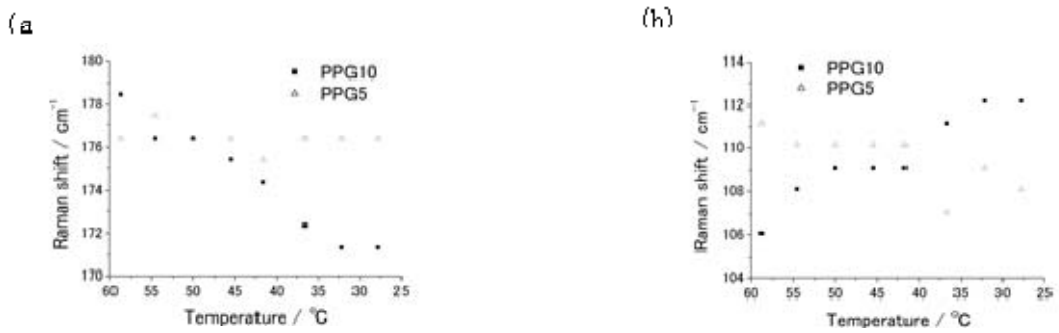

Figure 3 The peak position of PPG10 and PPG5 at around (a) 175 cm^{-1} (b) 109 cm^{-1}.

Stress-induced crystal transition of poly(butylenesuccinate) studied by terahertz and low-frequency Raman spectroscopy

Harumi Sato

(*26th International Conference on Raman Spectroscopy, ICORS 2018*)

Poly (butylene succinate) (PBS; Fig.1 (a)) which shows the crystal transition from α to β crystal form [1-3] by stretching was measured by terahertz (THz) and low-frequency Raman spectra. For the assignment of the absorption peaks in the low-frequency region, we performed quantum chemical calculations with Cartesian-coordinate tensor transfer (CCT) method. Four major peaks appeared in the THz spectra of PBS at around 58, 76, 90, and 100 cm^{-1}, and in the low-frequency Raman spectra a peak was observed at 88 cm^{-1}. The THz peak at 100 cm^{-1} and the Raman peak at 88 cm^{-1} show a shift to a lower wavenumber region with increasing temperature. The quantum chemical calculation of β crystal form reveals the new peak appears above 100 cm^{-1}.

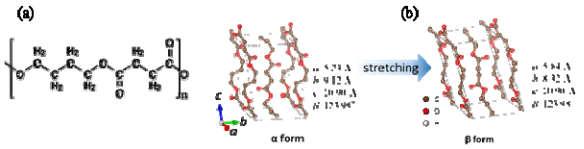

Figure 1. (a) Chemical structure and (b) α and β crystal forms of poly (butylene succinate).

Figure 2 shows the THz absorption spectra of undrawn and 2, 2.5, 3, 3.5, 4, and 4.5 times drawn films of PBS at room temperature. There are four major peaks in both spectra (parallel and perpendicular polarization) at around 58, 76, 90, and 100 cm^{-1}. The results of quantum chemical calculations indicate that the peak at 76 cm^{-1} is due to the twist motion of the main chain. The peak at 76 cm^{-1} does not show a significant shift with stretching. In both parallel and perpendicular THz spectra, however, the peak at around 100 cm^{-1} showed shifts with the opposite directions with stretching. The position of the peak at around 100 cm^{-1} in the perpendicular polarization changes to a lower wavenumber region with stretching, while the peak at 100 cm^{-1} in the parallel polarization shows a shift to a higher wavenumber region by stretching.

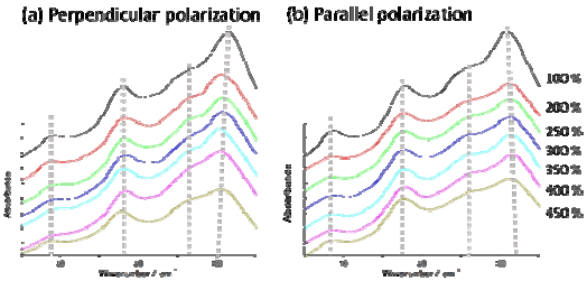

Figure 2. THz polarization spectra of PBS at room temperature with several drawn ratios.

It was found that two kinds of peaks overlapped at around 100 cm^{-1} in the THz spectra of PBS. One of them can be assigned to a weak hydrogen bond between the C=O and CH_2 groups in the intermolecular chains, which is perpendicular to the molecular chain of the α crystal form. Another one showed a parallel polarization which can be assigned to the intramolecular interaction between O (ether) and H-C groups in the β crystal form. The position of the peak at around 100 cm^{-1} in the perpendicular polarization changed to a lower wavenumber region with stretching, because of the weakening of the intermolecular hydrogen bonding by increasing the interatomic distances. On the other hand, that of the parallel polarization shifts to a higher wavenumber region because of the shortening of the interatomic distance from α to β crystal form (the strength of the intramolecular hydrogen bonding became stronger) by stretching.

[1] Y. Ichikawa, J. Suzuki, J. Washiyama, Y. Moteki, K. Noguchi, and K. Okuyama, *Polymer*, 1994, **35** , 3338-3339.

[2] Y. Ichikawa, H. Kondo, Y. Igarashi, K. Noguchi, K. Okuyama, J. Washiyama, *Polymer*, 2000, **41**, 4719-4727.

[3] Y. Ichikawa, J. Washiyama, Y. Moteki, K. Nogushi, and K. Okuyama, *Polym. J.*, 1995, **27**, 1230-1238.

Molecular dependence of several collagen model peptides stuidied by low frequency Raman spectroscopy

Tomoki Nagahama, Harumi Sato

(*26th International Conference on Raman Spectroscopy, ICORS 2018*)

THz region reflects the vibration of molecular chain and the interactions between molecular chains. THz-Raman spectroscopy is a powerful tool for monitoring higher-order structures of polymer. Therefore, we tried to investigate the structural changes of collagen model peptides by low frequency Raman spectroscopy.

We used two kinds of collagen model peptides ($(Pro\text{-}Pro\text{-}Gly)_{10}$ (= PPG10) and $(Pro\text{-}Pro\text{-}Gly)_5$ (= PPG5)) as samples. PPG10 forms a triple-helical structure like collagen in aqueous solution, and denatures when it is heated. PPG10 shows a reversible structural change from a triple-helix to a random coil in aqueous solution [1]. PPG5 does not show such a conformational change [2].

Figure 1 shows temperature dependent THz-Raman spectral variations of PPG10/D_2O and PPG5/D_2O from 27.8 ºC to 63.2 ºC. There are some differences between the low frequency Raman spectra of PPG10 and that of PPG5. The broad peeks at 181 cm^{-1} are derived from D_2O. During cooling process, the intensity ratio (109 cm^{-1}/ 181 cm^{-1}) of PPG10 changes at around 45ºC. While the intensity ratio of PPG5 does not change with temperature (Figure 2). The peaks at 152 cm^{-1} and 203 cm^{-1} also show similar temperature dependence. It is already

known that the PPG10 forms a triple-helical structure from randam coil structure at around 45°C in aqueous solution. Therefore, it is very likely that these peaks are derived from the triple helical structure.

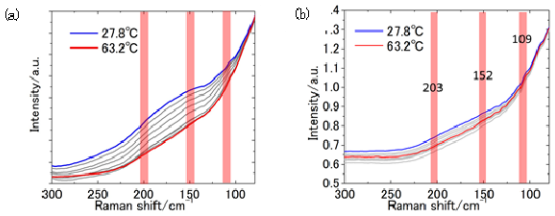

Figure 1 The Raman spectra of PPG10 (a) and PPG5 (b).

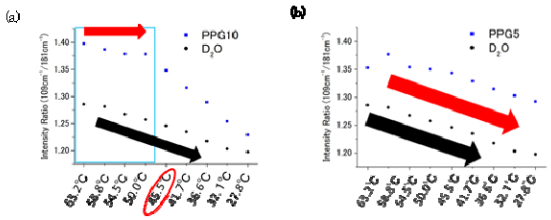

Figure 2 Intensity ratio (109 cm^{-1} / 181 cm^{-1}) of PPG10 (a) and PPG5 (b).

[1] T. Shikata, N. Yoshida, A. Minakawa, K. Okuyama, *J. Phys. Chem. B* (2009), **113** (43), 14504-14512.

[2] T. Shikata, N. Yoshida, A. Minakawa, K. Okuyama, *J. Phys. Chem. B* (2009), **113** (27), 9055-9058.

Study on Intermolecular Interaction of Polydioxanone by Terahertz and low frequency Raman spectroscopy

Natsumi Okazaki, Harumi Sato

(*26th International Conference on Raman Spectroscopy, ICORS 2018*)

Polydioxanone (PDS) is a biodegradable polymer which mainly used as surgical suture (Fig1). PDS shows a glass transition temperature (Tg) at around -10°C and crystallinity of about 55%. The degradation behavior, spherulite crystallization mechanism, mechanical and thermal characteristics of PDS have been reported. However, the detailed analysis of crystal structure and three-dimensional structure of PDS have not been reported yet. Thus, the aim of this study is to elucidate the thermal behavior and the higher order structure, and investigate the intermolecular interaction of PDS by using low-frequency Raman spectroscopy.

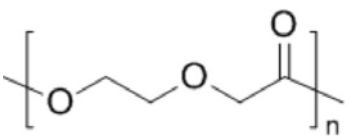

Figure 1 Chemical structure of PDS

PDS pelets was purchased from SIGMA-ALDRICH. Sample for measurement was obtained by melt the PDS pelets at 120°C, which is higher than the melting point (Tm = 110°C), sandwiched between Capton films, pressed, and naturally cooled film (T = 300 μm). The low wavenumber Raman spectrum was obtained from ONDAX XLF-CLM-830 Ondax SureBlock XLF series terahertz Raman spectroscopy system (laser excitation wavelength: 830 nm, resolution: 3.5 cm^{-1}) at room temperature.

Figure 2 shows the Raman and terahertz (THz) spectra of PDS at room temperature. In these spectra several peaks can be observed in both low-frequency Raman and THz spectra of PDS. The peak at 80 and 108 cm^{-1} were observed in the low-frequency Raman

spectrum, while the peak at 75, 93 and 121 cm^{-1} in the THz spectrum. It was found that the wavenumber of the peak in the low-frequency Raman and that of the THz spectra are different in the region of 40-150 cm^{-1}.

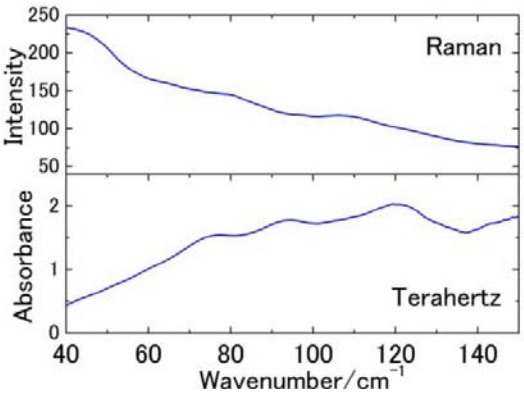

Figure 2 Raman and terahertz spectra of PDS at room temperature.

Study of higher order structure of poly (ethyleneterephthalate) and poly (butylene terephthalate) by low frequency Raman and terahertz spectoscopy

Yumiko Yamamoto, Harumi Sato

(*26th International Conference on Raman Spectroscopy, ICORS 2018*)

Poly (ethylene terephthalate) (PET: Fig.1(a)) has low crystallization rate and high crystallization temperature. On the other hand, poly (butylene terephthalate) (PBT: Fig.1(b)) containing two CH2 groups more than PET has high crystallization rate and it shows excellent moldability. THz region reflects the vibration of molecular chain and interaction between molecular chains such as hydrogen bond. Therefore, we can obtain information such as high order structure and crystal structure of polymers. If we can obtain information on higher order structure or interaction of PET and PBT by the low frequency Raman spectroscopy and THz spectroscopy, it may be possible to elucidate factors of difference in the crystallization process between PET and PBT.

The low frequency Raman spectra was measured using XLF-CLM-830 Ondax SureBlock XLF series THz Raman spectroscopy system (laser excitation wavelength: 830 nm, resolution: 3.5 cm^{-1}) manufactured by ONDAX Co.

(a)

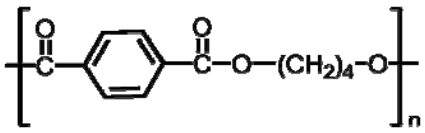

(b)

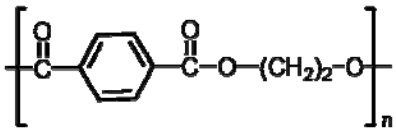

Figure 1 Chemical structure of (a) PET and (b) PBT.

Figure 2 shows the low frequency Raman spectra and THz spectra of PET and PBT at room temperature. Several peaks were observed at around 59 cm^{-1}, 204 cm^{-1}, 225 cm^{-1}, 276 cm^{-1} in both PET and PBT in the low frequency Raman spectra. On the other hand, peaks were observed at around 79 cm^{-1}, 113 cm^{-1}, 149 cm^{-1}, 240 cm^{-1} in the THz spectra. For the THz spectra of PBT, the peaks of 79 cm^{-1}, 113 cm^{-1}, 149 cm^{-1} shifted to the lower wavenumber

region during heating process. It is very likely that these peaks related to the inter- and intramolecular interactions of PBT.

(a)

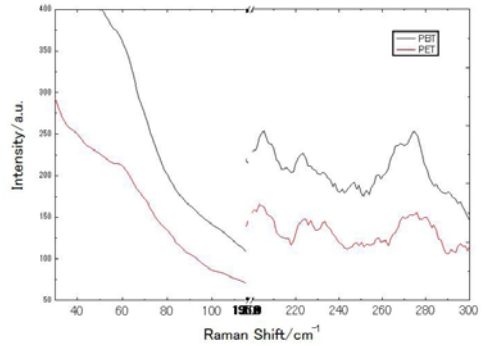

(b)

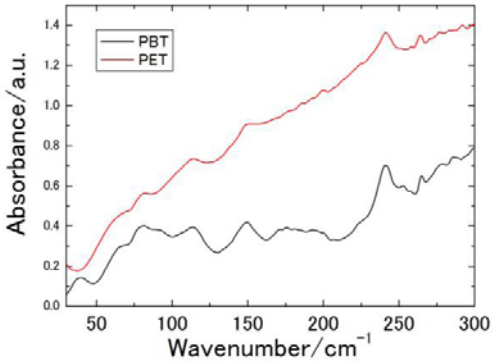

Figure 2. (a) Low frequency Raman spectra and (b) THz spectra of PET and PBT at room temperature.

The Study of Intermolecular Interaction in Polymer Blend of Polyethylene Glycol and Cellulose Acetate Butyrate by Low-Frequency Raman Spectroscopy

Marlina Dian, Harumi Sato

(*26th International Conference on Raman Spectroscopy, ICORS 2018*)

Polymer blending with natural polymers has attracted a great attention for the development of new polymeric materials, since the properties of the polymer can be significantly improved [1,2]. Polyethylene glycol (PEG) is condensation polymer of ethylene oxide and water that has been used for various applications. In order to improve the chemical properties, PEG is blended with Cellulose Acetate Butyrate (CAB). Low frequency vibrational modes which arise from inter- and intra-molecular interaction can directly provide valuable information about the interaction among polymer chains. In this study, we have investigated the intermolecular interaction between PEG and CAB by using low-frequency Raman spectroscopy.

PEG (Mn = 1.0x104) and CAB (Mn = 6.5x104) were purchased from Aldrich Chemical Co., Ltd., and were used as received. Samples of PEG/CAB blend were prepared by following method. At first, PEG and CAB with prescribed weight were dissolved in chloroform (CHCl3). After each solution dissolved perfectly, mixed them and stirred for 48 hours at 60oC. After that, the mixture was poured into a petri dish followed by evaporation at room temperature for 24 hours. Finally, the obtained film sample has been used for the investigation of their intermolecular interaction by using low-frequency Raman spectroscopy.

Figure 1 shows low-frequency Raman spectra of PEG, PEG/CAB (50/50), and CAB at room temperature in the region from about 60 – 1500 cm^{-1}. The spectra of pure PEG and CAB are different. On the other hand, PEG/CAB (50/50) shows the similar spectra with both PEG and CAB. Here some of the peaks appear due to PEG, CAB, or even an overlap between those two. Noted the origin of the spectra in the low-frequency vibrational region, therefore we

assumed that the obtained spectra here are related to the intermolecular interaction of PEG and CAB.

[1] Nattaporn S, el al., *Macromolecules* 2011; **44**: 3467 – 3477.

[2] Nattaporn S, el al., *Polymer* 2011; **52**: 461 – 471

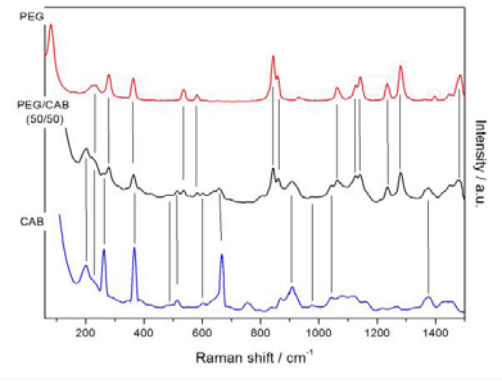

Figure 1. Low-Frequency Raman spectra of PEG, PEG/CAB (50/50), and CAB.

Inter- and intra-molecular interaction of PET and PBT studied by terahertz spectroscopy

Yumiko Yamamoto, Harumi Sato

(*International Conference on Advancing Molecular Spectroscopy, ICAMS*)

Poly (ethylene terephthalate) (PET: Fig 1(a)) and Poly (butylene terephthalate) (PBT: Fig 1(b)) are widely used as engineering plastics. PET has low crystallization rate and high crystallization temperature. On the other hand, PBT containing two CH_2 groups more than PET has high crystallization rate and is excellent in moldability. Terahertz (THz) region reflects the vibration of molecular chain and interaction between molecular chains such as hydrogen bond. Therefore, it may be possible to elucidate of the difference in the crystallization process between PET and PBT if we can obtain information about higher order structure or interaction of PET and PBT by THz spectroscopy.

The absorption peak in the THz spectra of PET film and PBT film were observed around 79 cm^{-1}, 113 cm^{-1}, 149 cm^{-1} and 240 cm^{-1} (Fig. 2). From the results of polarization measurement of PBT, it is indicated that peaks around 79 cm^{-1} and 149 cm^{-1} are derived from the parallel direction to the molecular chains, peaks around 113 cm^{-1} and 240 cm^{-1} are derived from both parallel and perpendicular directions to the molecular chains. In addition, the peak around 79 cm^{-1} shifted to the lower wavenumber region in both PET and PBT during heating process. It is suggested that the intramolecular interaction acts on the same part in PET and PBT, and that this interaction weakened because the mobility of the molecule improves as the temperature increasing. On the other hand, there was a difference in intensity ratio between 79 cm^{-1} and 113 cm^{-1} in PET and PBT.

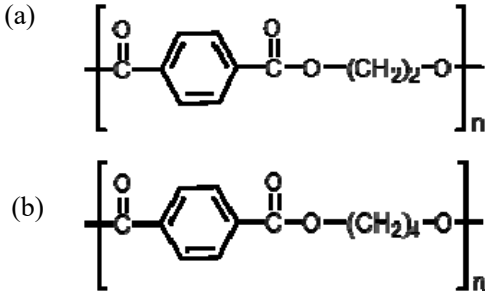

Figure 1. Chemical structure of (a) PET and (b)PBT.

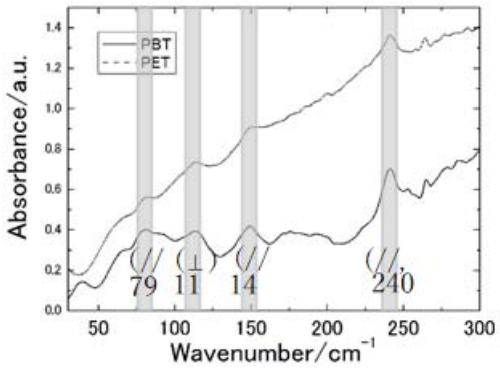

Figure 2. THz spectra of PET and PBT at room temperature.

Three different kinds of weak C-H…O=C inter- and intramolecular interactions in poly(ε-caprolactone) studied by terahertz spectroscopy, infrared spectroscopy and quantum chemical calculations

Harumi Sato, Chihiro Funaki

(*International Conference on Advancing Molecular Spectroscopy, ICAMS*)

The long range structure of poly(ε-caprolactone) (PCL) has been studied by THz spectroscopy, IR spectroscopy and quantum chemical calculations (QCCs). Natural bond orbital (NBO) analysis and the calculation of the interatomic distances between C-H and O=C groups in PCL crystalline indicate that the PCL chain has three kinds of weak intermolecular interactions between the CH_2 and C=O groups. In the IR spectra, significant changes due to the influence of hydrogen bondings were observed in the CH_2 and C=O stretching vibration regions. The results of QCCs performed by using the Cartesian Coordinate Tensor Transfer (CCT) method to assign the THz spectra of PCL suggest that the peaks at 47 and 67 cm^{-1} reflect the atomic motions of the C=O + CH_2 moiety derived from the weak CH…O=C hydrogen bondings. THz spectroscopy allows us to observe the intermolecular hydrogen bondings of the polymer separately, since hydrogen bondings with different strengths yield different peaks in a THz spectrum.

The results of THz and IR spectral analysis, and QCCs all indicate that PCL forms three kinds of weak intermolecular CH…O=C hydrogen bondings between the CH_2 and C=O groups. This may be one of the causes for the low melting temperature but high crystallinity of PCL. There are about six interactions in PCL and about sixteen interactions in polyglycolic acid (PGA), within the lamellar thickness. Therefore, it is suggested that the difference in the number of intermolecular interactions within the lamellar thickness leads to the difference in melting points between the two polymers.

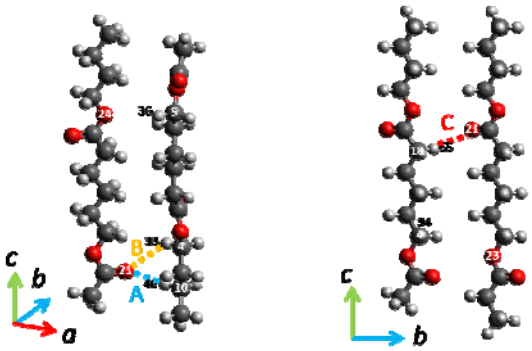

Figure 1. Model structures of PCL used in the NBO calculations. The structures are extracted from the crystal structure; the two chains are aligned perpendicularly along the (110) direction (a) and the b axis (b). Black balls: carbon atom; red balls:

oxygen atom; and gray balls: hydrogen atom.

Molecular weight dependence of Phase separation of poly(methyl methacrylate)/poly(4-vinyl phenol) ultra-thin film studied by infrared reflection absorption spectroscopy

Tomoki Nagahama, Morihisa Terasaki, Isao Takahashi[1], Yukihiro Ozaki[1], Harumi Sato

[1]Kwansei Gakuin University

(*International Conference on Advancing Molecular Spectroscopy, ICAMS*)

In the present study, the hydrogen bond between the carbonyl group of poly(methyl methacrylate) (PMMA) and the hydroxyl group of poly(4-vinyl phenol) (PVPh) in the ultra-thin PMMA/PVPh polymer blend films show were investigated by using reflection infrared spectroscopy (RAS). The purpose of this study is observation of the molecular weight dependence of polymer conformation and phase separation behavior of miscible polymer blend in the ultra-thin film.

PMMA (Mw; 15,000, Aldrich) and PVPh (Mw; 11,000, Aldrich) were used as the sample. Blended polymer were casted on the Au by spin coating. The IR spectra were obtained by infrared reflection absorption spectroscopy at 2 cm^{-1} resolution on a NICOLET6700(FT-IR).

Figure 1 shows the Intensity ratio of C=O free (1735 cm^{-1}) and hydrogen bonded band (1700 cm^{-1}) of PMMA/PVPh (50/50) polymer blend with several thickness during heating process. In our previous study, the thinner film of PMMA/PVPh (Mw = 1500) blend showed an inflection point of the intensity ratio at lower temperature. However, in this study, intensity ratio of the film with a thickness of 4.34 nm did not show a clear inflection point. It is indicated that PMMA and PVPh cannot separate in the ultra-thin film such as 4.34 nm thickness when the molecular weight of PVPh is large enough to make entanglement.

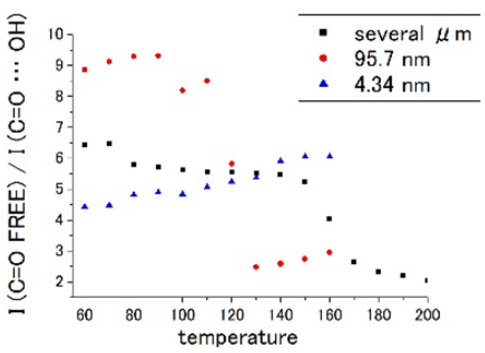

Figure 1. Intensity ratio between C=O free and hydrogen bond band.

Isothermal crystallization of poly(glycolic acid) studied by terahertz and infrared spectroscopy and SAXS/WAXD simultaneous measurements

Fumita Nishimur, Hiromichi Hoshina[1], Yukihiro Ozaki[2], Harumi Sato

[1]RIKEN

[2]Kwansei Gakuin University

(*Polymer J., 51, 237, 2018.*)

Isothermal crystallization of poly(glycolic acid) (PGA) has been studied using terahertz (THz) and infrared (IR) spectroscopy and simultaneous small-angle X-ray scattering (SAXS)/wide-angle X-ray diffraction (WAXD) measurements. Changes in the intermolecular interactions in PGA

during the isothermal crystallization were monitored using THz spectroscopy, which is an efficient technique for analyzing the higher-order structure of polymers. In the THz spectra, the temporal difference in the intensity observed in the isothermal crystallization is due to the difference in the vibrational origins of two bands at 192 and 65 cm^{-1}. The band at 192 cm^{-1} primarily originates from the intramolecular vibrational mode (twisting of the local structure of the PGA molecular chain). Furthermore, the band at 65 cm^{-1} exists due to the intermolecular vibration mode (C = O···H-C hydrogen bonds between polymer chains). In addition, these THz bands appeared after the appearance of the SAXS and WAXD peaks. When a lamellar structure is formed and the molecular chains are oriented, the THz band originating from the intermolecular vibration is observed. It is highly possible that the intermolecular vibration appearing in the THz spectra requires the molecular chains to be oriented.

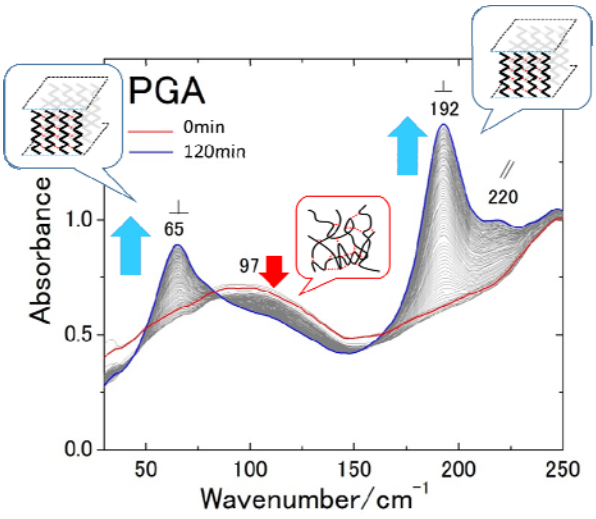

Figure 1 Time-dependent terahertz absorption spectra collected during the melt crystallization process of PGA at 185°C.

III Terahertz Material Physics Laboratory

III-A. HIGH FIELD ELECTRON SPIN RESONANCE (ESR) STUDIES OF QUANTUM SPIN SYSTEMS

The quantum effects and the spin frustration effects prevent long-range order due to strong quantum fluctuation and frustration. Their ground states at low temperature are attractive issue in field of solid state physics. High-frequency high-field ESR is a powerful spectroscopic method to investigate the ground state and lower excited state of the system, because the ESR observes directly magnetic excitation. Following the trends from a Grant-in-Aid for Scientific Research on Priority Areas “Novel states of matter induced by frustration” (No.473, 2007-2011, Headed by Prof. H. Kawamura (Osaka University) and H. Ohta was a member), we are studying these low dimensional antiferromagnets with frustration and related multiferroic materials intensively. High-field ESR measurements of S=1/2 distorted diamond chain $Cu_3(OH)_2(CH3CO_2)_2(H_2O)_xX_y$ (X_y=$EtC_6H_4SO_3$, 1,5-$Np(SO_3)_2$, 2,6-$Np(SO_3)_2$), which consists with Cu^{2+} (S=1/2 spin) diamond chain, has been studied. And S=1/2 Heisenberg antiferromagnetic chain with staggered D vector system $KCuMoO_4(OH)$ is also stadied. Temperature and wide-range frequency dependence measurements show clearly breather excitations. Following researches have been performed by the joint research program of Molecular Photoscience Research Center, Kobe University. For the spin frustration systems, high-field ESR measurements of S=1/2 kagome antiferromagnet $CaCu_3(OH)_6Cl_2\cdot 0.6H_2O$, S=1/2 frustrated magnet $KCu_3(SO_4)_2OCl$, triangular spin ring material have been performed with three joint groups. For quantum spin systems, high-field ESR measurements of S=1/2 low dimensional molecular magnets have been performed. For multiferroic and related materials, high-frequency ESR measurements of manganese perovskite $PbMnO_3$ and S=1/2 Ising spin antiferromagnet $BaCo_2V_2O_8$ have been performed. For the rest, high-field ESR and the magnetic susceptibility measurements of thin film of neodymium permanent magnet and fluorescent materials have been performed to obtain information of the magnetic anisotropy. And we also have joint research with theoretical groups for obtaining experimental parameter from quantum calculations. Totally, our joint research have been performed with 16 groups. And we have two scientific meetings with joint research groups.

H. Ohta gave an invited presentation at the workshop “BigMag@UCSB” (May 17-19, Santa Barbara, USA), and S. Okubo gave an invited presentation at "Modern Development of Magnetic Resonance 2018" (MDMR2018) (Sept. 24-28, Kazan, Russia).

In meantime H. Ohta finished the President (2015-2017) of International EPR (ESR) Society (IES) and continuing as the Immediate-Past President of IES (2018-2020). H. Ohta is also acting as the Advisory Council of APES (Asia-Pacific EPR/ESR Society), the President of the Japan Society of Infrared Science and Technology, and the Council Member of SEST.

Moreover, in order to strengthen the pulsed magnetic field researches in western Japan region, we have been continuing the activities of The KOFUC (Kobe-Osaka-Fukui Universities Centers) Network

since 2014. We have the 5th meeting on high magnetic field science in western Japan at Kobe University and 37 participants.

III-B. RESEARCHES ON VARIOUS SYSTEMS USING ESR AND DEVELOPMENTS OF ESR IMAGING

There are many unsolved basic properties of 3d-electron systems such as pressure dependence of the zero-field splitting energy due to technical difficulties. We have investigated the pressure dependence of the zero-field splitting of Fe(III) ion in bio-related model substance, hemin chloride, and observed substantial shift of the zero-field splitting upon pressure application. The results were discussed in relation to the pressure-induced structural changes of the molecule.

We also developed a new technique to investigate the electronic structure of microliter solution sample by multifrequency EPR. In this setup, a nanomembrane was used to detect a small change of EPR-induced magnetic moment of the frozen solution sample. EPR signals of 10 microliter solution sample of myglobin, which is known as a famous hemoprotein, was successfully observed. The paper by T. Okamoto was selected as "Editor's Pick" from APS.

Electron spin resonance (ESR) imaging is usually carried out in the low frequency region below 1 GHz (*L* band), and there have been few examples of ESR imaging in higher frequency region. However, high-frequency ESR imaging has a lot of advantages such high spectral resolution, high sensitivity, and high spatial resolution. Theoretically, a spatial resolution better than 100 μm is expected in the high-frequency region, which is more than one order of magnitude better than the low-frequency ESR imaging.

In this study, we developed ESR imaging system working at the millimeter-wave frequencies. For this purpose, null detection technique was adopted to increase the spin sensitivity, in combination with a Fermi-level-managed barrier (FMB) diode and a Gunn diode oscillator. Film-type wire-grid polarizers were used in this study. A minimum detectable spin number of 10^{13} spins was achieved using a double modulation technique at room temperature. One-dimensional ESR imaging at 120 GHz was successfully demonstrated for DPPH radicals which were spatially separated by a distance of 0.5 mm. The estimated spatial resolution was 0.4 mm, which could be improved with higher gradient fields in the future. We also measured mixed powders of DPPH and TEMPOL radicals, and their ESR spectra were clearly resolved at 260 GHz due to slightly different g factors. As a result, simultaneous ESR imaging of two spin species was successfully demonstrated.

T. Okamoto and S. Okubo succeed to observe transient phenomena of metal protein by high-frequency ESR. This work was carried out with H. Horitani Saga University by the joint research program of Molecular Photoscience Research Center, Kobe University.

Precise Determination of Zero-Field Splitting Parameters of Hemin by High-Field and High-Frequency Electron Paramagnetic Resonance

Tsubasa Okamoto[1], Eiji Ohmichi[1], Susumu Okubo[2], and Hitoshi Ohta[2]

[1]Graduate School of Science, Kobe University

[2]Molecular Photoscience Research Center, Kobe University

(*J. Phys. Soc. Jpn. 2018*)

The zero-field splitting (ZFS) parameters of Fe(III) protoporphyrin IX chloride, or hemin, a model substance of hemoproteins, were determined precisely by high-field and high-frequency electron paramagnetic resonance (HFEPR). From multi-frequency measurements up to 700 GHz, multiple EPR absorptions were clearly resolved, and the rhombic component of ZFS was directly determined, for the first time, as $|E| = 0.055 \pm 0.005$ cm^{-1}, in addition to the axial component $D = 6.90 \pm 0.01$ cm^{-1}. This finding indicates the essential role of the rhombic symmetry of excited states in the ZFS parameters.

Pressure Effect on Zero-Field Splitting Parameter of Hemin: Model Case of Hemoproteins under Pressure

Tsubasa Okamoto[1], Eiji Ohmichi[1], Yu Saito[2], Takahiro Sakurai[2], and Hitoshi Ohta[3]

[1]Graduate School of Science, Kobe University

[2]Research Facility Center for Science and Technology, Kobe University

[3]Molecular Photoscience Research Center, Kobe University

(*J. Phys. Chem. B, 2018*)

We experimentally studied the pressure dependence of the zero-field splitting (ZFS) parameter of hemin (iron(III) protoporphyrin IX chloride), which is a model complex of hemoproteins, via high-frequency and high-field electron paramagnetic resonance (HFEPR) under pressure. Owing to the large ZFS, the pressure effect on the electronic structure of iron − porphyrin complexes has not yet been explored using EPR. Therefore, we systematically studied this effect using our newly developed sub-terahertz EPR spectroscopy system in the frequency range of 80−515 GHz, under magnetic fields up to 10 T and pressure up to 2 GPa. We observed a systematic shift of the resonance fields of hemin upon pressure application, from which the axial component of the ZFS parameter was found to increase from D = 6.9 to 7.9 cm−1 at 2 GPa. In contrast to the previous methods used to study proteins under pressure, which mainly focused on conformational changes, our HFEPR technique can obtain more microscopic insights into the electronic structures of metal ions under pressure. In this sense, our technique provides novel opportunities to study the pressure effects on biofunctional active centers of versatile metalloproteins.

Force detection of high-frequency electron paramagnetic resonance spectroscopy of microliter solution sample

Tsubasa Okamoto[1], Hideyuki Takahashi[2], Eiji Ohmichi[1], Haruto Ishikawa[3], Yasuhisa Mizutani[3], and Hitoshi Ohta[4]

[1]Graduate School of Science, Kobe University

[2]Organization for Advanced and Integrated Research, Kobe University
[3]Graduate School of Science, Osaka University
[4]Molecular Photoscience Research Center, Kobe University
(*Appl. Phys. Lett., 2018*)

Force detection of magnetic resonance is now able to attain extremely high spin sensitivity. In these setups, microcantilevers were usually used as a sensitive force sensor and, in most cases, have been applied to solid-state samples such as paramagnetic impurities in solids. On the other hand, there are now growing demands for their applications to liquid-state samples in the research areas of life science because many proteins and enzymes are biofunctionally active only in solutions, where they interact with the surrounding water molecules. In this letter, we present an electron paramagnetic resonance (EPR) technique for solution samples using a SiNx nanomembrane and report high-frequency EPR spectroscopy of a microliter-volume frozen solution sample of hemin and myoglobin at multiple frequencies up to 350 GHz. This technique would be particularly useful to obtain more detailed insight into the electronic structure of metalloproteins/metalloenzymes under biologically active conditions.

III-C. DEVELOPMENT AND APPLICATION OF HIGH-PRESSURE THz ESR SYSTEM

Recently, the importance of the multiextreme condition including pressure and magnetic field has been increasingly recognized in ESR measurements. We developed the high-pressure high-field ESR system in which the maximum pressure is 2.5 GPa and the maximum magnetic field is 10 T so far, and we succeeded in extending the field region up to 25 T in 2018 by using the world's highest field cryogen-free superconducting magnet installed at IMR, Tohoku University. This development was done in collaboration with Prof. Nojiri et al. in Tohoku University. We can now perform ESR measurement under the extreme condition with a maximum pressure of 2.5 GPa and a maximum magnetic field of 25 T. Moreover, this system was successfully applied to the quantum magnet Cs2CuCl4 in collaboration with Dr. Zvyagin from Dresden High Magnetic Field Laboratory in Germany. Cs2CuCl4 has the anisotropic triangular lattice and is a good candidate to investigate the expected rich phase for the change of the anisotropy and the magnetic field. The exchange interactions were determined precisely and it was found that the anisotropic interactions changed to more isotropic ones by applying the pressure up to about 2 GPa. Moreover, we found new phases under the high field and pressure.

T. Sakurai gave an invited presentation about the pressure induced phase transition on $SrCu_2(BO_3)2$ at the Fall Meeting of the Physical Society of Japan. H. Ohta gave invited presentations at APES-IES2018 (Sept. 23-27, Brisbane, Australia) and IW-FIRT2019 (March 5-7, Fukui, Japan), and at one seminar (GPI, Moscow, Russia) concerning the developments of high pressure THz ESR.

Spectroscopic and magnetic properties of Fe^{2+} ($3d^6$; S=2) ions in Fe $(NH_4)_2(SO_4)_2 \cdot 6H_2O$ – Modeling zero-field splitting and Zeeman electronic parameters by microscopic spin Hamiltonian approach

MagdalenaZając[1], Czesław Rudowicz[2,3], H. Ohta[4,5] and T. Sakurai[6]

[1]Institute of Physics, West Pomeranian University of Technology

[2]Faculty of Chemistry, A. Mickiewicz University

[3]Modeling in Spectroscopy Group, Institute of Physics, West Pomeranian University of Technology Szczecin

[4]Graduate School of Science, Kobe University

[5]Molecular Photoscience Research Center, Kobe University

[6]Center for Supports to Research and Education Activities, Kobe University

(*J. Magn. Magn. Mat., 2018*)

Utilizing the package MSH/VBA, based on the microscopic spin Hamiltonian (MSH) approach, spectroscopic and magnetic properties of Fe^{2+} ($3d^6$; S=2) ions at (nearly) orthorhombic sites in $Fe(NH_4)_2(SO_4)_2 \cdot 6H_2O$ (FASH) are modeled. The zero-field splitting (ZFS) parameters and the Zeeman electronic (Ze) factors are predicted for wide ranges of values of the microscopic parameters, i.e. the spin-orbit (λ), spin-spin (ρ) coupling constants, and the crystal-field (ligand-field) energy levels (Δi) within the ^5D multiplet. This enables to consider the dependence of the ZFS parameters bkq (in the Stevens notation), or the conventional ones (e.g., D and E), and the Zeeman factors gi on λ, ρ, and Δi. By matching the theoretical SH parameters and the experimental ones measured by electron magnetic resonance (EMR), the values of λ, ρ, and Δi best describing Fe^{2+} ions in FASH are determined. The novel aspect is prediction of the fourth-rank ZFS parameters and the ρ(spin-spin)-related contributions, not considered in previous studies. The higher-order contributions to the second- and fourth-rank ZFSPs are found significant. The MSH predictions provide guidance for high-magnetic field and high-frequency EMR (HMF-EMR) measurements and enable assessment of suitability of FASH for application as high-pressure probes for HMF-EMR studies. The method employed here and the present results may be also useful for other structurally related Fe^{2+} (S=2) systems.

Direct Observation of the Quantum Phase Transition of $SrCu_2(BO_3)_2$ by High-Pressure and Terahertz Electron Spin Resonance

T. Sakurai[1], Y. Hirao[2], K. Hijii[3], S. Okubo[3], H, Ohta[3], Y. Uwatoko[4], K. Kudo[5], Y. Koike[6]

[1]Research Facility Center for Science and Technology, Kobe University

[2]Graduate School of Science, Kobe University

[3]Molecular Photoscience Research Center, Kobe University

[4]Institute for Solid State Physics, University of Tokyo

[5]Research Institute for Interdisciplinary Science, Okayama University

[6]Department of Applied Physics, Tohoku University

(*J. Phys. Soc. Jpn., 2018*)

High-pressure and high-field electron spin resonance (ESR) measurements have been performed on a single crystal of the

orthogonal-dimer spin system $SrCu_2(BO_3)_2$. With frequencies below 1 THz, ESR signals associated with transitions from the singlet ground state to the one-triplet excited states and the two-triplet bound state were observed at pressures up to 2.1 GPa. We obtained directly the pressure dependence of the gap energies, finding a clear first-order phase transition at Pc = 1.85 ± 0.05 GPa. By comparing this pressure dependence with the calculated excitation energies obtained from an exact diagonalization, we determined the precise pressure dependence for inter- (*J'*) and intra-dimer (*J*) exchange interactions considering the Dzyaloshinski‐Moriya interaction. Thus this system undergoes a first-order quantum phase transition from the dimer singlet phase to a plaquette singlet phase above the ratio $(J'/J)c = 0.660 \pm 0.003$.

Development and application of 2.5 GPa–25 T high-pressure high-field electron spin resonance system using a cryogen-free superconducting magnet

T. Sakurai[1], S. Kimura[2], M. Kimata[2], H. Nojiri[2], S. Awaji[2], S. Okubo[3], H. Ohta[3], Y. Uwatoko[4], K. Kudo[5], Y. Koike[6]

[1]Research Facility Center for Science and Technology, Kobe University

[2]Institute for Materials Research, Tohoku University

[3]Molecular Photoscience Research Center, Kobe University

[4]Institute for Solid State Physics, University of Tokyo

[5]Research Institute for Interdisciplinary Science, Okayama University

[6]Department of Applied Physics, Tohoku University

(*J Magn Reson., 2018*)

We have developed a high-pressure electron spin resonance probe and successfully installed into the world's highest-field cryogen-free superconducting magnet having a maximum central field of 24.6 T. The high pressure of 2.5 GPa is achieved by the specially designed piston-cylinder pressure cell using THz-wave-transparent components. In the first application of this high-pressure high-field ESR system, we observed that the orthogonal dimer spin system $SrCu_2(BO_3)_2$ undergoes a quantum phase transition from the dimer singlet ground to the plaquette singlet ground states.

Pressure-tuning the quantum spin Hamiltonian of the triangular lattice antiferromagnet Cs_2CuCl_4

S. A. Zvyagin[1], D. Graf[2], T. Sakurai[3], S. Kimura[4], H. Nojiri[4], J. Wosnitza[1], H. Ohta[5], T. Ono[6], H. Tanaka[7]

[1]Dresden High Magnetic Field Laboratory, Helmholtz-Zentrum Dresden-Rossendorf

[2]National High Magnetic Field Laboratory, Florida State University

[3]Research Facility Center for Science and Technology, Kobe University

[4]Institute for Materials Research, Tohoku University

[5]Molecular Photoscience Research Center, Kobe University

[6]Department of Physical Science, Osaka Prefecture University

[7]Department of Physics, Tokyo Institute of Technology

(*Nature Communications, 2019*)

Quantum triangular-lattice antiferromagnets are important prototype systems to investigate numerous phenomena of the geometrical frustration in condensed matter. Apart from highly unusual magnetic properties, they possess a rich phase diagram (ranging from an unfrustrated square lattice to a quantum spin liquid), yet to be confirmed experimentally. One major obstacle in this area of research is the lack of materials with appropriate (ideally tuned) magnetic parameters. Using Cs_2CuCl_4 as a model system, we demonstrate an alternative approach, where, instead of the chemical composition, the spin Hamiltonian is altered by hydrostatic pressure. The approach combines high-pressure electron spin resonance and r.f. susceptibility measurements, allowing us not only to quasi-continuously tune the exchange parameters, but also to accurately monitor them. Our experiments indicate a substantial increase of the exchange coupling ratio from 0.3 to 0.42 at a pressure of 1.8 GPa, revealing a number of emergent field-induced phases.

III-D. DEVELOPMENT OF BROADBAND FORCE-DETECTED ESR TECHNIQUES USING MICRO-CANTILEVER AND NANOMEMBRANE

A new force-detected ESR technique in the terahertz region is developed for sensitive detection of small samples. In this setup, two types of nanomembranes were used to detect ESR-induced magnetization/torque changes of the sample in high magnetic fields. One is based on a piezoresistive membrane, which enabled compact setup, and easy detection. Indeed, multi-frequency and angle-dependent ESR measurements were successfully demonstrated for a tiny single crystal of Co Tutton salt. The other is ultrathin SiN_x membranes, which enabled highly sensitive detection and high signal-to-noise ratio. H. Takahashi modulated the sample temperature by slow modulation of electromagnetic waves and succeeded in mechanical EPR detection of magnetic samples with fast relaxation times for the first time.

H. Takahashi precisely measured the magnetic torque of FeSe superconductor in the superconducting state, and discussed the superconducting fluctuations of the system, in comparison with the previous reports.

H. Takahashi joined the JST-PRESTO's program "Thermal Science and Control of Spectral Energy Transport". He started the new project to investigate the heat transport in magnetic materials by high-frequency ESR spectroscopy.

E. Ohmichi gave an invited presentation on his broadband force-detected ESR system at 1st India-Japan NMR workshop (June 21, Yokohama, Japan). H. Takahashi gave an invited presentation on his developments of membrane type force-detected ESR system at the Spring Meeting of the Physical Society of Japan. H. Ohta gave a seminar (GPI, Moscow, Russia) concerning these developments.

Mechanically detected terahertz electron spin resonance using SOI-based thin piezoresistive microcantilevers

E. Ohmichi[1], T. Miki[1], H. Horie[1], T. Okamoto[1], H. Takahashi[2], Y. Higashi[3], S. Itoh[3], H. Ohta[4]

[1]Graduate School of Science, Kobe University

[2]Organization for Advanced and Integrated Research, Kobe University

[3]Graduate School of Science, Kyoto University

[4]Molecular Photoscience Research Center, Kobe University

(*J. Mag. Res., 2018*)

We developed piezoresistive microcantilevers for mechanically detected electron spin resonance (ESR) in the millimeter-wave region. In this article, fabrication process and device characterization of our self-sensing microcantilevers are presented. High-frequency ESR measurements of a microcrystal of paramagnetic sample is also demonstrated at multiple frequencies up to 160 GHz at liquid helium temperature. Our fabrication is based on relatively simplified processes with silicon-on-insulator (SOI) wafers and spin-on diffusion doping, thus enabling cost-effective and time-saving cantilever fabrication.

Force- and torque-detection of high-frequency electron spin resonance using a membrane-type surface-stress sensor

Hideyuki Takahashi[1], Kento Ishimura[2], Tsubasa Okamoto[2], Eiji Ohmichi[2], and Hitoshi Ohta[3]

[1]Organization for Advanced and Integrated Research, Kobe University

[2]Graduate School of Science, Kobe University

[3]Molecular Photoscience Research Center, Kobe University

(*Rev. Sci. Instrum., 2018*)

We developed a practical useful method for force- and torque-detected electron spin resonance (FDESR/TDESR) spectroscopy in the millimeter wave frequency region. This method uses a commercially available membrane-type surface-stress (MSS) sensor. The MSS is composed of a silicon membrane supported by four beams in which piezoresistive paths are integrated for detecting the deformation of the membrane. Although this device has a lower spin sensitivity than a microcantilever, it offers several distinct advantages, including mechanical strength, ease of use, and versatility. These advantages make this device suitable for practical applications that require FDESR/TDESR.

Force-detected high-frequency electron spin resonance spectroscopy using magnet- mounted nanomembrane: Robust detection of thermal magnetization modulation

Hideyuki Takahashi[1], Tsubasa Okamoto[2], Kento Ishimura[2], Shigeo Hara[3], Eiji Ohmichi[2], and Hitoshi Ohta[4]

[1]Organization for Advanced and Integrated

Research, Kobe University

[2]Graduate School of Science, Kobe University

[3]Research Facility Center for Science and Technology, Kobe University

[4]Molecular Photoscience Research Center, Kobe University

(*Rev. Sci. Instrum., 2018*)

In this study, we report a conceptually novel broadband high-frequency electron spin resonance (HFESR) spectroscopic technique. In contrast to the ordinary force-detected electron spin resonance (ESR) technique, which detects the magnetization change due to the saturation effect, this method measures the magnetization change due to the change of the sample temperature at resonance. To demonstrate its principle, we developed a silicon nitride nanomembrane-based force-detected ESR spectrometer, which can be stably operated even at high magnetic fields. Test measurements were performed for samples with different spin relaxation times. We succeeded in obtaining a seamless ESR spectrum in magnetic fields of 15 T and frequencies of 636 GHz without significant spectral distortion. A high spin sensitivity of 1012 spins/G s was obtained, which was independent of the spin relaxation time. These results show that this technique can be used as a practical method in research fields where the HFESR technique is applicable.

Superconducting fluctuations in FeSe investigated by precise torque magnetometry

Hideyuki Takahashi[1,2], Fuyuki Nabeshima[3], Ryo Ogawa[3], Eiji Ohmichi[4], Hitoshi Ohta[5], and Atsutaka Maeda[3]

[1]Organization for Advanced and Integrated Research, Kobe University

[2]Japan Science and Technology Agency, PRESTO

[3]Department of Basic Science, the University of Tokyo

[4]Graduate School of Science, Kobe University,

[5]Molecular Photoscience Research Center, Kobe University

(*Phys. Rev. B, 2019*)

We investigated the superconducting fluctuation in FeSe, which is assumed to be located in the BCS-BEC crossover region, via magnetic torque measurements. In our method, the absolute cantilever displacement is measured by detecting the interference intensity of the Fabry-Pérot cavity formed between the cantilever and optical fiber. Our findings are different from the results of previous torque magnetometry studies using a piezoresistive cantilever; the “giant” fluctuation diamagnetism related to the BCS-BEC crossover does not exist. Instead, a considerably smaller fluctuation signal originating from the vortex liquid was observed that showed qualitatively similar behavior to that in cuprate superconductors. We also discuss the inconsistency between our torque data and the existence of a pseudogap proposed by an NMR experiment.

III-E. MAGNETIZATION MEASUREMENTS USING SQUID MAGNETOMETER

The installation of SQUID magnetometer in 2010 by a Grant-in-Aid Creative Scientific Research "Development of properties and functionalities by precise control of rare-earth doping" (2007-2011, Prof. Y. Fujiwara (Osaka University)) opened up wide varieties of collaborative researches. From 2010 applications of SQUID magnetometer to various material researches spread out continuously. It is also supporting the user programs of Molecular Photoscience Research Center, Kobe University since 2017. Users of SQUID magnetometer are Mochida and Takahashi groups, Uchino group (Department of Chemistry, Kobe University), Sugawara and Matsuoka group (Department of Physics, Kobe University), T. Sakurai and S. Hara (Center for Supports to Research and Education Activities, Kobe University). It is also used for the development of SQUID ESR. T. Okamoto, T. Sakurai, E. Ohmichi and H. Ohta received the Excellent Paper Award from the Japan Society of Infrared Science and Technology on May, 2018 by the paper concerning the SQUID ESR of hemoproteins.

Possible Frustration Effects on a New Antiferromagnetic Compound $Ce_6Pd_{13}Zn_4$ with the Octahedral Ce Sublattices

E. Matsuoka[1], A. Oshima[1], H. Sugawara[1], T. Sakurai[2], H. Ohta[3]

[1]Department of Physics, Graduate School of Science, Kobe University

[2]Research Facility Center for Science and Technology, Kobe University

[3]Molecular Photoscience Research Center, Kobe University

(*J. Phys. Soc. Jpn., 2018*)

Magnetization, specific heat, and electrical resistivity measurements have been performed on polycrystalline samples of a new cubic compound, $Ce_6Pd_{13}Zn_4$. This compound exhibits metallic behavior and is classified as a Kondo-lattice system. The trivalent Ce ions are responsible for the antiferromagnetic transition at T_N = 3.3 K and the phase transition at T'_N = 1.3 K with the formation of superzone gaps. The increase in magnetic susceptibilities below T_N and the considerably large value of the specific heat divided by temperature (1.25 $J \cdot Ce\text{-}mol^{-1} \cdot K^{-2}$) imply the existence of non-ordered Ce magnetic moments due to the geometrical frustration on the octahedral Ce sublattice.

Paramagnetic ionic plastic crystals containing the octamethylferrocenium cation: counteranion dependence of phase transitions and crystal structures

T. Mochida[1], M. Ishida[1], T. Tominaga[1], K. Takahashi[1], T. Sakurai[2], H. Ohta[3,4]

[1]Department of Chemistry, Graduate School of Science, Kobe University

[2]Research Facility Center for Science and Technology, Kobe University

[3]Department of Physics, Graduate School of Science, Kobe University

[4]Molecular Photoscience Research Center, Kobe University

(*Phys. Chem. Chem Phys., 2018*)

In recent years, ionic plastic crystals have attracted much attention. Many metallocenium salts exhibit

plastic phases, but factors affecting their phase transitions are yet to be elucidated. To investigate these factors, we synthesized octamethylferrocenium salts with various counteranions $[Fe(C_5Me_4H)_2]X$ ([**1**]X; X^- = $B(CN)_4^-$, $C(CN)_3^-$, $N(CN)_2^-$, FSA (= $(SO_2F)_2N^-$), $FeCl_4^-$, $GaCl_4^-$ and CPFSA (= $CF_2(SO_2CF_2)_2N^-$)) and elucidated their crystal structures and phase behavior. Correlations between the crystal structures and phase sequences, and the shapes and volumes of the anions are discussed. Except for [**1**][CPFSA], these salts exhibit phase transitions to plastic phases at or above room temperature (T_C = 298–386 K), and the plastic phases exhibit either NaCl- or anti-NiAs-type structures. X-ray crystal structure analyses of these salts at 100 K revealed that they have structures in which cations and anions are alternately arranged, with the exception of [**1**][CPFSA]. [**1**][CPFSA] exhibits a structure in which anions and cations are separately stacked to form columns. [**1**][$N(CN)_2$] exhibits a polar crystal structure that undergoes a monotropic phase transition to a centrosymmetric structure. The magnetic susceptibilities of room-temperature plastic crystals [**1**][$GaCl_4$] and [**1**][$FeCl_4$] were investigated; the latter exhibits a small ferromagnetic interaction at low temperatures.

Contribution of Coulomb Interactions to a Two-Step Crystal Structure Phase Transformation Coupled with a Significant Change in Spin Crossover Behavior for a Series of Charged FeII Complexes from 2,6-Bis(2-methylthiazol-4-yl)pyridine

K. Takahashi[1], M. Okai[1], T. Mochida[1], T. Sakurai[2], H. Ohta[3], T. Yamamoto[4], Y. Einaga[4], Y. Shiota[5], K. Yoshizawa[5], H. Konaka[6], and A. Sasaki[6]

[1]Department of Chemistry, Graduate School of Science, Kobe University

[2]Research Facility Center for Science and Technology, Kobe University

[3]Molecular Photoscience Research Center, Kobe University

[4]Department of Chemistry, Faculty of Science and Technology, Keio University

[5]Institute for Materials Chemistry and Engineering, Kyushu University

[6]XRD Application & Software Development, Rigaku Corporation

(*Inorg. Chem., 2018*)

A series of $[Fe^{II}(L)_2](BF_4)_2$ compounds were structurally and physically characterized (L = 2,6-bis(2-methylthiazol-4-yl)pyridine). A crystal structure phase transformation from dihydrate compound 1 to anhydrous compound 3 through partially hydrated compounds 2 and 2' upon dehydration was found. Compounds 1 and 3 exhibited a gradual spin crossover (SCO) conversion, whereas compounds 2 and 2' demonstrated two-step and one-step abrupt SCO transitions, respectively. An X-ray single-crystal structural analysis revealed that one-dimensional and two-dimensional Fe cation networks linked by π stacking and sulfur-sulfur interactions were formed in 1 and 3, respectively. A thermodynamic analysis of the magnetic susceptibility for 1, 2', and 3 suggests that the enthalpy differences may govern SCO transition behaviors in the polymorphic compounds 2' and 3. A structural comparison between 1 and 3 indicates that the

SCO behavior variations and crystal structure transformation in the present $[Fe^{II}(L)_2](BF_4)_2$ compounds can be interpreted by the relationship between the lattice enthalpies mainly arising from Coulomb interactions between the Fe cations and BF_4 anions as in typical ionic crystals.

Paramagntic ionic liquids exhibiting thermochromism based on monomer–dimer equilibrium of cationic half-sandwich complexes

T. Inagaki[1], T. Mochida[1], M. Takahashi[1], T. Sakurai[2], H. Ohta[3,4]

[1]Department of Chemistry, Graduate School of Science, Kobe University

[2]Research Facility Center for Science and Technology, Kobe University

[3]Molecular Photoscience Research Center, Kobe University

[4]Department of Physics, Graduate School of Science, Kobe University

(*J. Mol. Liq., 2018*)

We synthesized paramagnetic organometallic ionic liquids $[Fe(C_5Me_4Bu)(SC_6H_4R)(CO)\{P(OEt)_3\}][Tf_2N]$ (R = CF_3 (1), H (2), OMe (3)), comprising a cationic half-metallocenium iron-thiolate complex and a bis(trifluoromethanesulfonyl)amide (Tf_2N) anion. These liquids exhibited thermochromism based on the monomer–dimer equilibrium of the cation.

Phase Transitions, Crystal Structures, and Magnetic Properties of Ferrocenium Ionic Plastic Crystals with CF_3BF_3 and Other Anions

H. Kimata[1], T. Sakurai[2], H. Ohta[3,4] and T. Mochida[1]

[1]Department of Chemistry, Graduate School of Science, Kobe University

[2]Research Facility Center for Science and Technology, Kobe University

[3]Department of Physics, Graduate School of Science, Kobe University

[4]Molecular Photoscience Research Center, Kobe University

(*ChemistrySelect, 2019*)

Salts of cationic sandwich complexes often exhibit an ionic plastic phase; however, only a few exhibit a plastic phase at room temperature. To explore the use of the CF_3BF_3 anion to lower the transition temperature to the plastic phase, we prepared salts of CF_3BF_3 with various ferrocene derivatives, $[D][CF_3BF_3]$(D=$FeCp^*_2$,$Fe(C_5Me_4H)_2$,$Fe(C_5H_4Me)_2$,$FeCp(C_5H_4Me)$,$FeCp_2$; $Cp^*=C_5Me_5$, $Cp=C_5H_5$). Although $[FeCp^*_2][CF_3BF_3]$ exhibited a plastic phase above 417 K, the other salts formed room-temperature ionic plastic crystals with a phase transition to the plastic phase in the range 266–291 K. The crystal structure and thermal properties of $[FeCp_2][OTf]$ were elucidated for comparison. In addition, decamethylferrocenium salts with other anions were synthesized and structurally characterized: $[FeCp^*_2][X]$ (X=$N(SO_2F)_2$ and $B(CN)_4$) exhibited a phase transition to the plastic phase above 400 K, whereas carborane-containing salts$[FeCp^*_2]_2[B_{12}F_{12}]$ and $[FeCp^*_2][Co(C_2B_9H_{11})_2]$ did not exhibit a plastic phase.

III-F. SPIN AND LATTICE DYNAMICS STUDIED BY PUMP-PROBE AND TERAHERTZ SPECTROSCOPIES

The terahertz region in the electromagnetic spectrum has attracted research attention in solid-state physics, because elementary excitations in solid-state materials such as phonons and magnons play important roles, and many of those dynamics appear in this energy region. The ultrafast spin dynamics and optical spin control in magnetic materials are attractive topics because of the potential applications in the developments of ultrafast spin control, spintronics, quantum computing, and optical control of correlated spin systems. We studied the spin and lattice dynamics in solid-state materials using optical pump-probe spectroscopy and terahertz time-domain spectroscopy (THz-TDS). The generation and detection of magnetization and birefringence using optical and electric pulses are very useful to observe the spin and lattice dynamics in ferromagnetic, antiferromagnetic, multiferroic, and magnetoelectric materials. The time-domain spectroscopy has a large potential for the ultrafast, broadband, and accurate observation of elementary excitation dynamics in the terahertz region.

Dynamics of the electric-field induced magnetization in antiferromagnetic chromium oxide observed by Faraday rotation

Ryo Hikita[1], Hiroki Taniguchi[1], Takahiro Shinkai[1] and Toshiro Kohmoto[1,2]

[1]Graduate School of Science, Kobe University

[2]Molecular Photoscience Research Center, Kobe University

(*J. Phys.: Conf. Ser., 2019*)

In recent years, various types of multiferroic materials, in which ferroelectric and magnetic orders coexist, have been found. Many of them are antiferromagnets which have spin structures of spiral type, and their giant magnetoelectric effect has been attracting attention. Antiferromagnetic chromium oxide (Cr_2O_3, Néel temperature T_N = 307 K) is not multiferroic, but is known to show the linear magnetoelectric effect, in which the electric polarization is induced in proportion to the applied magnetic field and the magnetization is induced in proportion to the applied electric field.

The electric-field induced magnetization has been observed as the response to the applied alternating electric field. The electromotive force in a pickup coil or Faraday rotation of a probe light was detected as the magnetization signal, where the alternating frequency of 10^3-10^6 Hz was used. However, the dynamics of electric-field induced magnetization in the time regions shorter than microseconds has not been reported so far.

We observed the dynamics of the electric-field induced magnetization in an antiferromagnet Cr_2O_3 by the Faraday-rotation measurement using a continuous-wave probe light in the millisecond and a pulse probe light in the nanosecond region. In the millisecond region, it was found that the Faraday-rotation amplitude linearly depends on the electric field. This result suggests the linear magnetoelectric effect. In the nanosecond region, the Faraday-rotation amplitude linearly depends on the electric field, decreases with increasing temperature, and disappears above T_N. In our experiment, the response time of the

electric-field induced magnetization to the electric field could not be determined, but it was found that the response time is faster than 5 ns.

Electric-field induced magnetization in YIG observed by Faraday rotation

Keisuke Fujimoto[1], Takashi Hasunuma[1], and Toshiro Kohmoto[1,2]

[1]Graduate School of Science, Kobe University

[2]Molecular Photoscience Research Center, Kobe University

(*J. Phys.: Conf. Ser., 2019*)

Yttrium iron garnet (YIG, $Y_3Fe_5O_{12}$) is a ferrimagnetic material with a Curie temperature of 560 K and is known to show a large Faraday effect. YIG is also known to show the magnetoelectric (ME) effect. The second-order ME effect (magnetic-field induced electric polarization) at room temperature and the first-order ME effect (electric-field induced magnetization) below 125 K have been reported. Recently, the magnetocapacitance effect and the magnetic-field induced electric polarization in YIG were investigated in detail.

We observed the electric-field dependence and the magnetic-field dependence of the electric-filed induced magnetization in YIG by Faraday rotation. The Faraday-rotation amplitude can be given by a sum of two components linear and quadratic in the electric field, and we evaluated the coefficients for the two components from the two measurements independently. It was found that the linear and quadratic components coexist below 250 K in the electric-field induced magnetization in YIG. The linear component is dominant below 150 K, the ratio of the linear component to the quadratic one decreases around 180 K, and the sign of its coefficient is inverted above 180 K.

Ultrafast Magnon Dynamics in Antiferromagnetic Nickel Oxide Observed by Optical Pump-Probe and Terahertz Time-Domain Spectroscopies

Toshiro Kohmoto[1,2] and Takeshi Moriyasu[3]

[1]Graduate School of Science, Kobe University

[2]Molecular Photoscience Research Center, Kobe University

[3]University of Fukui

(*IRMMW-THz 2018*)

We have investigated the magnons in an antiferromagnetic 3d transition metal monoxide NiO, whose Néel temperature T_N is 523 K, using the pump-probe spectroscopy and terahertz time-domain spectroscopy (THz-TDS).

The magnon frequencies, which are the magnon precession frequencies, were observed at 1.3, 1.1, 0.5, and 0.1 THz at low temperatures. Magnon modes of 1.3, 1.1, and 0.1 THz were observed in the optical pump-probe spectroscopy experiment, while magnon modes of 1.1 and 0.5 THz were observed in the THz-TDS experiment. Note that the magnon mode of 1.1 THz was observed in both experiments. Both Raman- and IR-active modes are included in the NiO magnon modes. This is in contrast to MnO, for which the magnon signal was not observed in the optical

pump-probe spectroscopy experiment, but was observed in the THz-TDS experiment; thus the Raman activity of the magnon mode in MnO is low.

The magnon relaxation rate observed using THz-TDS was found to be almost constant up to T_N and to increase abruptly near that temperature. Temperature-independent spin-spin relaxation is thought to dominate below T_N.

Using optical pump-probe spectroscopy and THz-TDS, we can observe the softening of the magnon frequency near T_N more clearly than in other experiments involving techniques such as infrared and Raman spectroscopy. These results show that optical pump-probe spectroscopy and THz-TDS have high frequency resolution and a high S/N ratio in the THz region.

To explain the temperature dependence of the magnon frequency, we attempted to fit the observed magnon frequency using three different molecular field theories: the classical molecular field, the square root of the classical molecular field, and the molecular field including the biquadratic exchange. The observed temperature dependence of the magnon frequencies suggest that the biquadratic contribution of the exchange interaction is important and that the sublattice magnetization does not follow the Brillouin function in the cubic antiferromagnetic oxides.

We showed that complementary studies using optical pump-probe spectroscopy and THz-TDS are very useful for investigating the details of the magnon energy states in magnetic materials.

Original Papers 発表論文

authors	title	journal	Vol.	page	year
F. Ema, M. Tanabe, S. Saito, T. Yoneda, K. Sugisaki, T. Tachikawa, S. Akimoto, S. Yamauchi, K. Sato, A. Osuka, T. Takui, Y. Kobori	Charge-Transfer Character Drives Möbius Antiaromaticity in the Excited Triplet State of Twisted [28]Hexaphyrin	*J. Phys. Chem. Lett.*	**9**	2685-2690	2018 May 9
H. Sakai, R. Inaya, H. Nagashima, S. Nakamura, Y. Kobori, N. V. Tkachenko, T. Hasobe	Multiexciton Dynamics Depending on Intramolecular Orientations in Pentacene Dimers: Recombination and Dissociation of Correlated Triplet Pairs	*J. Phys. Chem. Lett.*	**9**	3354-3360	2018 May 31
H. Nagashima, S. Kawaoka, Y. Matsui, T. Tachikawa, H. Ikeda, Y. Kobori	Time-Resolved EPR Study on Singlet-Fission Induced Quintet Generation and Subsequent Triplet Dissociation in TIPS-Phenyl-Tetracene Aggregates	*J. Photopolym. Sci. Technol.*	**31**	163-167	2018 June25
R. Matsubara, T. Yabuta, U. M. Idros, M. Hayashi, F. Ema, Y. Kobori, K. Sakata, K.	UVA- and Visible-Light-Mediated Generation of Carbon Radicals from Organochlorides Using Nonmetal Photocatalyst	*J. Org. Chem.*	**83**	9381-9390	2018 July 13
H. Nagashima, S. Kawaoka, S. Akimoto, T. Tachikawa, Y. Matsui, H. Ikeda, Y. Kobori	Singlet-Fission-Born Quintet State: Sublevel Selections and Trapping by Multiexciton Thermodynamics	*J. Phys. Chem. Lett.*	**9**	5855-5861	2018 September 18
I. Karimata, K. Ohta, Y. Kobori, T. Tachikawa	The Development of Functional Mesocrystals for Energy Harvesting, Storage, and Conversion	*ACS Appl. Mater. Inter.*	**10**	37057-37066	2018 October 2
D. Lubert-Perquel, E. Salvadori, M. Dyson, P. N. Stavrinou, R. Montis, H. Nagashima, Y. Kobori, S. Heutz, C. W. M. Kay	Identifying triplet pathways in dilute pentacene films	*Nat. Commun.*	**9**	4222	2018 October 11
S. Nakamura, H. Sakai, H. Nagashima, Y. Kobori, N. V. Tkachenko, T. Hasobe	Quantitative Sequential Photoenergy Conversion Process from Singlet Fission to Intermolecular Two-Electron Transfers Utilizing Tetracene Dimer	*ACS Energy Lett.*	**4**	26-31	2019 January 11
Y. Kimura, I. Karimata, Y. Kobori, and T. Tachikawa	Mechanistic Insights into Photochemical Reactions on $CH_3NH_3PbBr_3$ Perovskite Nanoparticles from Single-Particle Photoluminescence Spectroscopy	*ChemNanoMat*	**5**	340 –345	2019 March 5
Izuru Karimata, Kaoru Ohta, Yasuhiro Kobori, and Takashi Tachikawa	Several Orders of Magnitude Difference in Charge-Transfer Kinetics Induced by Localized Trapped Charges on Mixed-Halide Perovskites	*ACS Appl. Mater. Interfaces*	**10**	37057-37066	2018.10.2
Yuki Kimura, Izuru Karimata, Yasuhiro Kobori, and Takashi Tachikawa	Mechanistic Insights into Photochemical Reactions on $CH_3NH_3PbBr_3$ Perovskite Nanoparticles from Single-Particle Photoluminescence Spectroscopy	*ChemNanoMat*	**5**	340-345	2019.1.11
Sayaka Uchida, Tomoki Okunaga, Yuki Harada, Shotaro Magira, Yasuto Noda, Takashi Mizuno, and Takashi Tachikawa	Rapid Formation of Small Mixed-Valence Luminescent Silver Clusters via Cation-Coupled Electron-Transfer in Redox-Active Porous Ionic Crystal Based on Dodecamolybdophosphate	*Nanoscale*		in press	
Sayaka Nagai, Maho Yamashita, Takashi Tachikawa, Takashi	Efficient and versatile mechanochromic luminescence of phenanthroimidazolylbenzothiadiazoles:	*J. Mater. Chem. C*	**50**	in press	

Ubukata, Masatoshi Asami, and Suguru Ito	tricolor switching and directional control over the chromism				
Fumita Nishimura, Hiromichi Hoshina, Yukihiro Ozaki and Harumi Sato	Isothermal crystallization of poly(glycolic acid) studied by terahertz and infrared spectroscopy and SAXS/WAXD simultaneous measurements	*Polymer J.*	**51**	237-245	2018.11.16
M. Kozanecki, C. Rudowicz, H. Ohta, T. Sakurai	Spectroscopic and magnetic properties of Fe^{2+} ($3d^6$; S = 2) ions in Fe $(NH_4)_2(SO_4)_26H_2O$ – Modeling zero-field splitting and Zeeman electronic parameters by microscopic spin Hamiltonian approach	*J. Magn. Magn. Mat*	**449**	94–104	2018.3
T. Okamoto, E. Ohmichi, S. Okubo, and H. Ohta	Precise Determination of Zero-Field Splitting Parameters of Hemin by High-Field and High-Frequency Electron Paramagnetic Resonance	*J. Phys. Soc. Jpn.*	**87**	013702/1-4	2018.1
E. Matsuoka, A. Oshima, H. Sugawara, T. Sakurai, H. Ohta	Possible Frustration Effects on a New Antiferromagnetic Compound $Ce_6Pd_{13}Zn_4$ with the Octahedral Ce Sublattices	*J. Phys. Soc. Jpn.*	**87**	013705/1-4	2018.1
E. Ohmichi, T. Miki, H. Horie, T. Okamoto, H. Takahashi, Y. Higashi, S. Itoh, H. Ohta	Mechanically detected terahertz electron spin resonance using SOI-based thin piezoresistive microcantilevers	*J. Mag. Res.*	**287**	41-46	2018.2
T. Mochida, M.Ishida, T. Tominaga, K. Takahashi, T. Sakurai and H. Ohta	Paramagnetic ionic plastic crystals containing the octamethylferrocenium cation: counteranion dependence of phase transitions and crystal structures	*J. Phys. Chem. Chem Phys.*	**20**	3019-3028	2018.2
T. Sakurai, Y. Hirao, K. Hijii, S. Okubo, H. Ohta, Y. Uwatoko, K. Kudo, Y. Koike	Direct Observation of the Quantum Phase Transition of $SrCu_2(BO_3)_2$ by High-Pressure and Terahertz Electron Spin Resonance	*J. Phys. Soc. Jpn.*	**87**	033701/1-4	2018.3
K. Takahashi, M. Okai, T. Mochida, T. Sakurai, H. Ohta, T. Yamamoto, Y. Einaga, Y. Shiota, K. Yoshizawa, H. Konaka, and A. Sasaki	Contribution of Coulomb Interactions to a Two-Step Crystal Structure Phase Transformation Coupled with a Significant Change in Spin Crossover Behavior for a Series of Charged FeII Complexes from 2,6-Bis(2-methylthiazol-4-yl)pyridine	*Inorg. Chem.*	**57**	1277-1287	2018.1
H. Takahashi, K. Ishimura, T. Okamoto, E. Ohmichi, H. Ohta	Force- and torque-detection of high-frequency electron spin resonance using a membrane-type surface-stress sensor	*Rev. Sci. Instrum*	**89**	036108/1-3	2018.3
H. Takahashi, T. Okamoto, K. Ishimura, S. Hara, E. Ohmichi, and H. Ohta	Force-detected high-frequency electron spin resonance spectroscopy using magnet- mounted nanomembrane: Robust detection of thermal magnetization modulation	*Rev. Sci. Instrum*	**89**	083905/1-8	2018.7
T. Sakurai, S. Kimura, M. Kimata, H. Nojiri, S. Awaji, S. Okubo, H. Ohta, Y. Uwatoko, K. Kudo, Y. Koike	Development and application of 2.5 GPa–25 T high-pressure high-field electron spin resonance system using a cryogen-free superconducting magnet	*J. Mag. Res.*	**296**	1-4	2018.11
T. Okamoto, E. Ohmichi, Y. Saito, T. Sakurai, and H. Ohta	Pressure Effect on Zero-Field Splitting Parameter of Hemin: Model Case of Hemoproteins under Pressure	*J. Phys. Chem. B*	**122**	6880-6887	2018.6

T. Okamoto, H. Takahashi, E. Ohmichi, H. Ishikawa, Y. Mizutani, and H. Ohta	Force detection of high-frequency electron paramagnetic resonance spectroscopy of microliter solution sample	*Appl. Phys. Lett.*	**113**	223702/1-4	2018.11
T. Inagaki, T. Mochida, K. Takahashi, T. Sakurai, H. Ohta	Paramagntic ionic liquids exhibiting thermochromism based on monomer–dimer equilibrium of cationic half-sandwich complexes	*J. Mol. Liq.*	**269**	882-885	2018.8
H. Kimata, T. Sakurai, H. Ohta and T. Mochida	Phase Transitions, Crystal Structures, and Magnetic Properties of Ferrocenium Ionic Plastic Crystals with CF_3BF_3 and Other Anions	*ChemistrySelect*	**4**	1-7	2019.1
H. Takahashi, F. Nabeshima, R. Ogawa, E. Ohmichi, H. Ohta, and A. Maeda	Superconducting fluctuations in FeSe investigated by precise torque magnetometry	*Phys. Rev. B*	**99**	060503(R)/1-5	2019.2
S. A. Zvyagin, D. Graf, T. Sakurai, S. Kimura, H. Nojiri, J. Wosnitza, H. Ohta, T. Ono, H. Tanaka	Pressure-tuning the quantum spin Hamiltonian of the triangular lattice antiferromagnet Cs_2CuCl_4	*Nature Communications*	10	1064/1-5	2019.3
R. Hikita, H. Taniguchi, T. Shinkai, and T. Kohmoto	Dynamics of the electric-field induced magnetization in antiferromagnetic chromium oxide observed by Faraday rotation	*J. Phys.: Conf. Ser.*		in press	2019
K. Fujimoto, T. Hasunuma, and T. Kohmoto	Electric-field induced magnetization in YIG observed by Faraday rotation	*J. Phys.: Conf. Ser.*		in press	2019

Invited Talks (domestic and international) 招待講演(国内および国際研究集会)

発表者氏名	開催時期	開催地	plenary or invite	学会名	講演題目
小堀康博 Y. Kobori	2018.06.25-28	幕張メッセ	invite	The 35th International Conference of Photopolymer Science and Technology Materials & Processes for Advanced Microlithography, Nanotechnology and Phototechnology	Time-Resolved EPR Study on Singlet Fission and Subsequent Triplet Dissociation Dynamics
	2018.5.13 –5.17	Seatle, USA	invite	233rd ECS Meeting	Time Resolved EPR Study on Photoinduced Charge-Transfer Trap States in Thiophene-Thiazolothiazole Copolymers Films
	2018.9.10 – 15,	Novosibirsk, Russia	invite	Spin Physics, Spin Chemistry, Spin Technology (SPCT2018)	Singlet-Fission-Born Quintet State: Sublevel Selections and Trapping by Multiexciton Thermodynamics
	2018.11.24	群馬大学・桐生キャンパス	invite	4th Kanto Area Spin Chemistry Meeting (4th KASC)	Geometry and motion of seconddary charge-separated states in Cryptochrome
	2019.3.26-27	静岡大学・静岡キャンパス	invite	第 19 回分子分光研究会	時間分解電子スピン共鳴法を用いた光エネルギー変換初期過程の観測
	2019.3.28	大阪市立大学･杉本キャンパス	invite	The 6th OCU International Workshop on Quantum Chemistry/Quantum Chemical Calculations on Quantum Computers: Quantum Algorithms	Three-Dimension Visualizations of Electron Spin Polarization for Elucidating Photo-Energy Conversion Mechanisms
	2018.9.15-17	岡山大学・津島キャンパス	invite	第 56 回日本生物物理学会年会	Electron Spin Polarization Imaging Analyses of Primary Charge Separations in Photosynthesis
立川貴士 T. Tachikawa	2018.9.20	横浜	invite	横浜国立大学講演会	光機能性材料の単一分子・単一粒子発光観測
	2018.10.5	大阪	invite	IEEE EPS イブニングミーティング	メソ結晶光触媒の開発と単一分子・単一粒子研究
	2018.10.31	神戸	invite	Indo-Japan mini-workshop Frontiers in Molecular Spectroscopy: From	Single-molecule, single-particle study toward development of efficient photocatalysts
	2018.11.30	神戸	invite	日本分光学会 関西支部 平成 30 年度 第 2 回講演会	光エネルギー変換プロセスの単一分子・単一粒子発光観測
	2018.12.8	Taipei, Taiwan	invite	2018 Taiwan-Japan Bilateral Symposium on Green Energy	Development of Hierarchical Superstructures for Efficient Photocatalysis
	2019.3.5	東京	invite	JST 新技術説明会	金属酸化物メソ結晶の開発と応用
富永圭介 K. Tominaga	2018.6.6-9	Palawan, Philippines	plenary	36th Samahang Pisikang Pilipinas (Physics Conference and Annual	Terahertz Molecular Science in Condensed Phases

				Meeting)	
	2018.6.25-29	Seoul, Korea	invite	9th International Conference on Coherent Multidimensional Spectroscopy	Vibrational frequency fluctuations of solute in aqueous solutions: Effects of hydrophobic and hydrophilic groups
	2018.9.18-21	Los Banos, Philippines	invite	Symposium on Advanced Spectroscopic Techniques	Terahertz Spectroscopy of Condensed Matter
	2018.9.18-21	Los Banos, Philippines	invite	Symposium on Advanced Spectroscopic Techniques	Ultrafast Spectroscopy Workshop I, II
	2018.11.4-8	名古屋	invite	Joint Conference of EMLG/JMLG Meeting 2018 and 41st Symposium on Solution Chemistry of Japan	Dynamics of water, aqueous solutions, and proteins studied by nonlinear IR spectroscopy and broadband dielectric spectroscopy
	2018.12.19-20	Bangalore, India	invite	Indo-Japan Meeting	Dynamics of water, aqueous solutions, and proteins studied by nonlinear IR Spectroscopy and broadband dielectric spectroscopy
	2018.12.22	Kanpur, India	invite	One-Day Symposium on Spectroscopic and computational studies of complex chemical systems at different time and length scales	Dynamics of water, aqueous solutions, and proteins studied by nonlinear IR Spectroscopy and broadband dielectric spectroscopy
	2019.1.4-6	Hefei, China	invite	International Symposium of Nonlinear Optical Spectroscopy	Hydrogen-bond Dynamics of 9-Fluorenone Derivatives in Water Probed by 2D-IR Spectroscopy
	2019.3.5-7	福井	invite	The 7th International Workshop on Far-Infrared Technologies	Broadband Dielectric Spectroscopy on Proteins and Lipid Bilayers from sub-GHz to THz region
太田薫 K. Ohta	2018.10.30-11.2	神戸	invite	Indo-Japan mini-workshop Frontiers in Molecular Spectroscopy: From Fundamentals to Applications in Chemistry and Biology	Charge Carrier Dynamics in Diketopyrrolopyrrole-Linked Tetrabenzoporphyrin Based Bulk Heterojunction Thin Films Probed by Time-Resolved Terahertz Spectroscopy
	2019.3.7	福井	invite	平成 30 年度福井大学遠赤外領域開発研究センター共同研究成果報告会	時間領域サブテラヘルツ分光装置の開発とその分子科学への応用
佐藤春実 H. Sato (人間発達環境学研究科)	2019.1.12-14	東海大学高輪キャンパス	invite	レーザー学会　第 39 回年次大会	テラヘルツ光源による高分子モルフォロジー観察
	2018.12.15	京都工芸繊維大学松ヶ崎キャンパス	invite	IEEE MTT-S Kansai Chapter テクニカルワークショップ	テラヘルツ分光の高分子材料への応用
	2018.11.30	神戸大学	invite	日本分光学会関西支部 第 2 回講演会・見学会	テラヘルツ分光を利用した高分子材料の高次構造と物性評価

	2018.11.13-15	科学技術館	invite	テラヘルツ波オープンセミナー	テラヘルツ分光による有機・生体分子の計測応用
	2018.12.15	Kobe University	invite	Indo-Japan mini-workshop Frontiers in Molecular Spectroscopy:	Terahertz Spectroscopy on Polymers : Intermolecular Interaction and Higher-Order Structure
	2018.10.6	Harris Hotel Semarang, Indonesia,	invite	International Conference on Education and Social Science Research	Structure and Physical Properties of Polymers Studied by Spectroscopy
	2018.8.26-31	Jeju Island, Korea	invite	the 26th International Conference on Raman Spectroscopy (ICORS 2018)	Stress-induced crystal transition of poly(butylenesuccinate) studied by terahertz and low-frequency Raman spectroscopy
太田仁 H. Ohta	2018.5.11-13	八王子	invite	第 14 回 ESR 入門セミナー	超入門
	2018.5.11-13	八王子	invite	第 14 回 ESR 入門セミナー	スペクトル解析 I(固体)
	2018.5.17-19	Santa Barbara, USA	invite	BigMag@UCSB	Exotic magnetic orders at very high magnetic fields
	2018.8.8-10	大阪	invite	第 16 回 ESR 夏の学校	電子スピン共鳴(ESR)序論
	2018.9.23-27	Brisbane, Australia	invite	The Third Joint Conference of the Asia-Pacific EPR/ESR Society and The International EPR (ESR) Society (IES)	Multi-extreme THz ESR -the development of high pressure ESR
	2018.10.8	Moscow, Russia	invite	セミナー	Recent Developmets of multi-extreme THz ESR -the mechanically detected ESR and the high pressure ESR-
	2019.3.5-7	福井	invite	The 7th International Workshop on Far-Infrared Technologies (IW-FIRT 2019)	Multi-Extreme THz ESR -Recent Developments and Future-
大久保晋 S. Okubo	2018.9.24-28	Kazan, Russia	invite (基調講演)	MODERN DEVELOPMENT OF MAGNETIC RESONANCE 2018 (MDMR2018)	Developmet and Application of THz ESR in Kobe University
齋藤佑 Y. Saito (2018.4~9 研究基盤センター) (2018.10~2019.3 分子フォト)	2018.7.20	京都	invite	第二回電子スピンサイエンス若手研究会	活性酸素の分析と応用について
大道英二 E. Ohmichi (理学研	2018.5.18	大阪	invite	第四回強磁場実験入門セミナー	強磁場中計測技術入門

究科）	2018.6.21	横浜	invite	1st India-Japan NMR workshop	Mechanically Detected Terahertz Electron Paramagnetic Resonance
高橋英幸（先端融合研究環）	2019.3.14-17	福岡	invite	日本物理学会　第 74 回年次大会	メンブレン型メカニカルデバイスを用いた高感度磁気測定および電子スピン共鳴測定
櫻井敬博（研究基盤センター）	2018.9.9-12	京田辺	invite	日本物理学会　2018 年秋季大会	直交ダイマー系 $SrCu_2(BO_3)_2$ の圧力下 THz ESR による量子相転移の観測

Presentation at conferences (international and domestic) 一般講演

発表者氏名	開催時期	開催地	plenary or invite	学会名	講演題目
笠原俊二 S. Kasahara	2018.6	東広島	poster	34th Symposium on Chemical Kinetics and Dynamics	High-Resolution Laser Spectroscopy of $S_1 \leftarrow S_0$ transition of Fluorene and Carbazole
	2018.9	Bilbao (Spain)	poster	25th International Conference on High Resolution Molecular Spectroscopy	High-Resolution Laser Spectroscopy of Nitrogen Dioxide in the region of 14500-16800 cm^{-1}
	2018.9	福岡	oral	第 12 回分子科学討論会	NO_2 ラジカルの電子状態における超微細分裂
	2019.3	神戸	oral	第 99 回日本化学会春季年会	Rotationally-resolved High-resolution Laser Spectroscopy of S_1-S_0 Transition of Fluorene: Perturbation in the S_1 State
	2019.3	静岡	oral	第 19 回分子分光研究会	NO_2 ラジカルの A-X 遷移の高分解能レーザー分光
小堀康博 Y. Kobori	2019.12.16-12.20	Taipei, Taiwan	Oral	10th Asian Photochemistry Conference (APC2018)	Singlet-Fission-Born Quintet State: Sublevel Selections and Trapping by Entropy Enhancement in Disordered Aggregates
	2018.11.1-11.3	北海道大学	Oral	第 57 回電子スピンサイエンス学会年会（SEST2018）	分子内シングレットフィッションによる五重項励起子生成機構
立川貴士 T. Tachikawa	2018.7.9	University College Dublin (Ireland)	oral	27th IUPAC International Symposium on Photochemistry	Correlated dynamics of photogenerated charges and ions in organolead mixed-halide perovskites
	2018.9.6	関西学院大学・上ケ原キャンパス	oral	2018 年光化学討論会	混合ハロゲン化物ペロブスカイトにおける電荷キャリアダイナミクス
	2018.12.17	Howard Civil Service Internationl House (Taipei)	oral	10th Asian Photochemistry Conference (APC2018)	Development of Hierarchical Mesocrystals for Efficient Photocatalysis
富永圭介 K. Tominaga	2018.8.26-31	Brussels, Belgium	oral	10th Conference on Broadband Dielectric Spectroscopy and its Applications	Broadband Dielectric Spectroscopy on Proteins and Lipid Bilayers from sub-GHz to THz region
	2018.8.26-31	Brussels, Belgium	poster	10th Conference on Broadband Dielectric Spectroscopy and its Applications	Charge carrier localization in doped polyaniline composite with polyacrylic acid and bentonite
	2018.9.9-14	名古屋	poster	43rd International Conference on Infrared, Millimeter and Terahertz Waves	THz Dynamics of Hydrated Phospholipid Studied by Broadband Dielectric Spectroscopy
	2018.9.9-14	名古屋	poster	43rd International Conference on Infrared, Millimeter and Terahertz Waves	Temperature Dependence of THz Conductivities of Polyaniline Emeraldine Salt/Bentonite Pellets
太田薫 K. Ohta	2018.9.9-14	名古屋	oral	43rd International Conference on Infrared, Millimeter and Terahertz Waves	Ultrafast Charge Carrier Dynamics in Diketopyrrolopyrrole-Linked Tetrabenzoporphyrin Films Studied by Time-Resolved Terahertz Spectroscopy

	2018.9.10-13	博多	oral	第 12 回分子科学討論会	散乱体透過後の超短パルス光の伝播特性と波面制御
佐藤春実 H. Sato	2018.9.12-14	千葉	poster	第 67 回高分子討論会	テラヘルツ分光法による高分子の分子間相互作用の観測と物性評価への応用
	2017.9.18	Kiel, Germany	oral	Kobe-Kiel bilateral workshop	Terahertz spectroscopy and its applications in polymers
	2018.6.30-7.13	関西学院会館	poster	International Conference on Advancing Molecular Spectroscopy(ICAMS)	Three different kinds of weak C-H…O=C inter- and intramolecular interactions in poly(ε-caprolactone) studied by terahertz spectroscopy, infrared spectroscopy and quantum chemical calculations
太田仁 H. Ohta	2018.7.1-5	Nantes, France	poster	EUROMAR 2018	Multi-extreme THz ESR -the high-sensitive membrane ESR and the high pressure ESR
	2018.7.15-20	San Francisco, USA	oral	21st International Conference on Magnetism (ICM2018)	Direct Observation of the Pressure Induced Phase Transition in Shastry-Sutherland Model Substance $SrCu_2(BO_3)_2$ by High Pressure THz ESR
	2018.7.22-27	Utah, USA	oral	59th Annual Rocky Mountain Conference on Magnetic Resonance	Multi-Extreme THz ESR: Development of Mechanically Detected ESR up to the THz Region
	2018.9.6	神戸	poster	第五回西日本強磁場科学研究会	神戸大学における多重極限 THz ESR
	2018.9.9-14	名古屋	poster	IRMMW-THz 2018 (43rd International conference on Infrared, Millimeter and Terahertz Waves)	Recent Developments And Applications Of Multi-Extreme THz ESR
	2018.11.1-3	札幌	oral	第 57 回電子スピンサイエンス学会年会	多重極限 THz ESR の開発と展望
	2018.11.26-28	仙台	poster	強磁場コラボラトリにおける物性研究の現状と展望	神戸大学における多重極限強磁場 THz ESR
	2019.1.9-10	東海村	oral	第 13 回量子スピン系研究会	多重極限 THz ESR による量子スピン系の研究
大久保晋 S. Okubo	2018.9.6	神戸	poster	第五回西日本強磁場科学研究会	2次元正方格子磁性体 $Sr_2MnO_2Cl_2$ の強磁場 ESR 測定 II
	2018.9.9-12	京田辺	oral	日本物理学会　2018 年秋季大会	S=1/2 歪んだダイアモンド鎖化合物 $(Cu_3(OH)_2(CH_3O_2)_2(H_2O)_xX_y$
	2018.11.1-3	札幌	oral	第 57 回電子スピンサイエンス学会年会	S=1/2 歪んだダイアモンド鎖化合物 $(Cu_3(OH)_2(CH_3CO_2)_2(H_2O)_xX_y)$の ESR 測定 II
	2018.11.26-28	仙台	poster	強磁場コラボラトリにおける物性研究の現状と展望	ヌル検出法によるテラヘルツ電子スピン共鳴測定
	2018.12.27-28	東京	poster	東京大学物性研究所　短期研究会 「量子多体効果が生み出す液晶的電子状態」	S=1/2　量子スピン鎖 $NaCuMoO_4(OH)$の飽和磁場近傍の ESR 測定

	2019.1.9-10	東海村	oral	第 13 回量子スピン系研究会	S=1/2 歪んだダイヤモンド鎖化合物の基底状態の ESR による研究
	2019.3.14-17	福岡	oral	日本物理学会　第 74 回年次大会（2019 年）	幾何学的スピン構造を持つ反強磁性体の強磁場 ESR による研究 III
齋藤佑 (2018.4~9 研究基盤センター) (2018.10~2019.3 分子フォト)	2018.9.6	神戸	poster	第五回西日本強磁場科学研究会	*S*=1/2 歪んだダイアモンド鎖を有する銅水酸化物 $Cu_3(OH)_2(OAc)_2(H_2O)_x(2,6\text{-NpSA})_y$ (2,6-NpSA;2,6-Naphtalehesulfonic Acid)の強磁場 ESR
	2018.9.23-27	Brisbane, Australia	poster	The Third Joint Conference of the Asia-Pacific EPR/ESR Society and The International EPR (ESR) Society (IES)	Antioxidant Capacity Evaluation of Carotenoid Compounds against Singlet Oxygen via ESR spectroscopy under in vitr Condition
	2018.11.3	札幌	oral	第 57 回電子スピンサイエンス学会年会（SEST2018)	高スピン金属イオン型ヘキサアクア錯塩の高磁場 ESR 研究：高圧 ESR の圧力標準物質としてのタットン塩の評価
大道英二 (理学研究科)	2018.9.9-14	名古屋	poster	IRMMW-THz 2018 (43rd International conference on Infrared, Millimeter and Terahertz Waves)	Broadband Electron Paramagnetic Resonance Using A Tunable Continuous-Wave Terahertz Photomixer Source
	2019.9.25-29	柏	poster	The 16th International Conferenxe on Megagauss Magnetic Field Generation and Related Topics	High-Field Terahertz EPR Studies on Heme Compounds
高橋英幸 (先端融合研究環)	2018.9.6	神戸	poster	第五回西日本強磁場科学研究会	磁気トルク測定による FeSe の超伝導揺らぎ由来反磁性の精密評価
	2018.9.9-12	京田辺市	oral	日本物理学会　2018 年秋季大会	光干渉変位検出方式のカンチレバー磁化測定による FeSe の超伝導揺らぎ磁化の評価
	2018.9.23-27	Brisbane, Australia	oral	The Third Joint Conference of th Asia-Pacific EPR/ESR Society and The International EPR (ESR Society (IES)	Highly Sensitive and Practical Force-detected ESR Spectrometer Utilizing a Silicon Nitride Nanomembrane
	2018.11.1-3	札幌	oral	第 57 回電子スピンサイエンス学会年会（SEST2017)	SiNx ナノメンブレンを用いた力検出型高周波 ESR 測定法
櫻井敬博 (研究基盤センター)	2018.9.6	神戸	oral	第五回西日本強磁場科学研究会	高圧強磁場 ESR の開発と応用 -直交ダイマー系 $SrCu_2(BO_3)_2$ の結果を中心に-
	2018.9.25-29	柏	poster	The 16th International Conferenxe on Megagauss Magnetic Field Generation and Related Topics	Development of high-pressue high-field ESR system and application to orthogonal dimer spin system $SrCu_2(BO_3)_2$
	2018.11.26-28	岡山	oral	第 59 回高圧討論会	無冷媒型超伝導磁石を用いた高圧力下 ESR 測定の開発
	2019.1.28	神戸	oral	第 2 回スピン系物理研究会	Shastry-Sutherland 物質 $SrCu_2(BO_3)_2$ の高圧力下 ESR による量子相転移の観測
	2019.3.14-17	福岡	oral	日本物理学会　第 74 回年次大会（2019 年）	25T 無冷媒型超伝導磁石を用いた直交ダイマー系 $SrCu_2(BO_3)_2$ の高圧下 ESR

原茂生(研究基盤センター)	2018.9.6	神戸	poster	第五回西日本強磁場科学研究会	フラストレート磁性体 $K_2Mn_3(OH)_2(VO_4)_2$ の強磁場 ESR 測定
	2018.3.14-17	福岡	poster	日本物理学会　第 74 回年次大会(2019 年)	$RbMn_3Ge_2O_9$ 新規 S=2 カゴメ格子酸化物の構造と磁性
河本敏郎 T. Kohmoto	2018.9.9-14	名古屋	poster	43rd Int. Conf. on Infrared, Millimeter, and Terahertz Waves	Ultrafast Magnon Dynamics in Antiferromagnetic Nickel Oxide Observed by Optical Pump-Probe and Terahertz Time-Domain Spectroscopies
	2019.3.14-17	福岡	poster	日本物理学会第 74 回年次大会	CuO における格子とスピンの超高速ダイナミクス

Presentation by Graduate Students and Postdocs 院生、ポストドクの学会発表

指導教員	発表者氏名	学年	時期	学会名	講演題目
小堀康博 Y. Kobori	尾山 真也	M1	2017.6.18 – 21	2018 年光化学討論会	時間分解 EPR 法を用いた P3HT:PC70BM ブレンド膜に生成する光電荷分離状態の観測
	尾山 真也	M1	2018.11.1-11.3	第 57 回電子スピンサイエンス学会年会（SEST2018）	時間分解 EPR 法を用いた P3HT:PC70BM ブレンド膜に生成する光電荷分離状態の観測
	江間 文俊	D3	2018.9.5-7	2018 年光化学討論会	有機包接結晶における室温リン光発光性三重項電荷移動状態のゲスト分子依存性
	濱田 実里	M2	2018.9.5-7	2018 年光化学討論会	クリプトクロムに生成する光電荷分離状態の立体構造の観測
	長嶋 宏樹	PD	2018.9.5-7	2018 年光化学討論会	TREPR 法によるシングレットフィッションにおける五重項状態の生成機構
	長嶋 宏樹	PD	2018.9.10-9.13	第 12 回分子科学討論会 2018	時間分解 EPR による一重項分裂反応から生じた三重項励起子対のダイナミクスの解析
	濱田 守彦	PD	2018.11.1-11.3	第 57 回電子スピンサイエンス学会年会（SEST2018）	時間分解 EPR 法を用いた PC70BM 薄膜中における励起子拡散の観測
立川貴士 T. Tachikawa	狩俣 出	D2	2018.9.6	2018 年光化学討論会	ハロゲン交換反応によるペロブスカイトナノ粒子のコアーシェル空間制御
	村上 雄太	M2	2018.9.6	2018 年光化学討論会	新規金属酸化物メソ結晶の開発と高効率・高選択的光触媒への応用
	水谷 晟吾	M2	2018.9.6	2018 年光化学討論会	タンタル酸ナトリウム光触媒の発光特性と金属ドープ濃度の関係性
	木村 優季	M2	2018.9.5	2018 年光化学討論会	Mechanistic insights into photochemical reactions on organic lead halide perovskites from single-particle spectroscopy
	渡瀬 達也	M1	2018.9.5	2018 年光化学討論会	メソポーラスシリカ担持ルテニウム錯体の単一粒子発光観測：細孔内拡散と光触媒活性の関係
	櫻井 学	D1	2018.9.5	2018 年光化学討論会	Local environment mapping of lipid bilayer membranes using magnetic-field responsive fluorescence probes
	水谷 晟吾	M2	2018.9.21	日本化学会「低次元系光機能材料研究会」 第 8 回サマーセミナー	深紫外蛍光顕微鏡を用いたタンタル酸ナトリウム光触媒の単一粒子発光観測
	村上 雄太	M2	2018.9.21	低次元系光機能材料研究会 第 8 回サマーセミナー	酸化チタン超構造体の制御されたナノ空間における発光観測
	渡瀬 達也	M1	2018.9.21	低次元系光機能材料研究会 第 8 回サマーセミナー	ルテニウム修飾メソポーラスシリカの単一粒子発光観測
	狩俣 出	D2	2018.10.24	第 8 回 CSJ 化学フェスタ 2018	ハロゲン交換反応によるペロブスカイトナノ粒子のコアーシェル形成過程のその場観測
	狩俣 出	D2	2018.11.1	Indo-Japan mini-workshop Frontiers in Molecular Spectroscopy: From Fundamentals to Applications in Chemistry and Biology	In-situ observation of charge carrier and ion dynamics during halide exchange reaction on $CH_3NH_3PbBr_3$ crystal

	水谷 晟吾	M2	2018.12.17	10th Asian Photochemistry Conference (APC2018)	Single-Particle Emission Observation of $NaTaO_3$ Photocatalysts Using Deep Ultraviolet Fluorescence Microscope
	村上 雄太	M2	2018.12.17	10th Asian Photochemistry Conference (APC2018)	Development of Titanium Dioxide Mesocrystals for Highly Efficient and Selective Photocatalysis: Role of Oriented Nano-Space
	渡瀬 達也	M1	2018.12.17	10th Asian Photochemistry Conference (APC2018)	Single-Particle Emission Observation of Ruthenium Complex Supported on Mesoporous Silica
	狩俣 出	D2	2018.12.18	10th Asian Photochemistry Conference (APC2018)	Localized Trapped Charges Induce Slow Charge Transfer over a Few Nanoseconds on Heterostructured $CH_3NH_3PbBr_{3-x}I_x$
	狩俣 出	D2	2019.3.18	日本化学会 第99春季年会 (2019)	Single-Particle Photoluminescence Switching Induced by Ion Dynamics in Organic-Inorganic Perovskite Nanoparticles
	櫻井 学	D1	2019.3.17	日本化学会 第 99 春季年会 (2019)	Local Environment of Lipid Bilayer Membrane Monitored by Magnetic Field Effect-Based Fluorescence Imaging
	木村 優季	M2	2019.3.18	日本化学会 第 99 春季年会 (2019)	有機鉛ハロゲン化物ペロブスカイトにおける発光挙動の単一粒子発光観測
	村上 雄太	M2	2019.3.18	日本化学会 第 99 春季年会 (2019)	酸化チタンメソ結晶の制御されたナノ空間を利用した選択的光触媒反応
	渡瀬 達也	M1	2019.3.17	日本化学会 第 99 春季年会 (2019)	ルテニウム色素吸着メソポーラスシリカの単一粒子蛍光顕微鏡観測：細孔内拡散と光触媒活性の関係
	坂本 萌里	B4	2019.3.17	日本化学会 第 99 春季年会 (2019)	ハロゲン混合型有機無機ペロブスカイトナノ粒子の単一粒子発光イメージング
	山下 真帆	B4	2019.3.17	日本化学会 第 99 春季年会 (2019)	ソフトクリスタルにおける刺激応答構造変化の蛍光顕微鏡観測
富永圭介 K. Tominaga	Feng Zhang	PD	2018.7.10-11	Interdisciplinary symposium on the development of THz techniques	THz spectroscopy of molecular crystals and crystalline polymers
	Feng Zhang	PD	2018.9.9-14	43rd International Conference on Infrared, Millimeter and Terahertz Waves	Analysis of Disorder in a Molecular Crystal with Terahertz Spectroscopy and Solid-state Density Functional Theory
	Feng Zhang	PD	2018.10.31	Indo-Japan mini-workshop frontiers in molecular spectroscopy	Low-frequency modes of molecular crystals and crystalline polymers studied by terahertz spectroscopy and solid-state density functional theory
	Feng Zhang	PD	2018.12.25-27	The fourth young-scholars forum of Southwest University	THz spectroscopy of molecular crystals and crystalline polymers
	門村 友	M2	2018.6.6-9	36th Samahang Pisika ng Pilipinas (Physics Conference and Annual Meeting)	Hydration effect on the dynamics of phospholipids studied by broadband dielectric spectroscopy
	門村 友	M2	2018.9.9-12	日本物理学会 2018 年 秋季大会［物性］	広帯域誘電分光法によるリン脂質の動的挙動に及ぼす水和の影響
	門村 友	M2	2018.11.4-8	Joint Conference of EMLG/JMLG Meeting 2018 and 41st Symposium on Solution Chemistry of Japan	Hydration effect on the dynamics of phospholipid studied by broadband dielectric spectroscopy

	平松 優一	M2	2018.6.6-9	36th Samahang Pisika ng Pilipinas (Physics Conference and Annual Meeting)	Charge Carrier Dynamics in Bulk Heterojunction Organic Semiconductor by Optical-Pump Terahertz-Probe Spectroscopy
	平松 優一	M2	2018.9.5-7	2018 年光化学討論会	光ポンプ-テラヘルツプローブ分光法によるバルクヘテロ接合型有機半導体における電荷キャリアダイナミクス
	平松 優一	M2	2018.11.4-8	Joint Conference of EMLG/JMLG Meeting 2018 and 41st Symposium on Solution Chemistry of Japan	Adsorbed water dynamics on TiO_2 surface by broadband dielectric spectroscopy
	Lou Serafin M. Lozada	Research student	2018.11.4-8	Joint Conference of EMLG/JMLG Meeting 2018 and 41st Symposium on Solution Chemistry of Japan	Terahertz investigation of the temperature dependence of charge localization of polyaniline composite
	Lou Serafin M. Lozada	Research student	2019.3.5-7	7th International Workshop on Far-Infrared Technologies	Conductivity and carrier density of polyaniline containing polymer-clay composite studied by terahertz time-domain spectroscopy
佐藤春実 H. Sato	三輪 泰大	M1	2018.12.21	若手フロンティア研究会 2018	TBAB hydrate の THz 吸収分光とラマン分光の比較
	Dian Marlina	D2	2018.12.5-7	テラヘルツ科学の最先端 V	Hydrogen-Bonding Interactions of Poly(3-hydroxybutyrate) / Poly(4-vinylphenol) Studied by Low Frequency-Raman Spectroscopy
	那須 達郎	B4	2018.12.5-7	テラヘルツ科学の最先端 V	低波数ラマンを用いた高吸水性樹脂の水和に関する研究
	西前 篤志	B4	2018.12.5-7	テラヘルツ科学の最先端 V	ポリ（グリコリド-co-ラクチド）共重合体の THz 分光法による高次構造の研究
	山元 優美子	M1	2018.12.5-7	テラヘルツ科学の最先端 V	テラヘルツ分光法および低波数ラマン分光法を用いた結晶性エンジニアリングプラスチックの相互作用の研究
	長濱 朋輝	M2	2018.12.2-5	The 3rd Aquaphotomics International Symposium	Molecular dependence of collagen model peptide stuidied by low frequency Raman spectroscopy
	三輪 泰大	M1	2018.12.2-5	The 3rd Aquaphotomics International Symposium	Study of Tetrabutylammonium Bromide Hydrate by Two spectroscopies in THz region
	山元 優美子	M1	2018.9.12-14	第 67 回高分子討論会	テラヘルツ分光法によるポリブチレンテレフタレートの高次構造と結晶構造形成過程の研究
	岡崎 なつ実	M1	2018.9.12-14	第 67 回高分子討論会	テラヘルツ分光法によるポリジオキサノンの結晶構造における相互作用の解明
	長濱 朋輝	M2	2018.9.12-14	第 67 回高分子討論会	赤外分光法及び低波数ラマン分光法におけるコラーゲンモデル化合物の分子量依存性
	Dian Marlina	D2	2018.9.12-14	第 67 回高分子討論会	A Study of Hydrogen Bonding of Polyethylere Glycol / Chitosan Blends in the Low-frequency Region
	岡崎 なつ実	M1	2018.8.26-31	the 26th International Conference on Raman Spectroscopy (ICORS 2018)	Study on Intermolecular Interaction of Polydioxanone by Terahertz and low frequency Raman spectroscopy

	長濱 朋輝	M2	2018.8.26-31	the 26th International Conference on Raman Spectroscopy (ICORS 2018)	Molecular dependence of several collagen model peptides stuidied by low frequency Raman spectroscopy
	山元 優美子	M1	2018.8.26-31	the 26th International Conference on Raman Spectroscopy (ICORS 2018)	Study of higher order structure of poly (ethylene terephthalate) and poly (butylene terephthalate) by low frequency Raman and terahertz spectoscopy
	Dian Marlina	D2	2018.8.26-31	The 26th International Conference on Raman Spectroscopy (ICORS 2018)	The Study of Intermolecular Interaction in Polymer Blend of Polyethylene Glycol and Cellulose Acetate Butyrate by Low-Frequency Raman Spectroscopy
	三輪 泰大	M1	2018.8.26-31	the 26th International Conference on Raman Spectroscopy (ICORS 2018)	Observation of THz-Raman Spectrum in Tetrabutylammonium Bromide Hydrate
	長濱朋輝	M2	2018.7.13	高分子研究発表会（神戸）	高感度反射赤外分光法を用いたポリメタクリル酸メチルとポリ4ービニルフェノール超薄膜の相分離挙動と分子量依存性
	山元優美子	M1	2018.7.13	高分子研究発表会（神戸）	振動分光法によるポリブチレンテレフタレートの分子間・分子内相互作用の研究
	Dian Marlina	D2	2018.7.13	高分子研究発表会（神戸）	Intermolecular Interaction of Polyethylene Glycol / Cellulose Acetate Butyrate Blends by Terahertz Spectroscopy
	岡崎なつ実	M1	2018.7.13	高分子研究発表会（神戸）	赤外およびテラヘルツ分光法によるポリジオキサノンの分子間相互作用に関する研究
	Dian Marlina	D2	2018.6.30-7.13	International Conference on Advancing Molecular Spectroscopy (ICAMS)	Hydration Study of Polyethylene Glycol Based Polymer Blend by Low-Frequency Raman Spectroscopy
	長濱朋輝	M2	2018.6.30-7.13	International Conference on Advancing Molecular Spectroscopy (ICAMS)	Molecular weight dependence of phase separation of poly(methyl methacrylate)/poly(4-vinyl phenol) ultra-thin film studied by infrared reflection absorption spectroscopy
	山元優美子	M1	2018.6.30-7.13	International Conference on Advancing Molecular Spectroscopy (ICAMS)	Inter- and intra-molecular interaction of PET and PBT studied by terahertz spectroscopy
	三輪 泰大	M1	2018.6.30-7.13	International Conference on Advancing Molecular Spectroscopy (ICAMS)	Observation of THz- Raman Spectrum in Tetrabutylammonium Bromide Hydrate
	岡崎なつ実	M1	2018.6.30-7.13	International Conference on Advancing Molecular Spectroscopy (ICAMS)	Intermolecular interaction of polydioxanone studied by terahertz spectroscopy
	Dian Marlina	D2	2018.5.23-25	高分子年次大会	Higher-Order Structure of Polyethylene Glycol and Its Blends Studied by Terahertz Spectroscopy
	岡崎なつ実	M1	2018.5.23-25	高分子年次大会	赤外及びテラヘルツ分光法によるポリジオキサノンの結晶構造と分子間相互作用に関する研究
	山元優美子	M1	2018.5.23-25	高分子年次大会	テラヘルツおよび赤外分光法によるポリブチレンテレフタレートの高次構造の研究
太田仁 H. Ohta	岡本翔	D3	2018.5.11-13	第14回ESR入門セミナー	研究講演I　マイクロカンチレバーを用いた高周波電子スピン共鳴法の開発とその生体関連物質への応用

岡本翔	D3	2018.9.6	第五回西日本強磁場科学研究会	SiN_x ナノメンブレンを用いた微量試料の強磁場 ESR 測定法
下城世那	M2	2018.9.6	第五回西日本強磁場科学研究会	幾何学的スピン構造をもつ反強磁性体の強磁場 ESR 測定
出口健太	M2	2018.9.6	第五回西日本強磁場科学研究会	高感度 ESR 測定のためのマグネットオンカンチレバーの開発
石村謙斗	M2	2018.9.6	第五回西日本強磁場科学研究会	改良されたメンブレン型ピエゾ抵抗センサーを用いた強磁場 ESR 測定
藤本達也	M2	2018.9.6	第五回西日本強磁場科学研究会	波長可変テラヘルツ光源を用いた強磁場中 ESR 分光法の開発
松本蓮	M1	2018.9.6	第五回西日本強磁場科学研究会	ナノメンブレンを用いた周波数掃引型強磁場電子スピン共鳴法の開発
奥藤涼介	M1	2018.9.6	第五回西日本強磁場科学研究会	多重極限 ESR 装置におけるハイブリッド型圧力セルの最適化と応用
鈴木哲平	M1	2018.9.6	第五回西日本強磁場科学研究会	S=1/2 カゴメ格子反強磁性体 Ca-kapellasite の圧力下の帯磁率測定
大島健太郎	M1	2018.9.6	第五回西日本強磁場科学研究会	ペロブスカイト型化合物 $PbMnO_3$ の強磁場 ESR 測定
Paul Bruand	Intern INSA, France	2018.9.6	第五回西日本強磁場科学研究会	Development of High-field ESR system using the null detection
港啓介	M1	2018.9.9-12	日本物理学会　2018 年秋季大会	光伝導アンテナを用いた連続周波数可変テラヘルツ電子スピン共鳴法の開発
奥藤涼介	M1	2018.9.9-12	日本物理学会　2018 年秋季大会	ハイブリッド型圧力セルを用いた多重極限 ESR 装置の開発と応用
鈴木哲平	M1	2018.9.9-12	日本物理学会　2018 年秋季大会	S=1/2 カゴメ格子反強磁性体 Ca-kapellasite の圧力下の磁性
石村謙斗	M2	2018.9.9-12	日本物理学会　2018 年秋季大会	改良されたメンブレン型ピエゾ抵抗センサーを用いた高感度磁気測定
松本蓮	M1	2018.9.9-12	日本物理学会　2018 年秋季大会	ナノメンブレンを用いた周波数掃引型高周波電子スピン共鳴法の開発
大島健太郎	M1	2018.9.9-12	日本物理学会　2018 年秋季大会	ペロブスカイト型化合物 $PbMnO_3$ の高周波 ESR 測定
下城世那	M2	2018.9.9-12	日本物理学会　2018 年秋季大会	幾何学的スピン構造をもつ反強磁性体の強磁場 ESR による研究 II
岡本翔	D3	2018.9.23-27	The Third Joint Conference of the Asia-Pacific EPR/ESR Society and The International EPR (ESR)	Pressure Effect on Zero-Field Splittng Parameter of Iron-Porphyrin Complexes Revealed by High-Frequency and High-Field Electron Paramagnetic Resonance

				Society (IES)	
	奥藤涼介	M1	2018.9.23-27	The Third Joint Conference of the Asia-Pacific EPR/ESR Society and The International EPR (ESR) Society (IES)	Development of high-field and high-pressure ESR system and application to trangular antiferromagnet $CsCuCl_3$
	岡本翔	D3	2018.9.23-27	The Third Joint Conference of the Asia-Pacific EPR/ESR Society and The International EPR (ESR) Society (IES)	Pressure Effect on Zero-Field Splittng Parameter of Iron-Porphyrin Com-plexes Revealed by High-Frequency and High-Field Electron Paramagnetic Resonance
	岡本翔	D3	2018.11.1-3	第 57 回電子スピンサイエンス学会年会	154GHz ジャイロトロンを用いた力検出型 ESR 測定法と金属タンパク質への応用
	下城世那	M2	2018.12.21	若手フロンティア研究会 2018	幾何学的なスピン構造を有する反強磁性体の強磁場 ESR による研究
	出口健太	M2	2018.12.21	若手フロンティア研究会 2018	高感度 ESR 測定のためのマイクロ磁気チップカンチレバーの作製
	石村謙斗	M2	2018.12.21	若手フロンティア研究会 2018	改良されたメンブレン型ピエゾ抵抗センサーを用いた角度回転高周波 ESR
	大島健太郎	M1	2018.12.21	若手フロンティア研究会 2018	ペロブスカイト型化合物 $PbMnO_3$ の ESR 測定
	奥藤涼介	M1	2018.12.21	若手フロンティア研究会 2018	２万気圧下でスピンを観る！
	藤本達也	M2	2018.12.21	若手フロンティア研究会 2018	ヌル検出を用いた高周波 ESR 測定法の開発
	岡本翔	D3	2018.12.21	若手フロンティア研究会 2018	SiNx ナノメンブレンを用いた力検出型電子スピン共鳴法
	港啓介	M1	2018.12.21	若手フロンティア研究会 2018	光伝導アンテナを使った連続周波数可変テラヘルツ帯電子スピン共鳴法の開発
	鈴木哲平	M1	2018.12.21	若手フロンティア研究会 2018	ヌル検出法による高周波電子スピン共鳴測定
	恒石一義	M1	2018.12.21	若手フロンティア研究会 2018	$KCuMoO_4(OH)$の ESR 測定
	松本蓮	M1	2018.12.21	若手フロンティア研究会 2018	ナノメンブレンを用いた周波数掃引型電子スピン共鳴法の開発
	奥藤涼介	M1	2019.3.14-17	日本物理学会　第 74 回年次大会（2019 年）	圧力下における三角格子反強磁性体 $CsCuCl_3$ の相互作用パラメータの評価
河本敏郎 T. Kohmoto	疋田崚	M2	2018.7.8-13	12th Int. Conf. on Excitonic and Photonic Processes in Condensed Matter and Nano Materials	Dynamics of the electric-field induced magnetization in antiferromagnetic chromium oxide observed by Faraday rotation

	藤本恵輔	M1	2018.7.8-13	12th Int. Conf. on Excitonic and Photonic Processes in Condensed Matter and Nano Materials	Electric-field induced magnetization in YIG observed by Faraday rotation
	小出大士朗	M1	2018.11.24	2018 年度日本物理学会北陸支部定例学術講演会	シリコンの透過テラヘルツ電場波形に対する光励起の影響
	疋田崚	M2	2018.12.7-8	第 29 回光物性研究会	反強磁性体 Cr_2O_3 における高速格子ダイナミクス
	藤本恵輔	M1	2018.12.7-8	第 29 回光物性研究会	YIG における電場誘起磁化
	釋佳祐	M1	2018.12.7-8	第 29 回光物性研究会	マルチフェロイック物質 CuO における格子とスピンの超高速ダイナミクス
	藤本恵輔	M1	2018.12.21	若手フロンティア研究会 2018	YIG の電場誘起磁化
	釋佳祐	M1	2018.12.21	若手フロンティア研究会 2018	マルチフェロイック物質 CuO における格子とスピンの超高速ダイナミクス
	疋田崚	M2	2018.12.21	若手フロンティア研究会 2018	反強磁性体 Cr_2O_3 における高速格子ダイナミクス
	小出大士朗	M1	2019.3.5-7	7th Int. Workshop on Far-Infrared Technologies	Influence of Photo-excitation on Terahertz Waveform Transmitted through Silicon
	藤本恵輔	M1	2019.3.14-17	日本物理学会第 74 回年次大会	YIG における電場誘起磁化
	疋田崚	M2	2019.3.14-17	日本物理学会第 74 回年次大会	反強磁性体 Cr_2O_3 における高速格子ダイナミクス

Books **著書**

著者（共著者も含む）	書名	出版社名	ページ数	発行年
Feng Zhang, Keisuke Tominaga, Michitoshi Hayashi, and Takashi Nishino	“Effects of non-covalent interactions on molecular and polymer individuality in crystals studied by THz spectroscopy and solid-state density functional theory” in *“Molecular Spectroscopy: A Quantum Chemistry Approach”* edited by Yukihiro Ozaki	Wiley		2019 In press

Other Publications **参考論文･記事･報告**

著者	タイトル	出版物名	巻・号・ページ	発行年
Feng Zhang, Houng-Wei Wang, Keisuke Tominaga, Michitoshi Hayashi, Tetsuo Sasaki	Structure Analysis of Disorder in a Molecular Crystal with Terahertz Spectroscopy and Solid-state Density Functional Theory	*abstract book IRMMW-THz 2018*	Th-A2-R1-2	2018
Yu Kadomura, Naoki Yamamoto, and Keisuke Tominaga	THz Dynamics of Hydrated Phospholipid Studied by Broadband Dielectric Spectroscopy	*abstract book IRMMW-THz 2018*	Tu-POS-12	2018
Yuichi Hiramatsu, Kaoru Ohta, Kohtaro Takahashi, Mitsuharu Suzuki, Hiroko Yamada, and Keisuke Tominaga	Charge Carrier Dynamics in Bulk Heterojunction Organic Semiconductor by Optical-Pump Terahertz-Probe Spectroscopy	*abstract book IRMMW-THz 2018*	Mo-POS-31	2018
Alvin Karlo G. Tapia, Lou Serafin M. Lozada, and Keisuke Tominaga	Temperature Dependence of THz Conductivities of Polyaniline Emeraldine Salt/Bentonite Pellets	*abstract book IRMMW-THz 2018*	Mo-POS-37	2018
Kaoru Ohta, Yuichi Hiramatsu, Kohtaro Takahashi, Mitsuharu Suzuki, Hiroko Yamada and Keisuke Tominaga	Ultrafast Charge Carrier Dynamics in Diketopyrrolopyrrole-Linked Tetrabenzoporphyrin Films Studied by Time-Resolved Terahertz Spectroscopy	*abstract book IRMMW-THz 2018*	Mo-P2-R1-2	2018
疋田崚，谷口弘樹，河本敏郎	反強磁性体 Cr_2O_3 における高速格子ダイナミクス	光物性研究会論文集	29 巻 93-96	2018
藤本恵輔，蓮沼貴史，河本敏郎	YIG における電場誘起磁化	光物性研究会論文集	29 巻 153-156	2018
釋佳祐，澤田幸宏，鄭旭光，河本敏郎	マルチフェロイック物質 CuO における格子とスピンの超高速ダイナミクス	光物性研究会論文集	29 巻 241-244	2018

Lecture to Public **講演、模擬授業など**

氏名	講演題目	集会名	日時	場所
小堀康博	光と磁石の力で世界を変える - 太陽光エネルギー変換の仕組み -	神戸大学 day セミナー	2018. 5. 22	神戸大学中等部
佐藤春実	ラマン分光の高分子化学への応用	日本分光学会第 54 回夏期セミナー「ラマン分光法」	2018.9.15	幕張メッセ国際会議場
佐藤春実	高分子のテラヘルツ分光と低波数ラマン分光	日本分光学会第 54 回夏期セミナー「テラヘルツ分光と低波数ラマン分光の基礎」	2018.9.15	幕張メッセ国際会議場
河本敏郎	光と色の科学	出前授業	2018.6.21	西宮東高校
河本敏郎	光と色の科学	理学部模擬授業 (明石高校)	2018.7.26	神戸大学
河本敏郎	レーザー光で見る電子や原子の超高速運動	神戸大学理学部サイエンスセミナー 2018	2018.7.28	神戸大学
河本敏郎	光と色の科学	理学部模擬授業 (東洋大姫路高校)	2018.11.14	神戸大学

Awards **受賞**

氏名	受賞研究題目	賞名	団体、学会名
木村 優季	Mechanistic insights into photochemical reactions on organic lead halide perovskites from single-particle spectroscopy	光化学討論会最優秀学生発表賞（ポスター）	光化学協会
狩俣 出	ハロゲン交換反応によるペロブスカイトナノ粒子のコアーシェル形成過程のその場観測	第 8 回 CSJ 化学フェスタ 2018　優秀ポスター発表賞受賞	日本化学会
岡崎 なつ実	Study on Intermolecular Interaction of Polydioxanone by Terahertz and low frequency Raman spectroscopy	Best Poster Award	the 26th International Conference on Raman Spectroscopy (ICORS 2018)（2018.8.31）
山元 優美子	Inter- and intra-molecular interaction of PET and PBT studied by terahertz spectroscopy	Best Poster Award	International Conference on Advancing Molecular Spectroscopy (ICAMS) (2018.7.1)
岡本 翔、櫻井 敬博、大道 英二、太田 仁	SQUID 磁束計を用いた高周波 ESR 測定法へのヘムタンパク質モデル錯体への応用	第４回論文賞	一般社団法人　日本赤外線学会（2018 年 5 月）
高橋　英幸	テラヘルツ領域における機械検出型磁気共鳴法の開発	第５回研究奨励賞	一般社団法人　日本赤外線学会（2018 年 5 月）
奥藤　涼介	ESR による圧力下の磁性体における電子状態の解析	優秀賞	平成 30 年度サイエンスフロンティア研究発表会（2018 年 10 月）
出口　健太	半導体ナノ加工技術の開発とマイクロ磁気チップ付きプローブへの応用	優秀発表賞	修士論文審査会（2019 年 3 月）
下城　世那	高次構造を持つ反強磁性四面体クラスターの強磁場 ESR による研究	優秀発表賞	修士論文審査会（2019 年 3 月）
藤本　達也	テラヘルツ領域における空間分解電子スピン共鳴法の開発	優秀発表賞	修士論文審査会（2019 年 3 月）

Conference Organization 学術集会の開催

氏名	学術集会	共同主催者	場所	時期	参加者概数
富永圭介	Indo-Japan Min-Workshop on “Frontiers in Molecular Spectroscopy: Fundamentals and Applications on Material Science and Biology”		理学研究科 Z201・202 教室	2018.10.30-11.2	約 40 名
小堀康博	森野レクチャー		北海道大学	2018.11.1	100 名
太田仁、大久保晋、富永圭介	スピン系物理研究会	神戸大学分子フォトサイエンス研究センター	神戸大学理学部 Z401 教室	2018.11.5	22 名
太田仁、大久保晋	平成 30 年度神戸大学物性実験研究セミナー	神戸大学分子フォトサイエンス研究センター	滝川記念学術交流会館	2018.12.1	60 名
太田仁、大久保晋	量子スピン研究会	神戸大学分子フォトサイエンス研究センター	東海村産業情報プラザ アイヴィル会議室 301	2019.1.9-10	20 名
太田仁、大久保晋、富永圭介	第 2 回スピン系物理研究会	神戸大学分子フォトサイエンス研究センター	神戸大学理学部 Z201／202 教室	2019.1.28	21 名
富永圭介、太田仁、大久保晋	分子フォト共同研究・共同利用　研究会	神戸大学分子フォトサイエンス研究センター	神戸大学理学部 Z302 教室	2019.03.8	33 名

Seminars

セミナー

Date	Name	Affiliation	Title
4.13.2018	John T. Fourkas	University of Maryland	When Complicated Things Happen to Simple Liquids: Acetonitrile at Silica Interfaces
5.10.2018	Malcolm D. E. Forbes	Bowling Green State University, USA	Not So Free Radicals
6.14.2018	Sergey Demishev	Prokhorov General Physics Institute of RAS, Russia	Electron nematic effect in CeB6: The ESR and magnetoresistance evidence
7.19.2018	羽曾部 卓	慶應義塾大学理工学部	励起状態制御に基づく光機能性有機材料の開発と応用展開
11.9.2018	Christopher W. M. Kay	University of Saarland, Germany	Room-Temperature, Solid-State Masers
2.22.2019	Armida V. Gillado	Institute of Mathematical Sciences and Physics, University of the Philippines, Los Baños	Composites of Polyaniline and Oxides: Structural, Electrical and Antimicrobial Properties
3.18.2019	Oliver Portugall	EMFL-LNCMI, Toulouse, France	Solid state spectroscopy beyond 100 Tesla: recent results and new developments
3.19.2019	Zhi-Heng Loh	Nanyang Technological University, Singapore	Femtosecond Electronic and Vibrational Dynamics of Ionized Aqueous Solutions

Molecular Photoscience Research Center
Kobe University,
Nada, Kobe 657-8501 Japan

Tel: +81-78-803-5761
URL: http://www.research.kobe-u.ac.jp/mprc/about/index_e.html (English)

〒657-8501
神戸市灘区六甲台町 1－1
神戸大学分子フォトサイエンス研究センター

電話番号　078-803-5761
http://www.research.kobe-u.ac.jp/mprc/index.html（日本語）